EXPERIMENTAL INVESTIGATION ON IMPACTS OF TSUNAMI-INDUCED FORCES ON COASTAL STRUCTURES

SADIA RAHMAN

DISSERTATION SUBMITTED IN FULFILMENT OF THE REQUIREMENTS FOR THE DEGREE OF MASTER OF ENGINEERING SCIENCE

FACULTY OF ENIGINEERING

UNIVERSITY OF MALAYA

KUALA LUMPUR

2014

UNIVERSITY OF MALAYA

ORIGINAL LITERARY WORK DECLARATION

Name of Candidate: Sadia Rahman

Registration/Matric No: KGA110094

Name of Degree: MASTER OF ENGINEERING SCIENCE

Title of Project Paper/Research Report/Dissertation/Thesis:

EXPERIMENTAL INVESTIGATION ON IMPACTS OF TSUNAMI-INDUCED FORCES ON COASTAL STRUCTURES

Field of Study: WATER RESOURCES ENGINEERING

I do solemnly and sincerely declare that:

(1) I am the sole author/writer of this Work;

(2) This Work is original;

(3) Any use of any work in which copyright exists was done by way of fair dealing and for permitted purposes and any excerpt or extract from, or reference to or reproduction of any copyright work has been disclosed expressly and sufficiently and the title of the Work and its authorship have been acknowledged in this Work;

(4) I do not have any actual knowledge nor do I ought reasonably to know that the making of this work constitutes an infringement of any copyright work;

(5) I hereby assign all and every rights in the copyright to this Work to the University of Malaya ("UM"), who henceforth shall be owner of the copyright in this Work and that any reproduction or use in any form or by any means whatsoever is prohibited without the written consent of UM having been first had and obtained;

(6) I am fully aware that if in the course of making this Work I have infringed any copyright whether intentionally or otherwise, I may be subject to legal action or any other action as may be determined by UM.

Candidate's Signature Date

Subscribed and solemnly declared before,

Witness's Signature Date

Name:

Designation:

ABSTRACT

The recent tsunamis have showed their terrifying impacts and disastrous destructions to the coastal region. Near shore, infrastructure systems comprising buildings, bridges, highways, other road facilities, utilities etc. are critically at risk of substantial damages by the exerted tsunami forces. Tsunamis are long oceanic waves caused mainly due to the rapid displacement of water induced by the earthquake in the ocean floor. Waves disseminate away from their generating source at significant speed and propagate toward the shore. Upon approaching the shallow water near the coast, their speed and wavelengths reduce; however, their wave height increases significantly. While propagating along the shore, waves contain tremendous energy and hit the nearby coastal zones violently. Recorded videos from the historical tsunamis showed that the tsunami waves propagated as hydraulic bores. Dam-break mechanism is the most studied method of producing waves that transmit like hydraulic bores. In this study, a comprehensive research was performed to examine the impact of tsunami-induced forces on two different types of coastal structures (bridge and building). Forces and wave heights were measured using the load cell and the wave probe, respectively. In the case with bridge structures, both broken and unbroken waves were simulated where the measured horizontal forces were larger for the broken waves. When the girder was located in a higher position, measured forces were larger. This fact indicated that the bridges with higher girder height are more vulnerable to the tsunami hazard. Experiments were also performed with about 16 % perforations in the girder and approximately 10 % to 18 % of force reductions were achieved. Results revealed that perforations in the girder are effective in reducing tsunami forces. For the case with square building model, the initial impact forces were larger than the hydrodynamic forces with larger reservoir depths. The hydrodynamic forces exceeded the impact forces at smaller reservoir depth. The average C_D (drag coefficient) value was 1.31 which was very close to FEMA 55 suggested values. The advantages of opening in

the building against tsunami forces were evaluated where approximately 10 % to 65 % of forces were reduced due to the presence of the opening. Seawall with enough height and positioned closer to the building model provided better performance by obstructing the incoming waves. Another research was performed with perforated seawall. As the amount of force reduction attained by the perforated seawall was almost similar to the solid seawall, this study proposed the use of the perforated wall instead of a solid wall. Perforated wall allows easy receding of water to go back to sea, whereas solid wall traps the coming water behind and thus, creating additional forces on the building. Less construction cost of the perforated wall makes it more attractive than the solid wall. The effects of the upstream barriers on the building model were assessed by placing different size barriers in different locations in front of the model. Thinner barrier placed closer to the model provided more protection against the tsunami.

ABSTRAK

Kejadian tsunami baru-baru ini telah meninggalkan kesan yang mendalam dan teruk di kawasan sekitar persisiran pantai negara. Infrastruktur binaan seperti bangunan, jambatan dan lebuh raya di kawasan persisiran pantai adalah berisiko tinggi kepada bahaya tsunami. Tsunami adalah ombak atau gelombang yang terhasil akibat gegaran gempa bumi di dasar laut. Gelombang dari punca gempa bumi bergerak dalam kelajuan yang tinggi tetapi dengan tenaga yang berkurangan. Semakin menghampiri kawasan daratan atau kawasan air cetek, tenaga dari pergerakan tsunami akan meningkat dan menyebabkan gelombang meninggi. Ini menyebabkan zon pantai sangat merbahaya kepada kesan tsunami. Rakaman video sejarah tsunami menunjukkan gelombang yang dihasilkan adalah secara renjatan hiraulik. Mekanisma keruntuhan dam adalah kaedah yang digunakan secara meluas dalam penghasilan gelombang secara renjatan hidraulik. Kajian ini meliputi perbincangan dan pemerhatian mengenai kesan tsunami ke atas bangunan dan jambatan di kawasan persisiran pantai. Tenaga dan ketinggian gelombang tsunami diukur menggunakan sensor dan probe gelombang. Bagi kes struktur jambatan, dua jenis ombak (pecah dan tak pecah) telah disimulasikan dan keputusan menunjukkan bacaan yang tinggi dalam aspek tenaga mendatar disebabkan ombak pecah. Apabila galang diletakkan pada posisi tinggi, tenaga yang diukur adalah besar. Eksperiman ini menunjukkan galang yang berada pada posisi yang tinggi adalah berisiko tinggi terhadapa kesan tsunami. Eksperimen dengan 16% tebukan pada galang menunjukkan kekurangan tenaga sebanyak 10% hingga 18%. Keputusan daripada eksperimen ini menunjukkan tebukan pada galang adalah efektif untuk mengurangkan kesan daripada kesan tenaga tsunami.

Bagi kes bangunan bentuk segiempat pula, tenaga impak awal adalah besar berbanding tenaga hidrodinamik dengan kedalaman takungan yang tinggi. Tenaga hidrodinamik mengatasi tenaga impak untuk takungan yang cetek. Nilai purata C_D (pekali seretan) adalah 1.31 dan ini menghampiri nilai C_D yang dianjurkan dalam rujukan FEMA 55. Bukaan pada bangunan dilihat membantu dalam mengurangkan kesan tenaga tsunami dalam anggaran sekitar 10% hingga 65% tenaga. Dinding laut yang diletakkan berdekatan bangunan memberi kesan yang sangat baik dalam menghalang ombak yang datang. Satu kajian yang lain dilakukan dengan menebuk dinding laut. Keputusan eksperimen mendapati tebukan pada dinding laut memberikan kesan yang sama seperti dinding laut tanpat tebukan. Melalui permerhatian ini, penggunaan dinding laut yang ditebuk adalah sangat dianjurkan. Tebukan pada dinding membolehkan air laut kembali ke laut manakala dinding tanpa tebukan menghasilkan tenaga tambahan pada bangunan. Kos yang rendah untuk dinding laut yang ditebuk membuatkan ia sangat disyorkan berbanding dinding laut yang tidak ditebuk. Kesan penghalang pada sebelah hulu digunakan dalam eksperimen dengan menggunakan saiz penghalang yang berbeza yang diletakkan di sebelah depan model bangunan. Eksperimen mendapati, penghalang yang nipis adalah lebih efektif dalam menghadapi kesan terhadap tsunami.

ACKNOWLEDGMENTS

All Praise to Allah. I am grateful to the Almighty Allah for giving me the patience, opportunity and courage to complete the thesis successfully.

I would like to express my deep and sincere gratitude to my supervisor Dr. Shatirah Binti Mohamed Akib. With her endless encouragements and appreciation, she has always motivated me to reach higher goals. Since we ever met, she always did all that was in her power to help me succeed both academically and professionally. I would like to sincerely thank Dr. Radianta Triatmadja for providing the facilities for performing the experiments in their laboratory. His endless support helps in fulfilling my experimental works. Again, I would like to thank everyone working in the Hydrology and Hydraulics laboratory at the University of Gadjah Mada, Indonesia for their significant help. I would like to acknowledge the help of Mr. M. Subhi Nurul Hadie of University of Gadjah Mada for the technical assistance during the experiments.

Finally, I would like to thank my family for all the endless support they have provided me, and to whom I owe everything.

Sadia Rahman

University of Malay, 2014

TABLE OF CONTENT

LIST OF FIGURES

LIST OF TABLES

LIST OF SYMBOLS

A	Projected area of the body normal to the direction of flow (cm^2)
A_0	Area of the opening (cm^2)
a	Tsunami wave height (cm)
b	Width of the wall (m)
C	Velocity coefficient
C_D	Drag coefficient (non-dimensional)
C_F	Coefficient of forces
C_f	Bulk coefficient
d	Distance between rear face of the barrier to the front face of the building (cm)
d_s	Inundation depth (cm)
f	friction coefficient
F_B	Buoyant force (N)
F_D	Total drag force acting in the direction of flow (N)
F_{HS}	Hydrostatic force per unit width (N/m)
F_i	Impact force (N)
F_r	Froude number
F_S	Total surge force per unit width of wall (N/m)
g	Gravitational acceleration (m/s^2)

h Static water depth (cm)

h_0 Reservoir depth (cm)

h_3 Initial downstream depth (cm)

L Distance between the gate and the location of interest (m)

L_r Length ratio

l_a Distance between the center of the model to the hinge (cm)

l_b Distance between the hinge to the centre point of load cell (cm)

m Mass of the body impacting the structure (Kg)

q Horizontal wave pressure (N/m^2)

t Time (s)

u Wave velocity (m/s)

u_i Approach velocity of the impacting body (m/s)

u_b velocity of the impacting body (m/s)

V Submerged volume of the structure (m^3)

W Seawall height (cm)

x Distance between the gate and the seawall position (m)

Z Girder height (cm)

z The distance from the base of the wall to the point of application of the resultant surge force (cm)

κ Ratio between the horizontal wave pressure and the static water pressure against the tsunami wave height

η_* Size of opening

Δ Reduction factor

θ Bed slope (non-dimensional)

ρ Density of water (kg/m^3)

σ Ratio of distance between the building and the barrier to the wave height

δ Ratio between the girder height to the tsunami wave height

Δs Distance between the stations (m)

Δt Impact duration (equals to the time between initial contact of the body with the building and the maximum impact force) (s)

CHAPTER 1

INTRODUCTION

1.1 General

In the last recent tsunami events, severe devastations were observed through terrific losses of life and significant damages on the coastal infrastructures that remind the world about the enormous vulnerability of the tsunami incident. The damages in Indian Ocean Tsunami in 2004 (Liu et al., 2005), in Chile tsunami in 2010 (Michelin et al., 2010) and in Tohoku Tsunami in 2011 (Mori et al., 2011) have renewed the public awareness about the destruction impact of the tsunami hazards on their life and property. Near shore, infrastructure systems comprising buildings, bridges, highways, utilities, other road facilities etc. are critically at risk of substantial damages by the exerted tsunami forces. Post tsunami field surveys have been well documented such tsunami devastations along with dreadful and crucial characteristics of tsunami (Bahlburg & Spike, 2012; Bahlburg & Weiss, 2007; Fritz et al., 2008; Goto et al., 2012; Kawashima et al., 2011; Lekkas et al., 2011; Liu et al., 2005; Richmond et al., 2012; Richmond et al., 2006; Synolakis & Okal, 2005). As of 2007, there was a greater chance of earthquake induced tsunami with a magnitude of 8 near Japan and that happened in March, 11th, 2011. A devastating tsunami took place along Tohoku, Japan that caused around 17 m inundation in some areas. In the U.S. Pacific northwest zone, the probability of an earthquake with magnitude of 9 is about 14 % that might trigger a 10 m inundation along the shore. Therefore, all these events emphasize on the necessity of clear understanding of the complex interaction between tsunami induced forces and impacted coastal structures for the further protection strategy. The performance of structures during these disasters indicated the dimness in the current design code.

Hence, more researches need to be conducted to understand the loading circumstances on the near shore structures based on both physical and numerical simulations.

Large tsunami waves propagate in the ocean over thousands of kilometers away from their generating source at considerable speeds. When an offshore subduction earthquake of significant magnitude occurs, the quick uplift motion of the seabed vertically displaces a large volume of water, inducing a rapid, localized change in the sea level. This results into one or several tsunami waves propagating in opposite directions, perpendicular to the fault line. In deep waters, these waves have relatively small amplitudes but their wavelengths often approach hundreds of kilometers. As these waves propagate towards the shoreline into shallow coastal waters, due to the compressing effect of the up-sloping seabed and the decreasing water depth, waves experience a deceleration and a reduction of their wavelength, as well as an increase in amplitude. In most cases, depending on the geographical features of the coastline, the front of the wave breaks when its height becomes approximately equal to the local water depth. From this point, the broken wave takes the form of a hydraulic bore, a rapidly advancing body of water with a relatively uniform depth and a steep turbulent front, and continues to propagate onshore as seen in Figure 1.1. In addition, although most often triggered by subduction earthquakes as explained above, tsunamis can also be due to the sudden displacement of water induced by subaerial and submarine landslides, volcanic eruptions, and meteor impacts.

Figure 1.1: Hydraulic bore induced by the 2011 Tohoku Tsunami, Iwanuma city, Miyagi prefecture, Japan (St-Germain et al., 2013)

1.2 Problem Statement

Within the past few years, although the phenomenon has been known for centuries in countries like Japan, several tsunamis around the globe brought to light the potential such events have for causing severe damage to the inland buildings and bridges and endangering human life. In the recent Tohoku tsunami, even though Japan had large coastal structures such as breakwaters and sea dikes specifically designed against tsunamis, these were no match for the unprecedented tsunami of March 11th, 2011, as shown in Figure 1.2. Triggered by a Mw 9.0 (St-Germain et al., 2013) subduction earthquake located northeast of the Tohoku region, the tsunami resulted in widespread destruction (Figure 1.3), claimed over 20,000 lives, and caused economic losses estimated at over 217 billion US dollars (EERI, 2011). In the aftermath of these events, as displayed in Figure 1.4, field surveys revealed that structures can severely be damaged or destroyed due to the action of extreme tsunami-induced hydrodynamic forces (EERI, 2011; Ghobarah et al., 2006; Nistor et al., 2005; Saatcioglu et al., 2006a,

2006b; Tomita et al., 2006; Yamamoto et al., 2006). Furthermore, after the latest 2011 Tohoku Tsunami it was observed that, although multiple-storey engineered concrete and steel buildings were previously believed to be tsunami-resistant (EERI, 2011; Mikami et al., 2012; Takahashi et al., 2011) as evidence in Figures 1.3 and 1.4b, they can also be destroyed. Motivated by these field observations, an extensive literature review of current design codes demonstrated that, in contrast to seismic forces, such hydrodynamic forces are not taken into proper consideration when designing structures for tsunami prone areas (Nistor et al., 2009).

Bridges are one of the most susceptible structural elements that can be viciously impacted by the tsunami disaster. During the latest few tsunami hazards, a number of bridges were affected severely due to the lack of proper incorporation of tsunami forces in the design guidelines (Figure 1.5). Such damages hampered the emergency and rescue activities. Therefore, the provisions of the seismic as well as the tsunami loading on the coastal structures should be considered in the design guideline.

Figure 1.2: Destruction of coastal structures by the 2011 Tohoku Tsunami: (a) Overturned caissons of the breakwater at Kamaishi city, Miyagi prefecture (Takahashi et al., 2011); (b) Concrete panels stripped from earthen sea dike at Tarou city, Miyagi Prefecture (EERI, 2011)

Figure 1.3: Widespread destruction of inland structures by the 2011 Tohoku Tsunami in Onagawa city, Miyagi prefecture (Mikami et al., 2012)

Figure 1.4: Destruction of inland structures due to tsunami-induced hydrodynamic forces: (a) 2004 Indian Ocean Tsunami, Phuket city, Thailand (CAEE, 2005); (b) 2011 Tohoku Tsunami, Onagawa city, Miyagi prefecture, Japan (Nistor et al., 2005)

Figure 1.5: Bridge damage due to tsunami attack: (a) Total Wash-Away of Deck in Banda Aceh (Unjoh, 2005); (b) Damaged steel truss bridge in Lhok Nga, Banda Aceh; (c) Utatsu bridge, the middle part was washed away

1.3 Research Objectives

This study aimed to understand the tsunami wave forces on the coastal structures. Specifically, the objectives of this study include:

1. To measure the tsunami wave forces on the solid and perforated bridge girder
2. To examine the effects of the breakwater in reducing the tsunami forces on the bridge structures
3. To study the tsunami wave effects on the buildings with openings and without openings.
4. To evaluate the effectiveness of using onshore solid and perforated seawall in controlling the tsunami forces.
5. To identify the effects of various upstream barriers in minimizing the tsunami forces on the building structures.

1.4 Scope of the Study

Tsunami waves originate in the deep ocean and propagate towards the shore. Before reaching the shore the waves break. The breaking of waves occur at the location where

the water level of the wave becomes equivalent to the water depth at that location. At this state, the wave turns into a hydraulic bore and flows along the shore with subsequently high velocity. In order to simulate such wave condition, dam-break mechanism was adopted where waves were produced by the quick opening of the gate located upstream of the flume. The impacts of the tsunami forces on the coastal bridges and buildings were assessed and the complex nature of wave-structures interaction was evaluated based on the experimental data.

1.5 Significance of the Study

The novelty of the present study resides in the investigation of the tsunami impacts on different coastal structures through the measurement of exerted forces. Limited studies on the unpredictable nature of the tsunami flow enable the researchers to concentrate much on the characteristics of tsunami flow. This thesis aims to enhance the understanding of the wave-structure interaction and the results obtained can provide a better understanding of the tsunami propagation nature that in turn would be helpful to modify the current guidelines for the construction of any coastal structures. In addition to the application of this study to improve the design guidelines, the research results are valuable for the validation of the numerical models. The most recently developed numerical methods, dealing with the interaction of fluid-structure at the cutting edge of multi-phase numerical modeling, must be validated with experimental data.

1.6 Outline of the Thesis

Chapter 1 provides an introduction to the present study. Main elements of the thesis, including objectives, research scope, significance, and thesis outlines are briefly explained. A detailed literature review is presented in Chapter 2, which includes a description of the characteristics of a tsunami-induced hydraulic bore, as well as

existing results of current research on the impact of hydraulic bores on walls and freestanding structures. The experimental set-up is described in detail in Chapter 3. The characteristics of the facility, preparation of the flume, and construction of the gate, together with the method of carrying out the experiments, are briefly described in this chapter. The calibration procedure and the position of instruments used in the experiments are also explained. All the results are evaluated with adequate discussion in Chapter 4. Conclusions based on the obtained data and results of the data analysis are presented in Chapter 5. The contributions of the present research are outlined in this chapter, along with recommendations for future work.

CHAPTER 2

LITERATURE REVIEW

2.1 Introduction

This chapter attempts to summarise the present state of understanding of the damage mechanism of the coastal bridges and the building structures during the tsunami event. The force time history was analysed to facilitate the understanding of the damage pattern. In this chapter, results of literature reviews are presented in order to identify gaps and shortcomings within the existing research. This chapter opens with a survey of the study performed on the dam-break flows. Then, the published research results on the forces exerted on the structures by hydraulic bores are reviewed.

Tsunamis are long oceanic waves caused mainly due to the rapid displacement of the water induced by the earthquake in the ocean floor. Waves disseminate away from their generating source at significant speed and propagate toward the shore. In the deep water, the waves remain unnoticeable because of their small amplitude. Upon approaching the shallow water near the coast, their speed and wavelengths reduce; however, their wave height increases significantly. While propagating along the shore, waves contain tremendous energy and hit the nearby coastal zones violently (FEMA, 2008).

2.2 Behaviors and Characteristics of Tsunamis

Information from the historical tsunami events indicates that the behaviors and characteristics of tsunami are quite distinct from other coastal hazards, and cannot be inferred from the common knowledge or intuition. The primary reason for this

distinction is the unique timescale associated with the tsunami phenomena. Unlike typical wind-generated water waves with periods between 5 and 20 seconds, tsunamis can have wave periods ranging from a few minutes to over 1 hour (FEMA, 2005). This timescale is also important because of the potential for wave reflection, amplification, or resonance within coastal features. Table 2.1 demonstrated the comparisons among various coastal hazard phenomena (FEMA, 2008).

Table 2.1: Comparison of relative time and loading scales for various coastal hazard phenomena

Coastal Hazard Phenomena	Time Scale (Duration of Loading)	Loading scale (Height of water)	Typical Warning Time
Wind generated waves	Tens of seconds	1 to 2 meters typical	Days
Tsunami run-up	Tens of minutes to an hour	1 to 10 meters	Several minutes to hours
Hurricane storm surge	Several hours	1 to 10 meters	Several hours to few days
Earthquake shaking	Seconds	N/A	Seconds to none

There is significant uncertainty in the prediction of the hydrodynamic characteristics of the tsunamis because they are highly influenced by the tsunami waveform and the surrounding topography and bathymetry (FEMA, 2008). They are generally different from the ordinary ocean waves as in the case of ocean waves energy is limited to the surface only and can be dissipated at the time of breaking. However, in case of the tsunami, energy does not readily release rather it push up a large volume of water with greater wavelength (Figure 2.1).

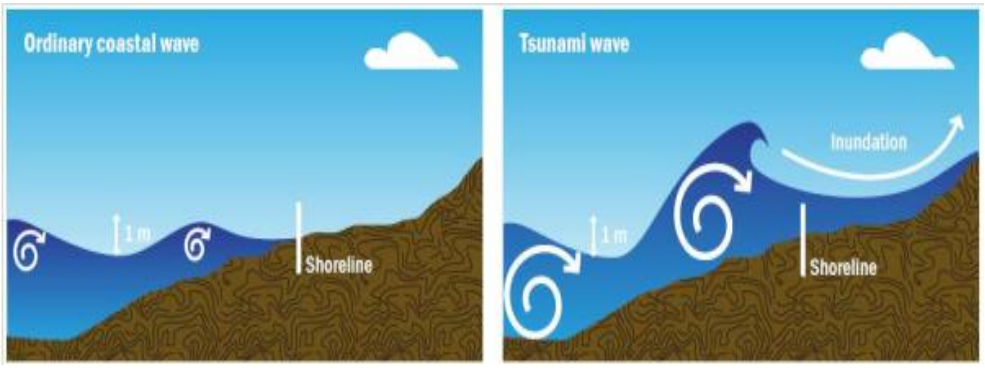

Figure 2.1: Difference between Tsunami and ordinary coastal waves

Tsunami energy propagation has robust directivity. The majority of its energy is emitted in a direction normal to the major axis of the tsunami source. The more elongated the tsunami source, the stronger the directivity; (Carrier & Yeh, 2005; Okal, 2003). Direction of approach can affect the tsunami characteristics at the shoreline, because of the sheltering or amplification effects of other land masses and offshore bathymetry (FEMA, 2005). Several factors are needed to understand the tsunami wave terminology viz., wavelength, wave height, period, run-up height etc. Wavelength is the distance between two sequential peaks. Wave period is the time required by the wave to pass two consecutive peaks. Tsunami wave height is the distance between the crest and the trough. Run-up height is the vertical measurement of height above sea level when the wave crest hit the onshore above the sea level.

2.3 Dam-Break Wave

Among the various ways in which a tsunami can propagate onshore, the common one is that of a rapidly advancing hydraulic bore which is formed by the breaking of the tsunami wave at the offshore reef or at the shoreline. This type of the wavefront is one of the most destructive forms of onshore propagation of tsunamis (Arnason et al., 2009).

A dam-break wave is one of the most studied examples of unsteady flow in the open channels. Catastrophes caused by the sudden failure of dams and the resulting wave have attracted physicists and scientists since the 19th century (Chanson, 2006). Shallow water equations, providing a simplified representation of the unsteady open channel flows, were derived by Saint-Venantin 1871, from depth integrated equations of momentum and mass conservation, based on the following assumptions:

1. One-dimensional flow,
2. Hydrostatic pressure,
3. Flow resistance being the same as a steady uniform flow for the same depth and velocity,
4. Negligible bed slope *(θ)*, i.e. $\sin\theta \approx \tan\theta \approx \theta$,
5. Constant water density, and
6. Boundaries of the channel are fixed.

It should also be noted that the sudden failure of a dam corresponds to a discontinuity in boundary conditions of the equations. However, despite all simplifying assumptions, taking discontinuous solutions into account is still a challenging feature of the equations. Moreover, analytical solutions exist for a very limited number of cases, due to the nonlinear characters of these equations. As a result, and with the advent of modern computers, numerical methods are widely utilized to solve the equations and capture the discontinuities of the solution. The method of characteristics is one of the earliest methods used to solve the Saint-Venant equations numerically and is based on a graphic interpretation of the problem. This process is efficient in giving a good understanding of the physical concept behind the problem. The method of characteristics is still studied because it is essential for defining boundary conditions for a few explicit schemes.

2.3.1 Experimental Work on Dam-Break Waves

Lauber and Hager (1998) performed a comprehensive literature review of the existing experimental studies on dam-break waves in horizontal and sloped channels. They summarized the existing understanding of the phenomena in horizontal channels where they demonstrated the flow mechanism of dam-break waves clearly with mentioning sufficient effect of tail water on the propagating waves. They presented that non-dimensional period of removal was smaller than $(g/h_0)^{1/2}t=2^{1/2}$, where g = gravitational acceleration, h_0 = reservoir depth and t = time. For a smooth prismatic and rectangular channel (h_0 > 300 mm), the flow should be governed by the Froude similarity law. They suggested that the boundary roughness had significant effects on the wavefronts for larger times.

Hence, Most of the studies have been focused on the commencement of the dam-break waves featured with positive wavefront. Maximum of the tests was performed in the horizontal flumes or flumes with small angle. Also, the test flumes were supposed to be as long as possible to approach the assumption of an infinitely long channel in the analytical solutions. Moreover, tests with dry or wet downstream and mobile or immobile beds have been performed to examine the effects of various parameters on the flow variables. Various researches had been performed on dam-break by many researchers (Bell et al., 1992; Briechle & Köngeter, 2002; Barr & Das, 1980; Dressler, 1954; Franco, 1996; Lauber & Hager, 1998; Leal, 1999; Leal et al., 2002; Miller & Hanif Chaudhry, 1989; Stansby et al., 1998; US Army Corps of Engineers, 1960 & 1961). Leal et al. (2006) conducted a comprehensive literature review of dam-break wave experiments in order to investigate the existing formulae and data sets on the dam-break wavefront velocity. Figure 2.2 showed a dimensionless representation of the data from several data sets: Bell et al.1992 (Bel); Briechle and Kotenger 2002 (Brl, Br2);

Franco, 1996 (Fr); Lauber and Hager 1998 (La); Leal 1999 (Lei); Leal et al.2002 (Lefbl) and Stansby et al. 1998 (Stl, St2). The results are presented in terms of the location ($X = L/h_0$) and time ($T = t\sqrt{g/h_0}$) where L = distance between the gate and the location of interest, t = measurement time after the gate opening, and h_0 = reservoir depth. Furthermore, Leal et al. (2006) developed a numerical model based on the shallow-water approach, assuming that the sediment transport was occurring dominantly in the form of contact-load and using recent developments in sheet flow studies. It was observed that the result from the numerical model provided the best description of the experimental data (Figure 2.2).

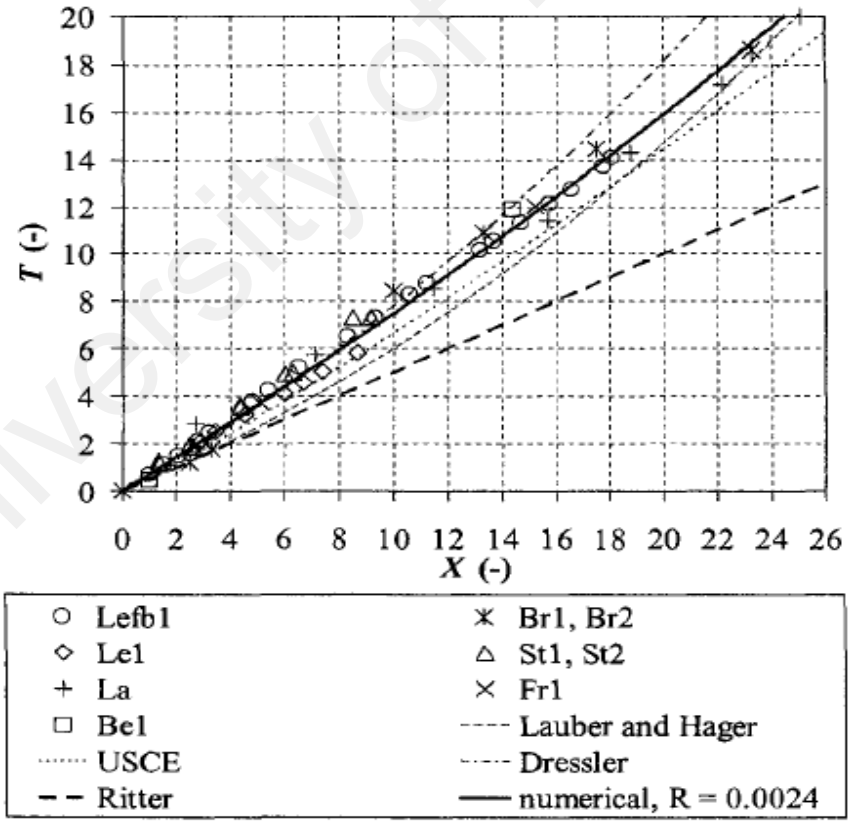

Figure 2.2: Wavefront locations in *(X, T)* space over dry fixed bed; comparison of experimental data sets (symbols) with proposed formulae (lines) (Leal et al., 2006).

2.3.2 Tsunami-Induced Hydraulic Bores

Tsunamis are long oceanic waves that are mainly caused by earthquake in the ocean floor. Near origin, waves maintain larger wavelength and smaller wave height. As they transmit towards the shore, their wavelength decreases, however, wave height and speed increase. During the transmission from the origin, they dissipate very little energy; as a consequence, reach the shore with nearly unchanged tremendous energy. As waves break offshore, they turn into hydraulic bore and engulf the near shore region. Tsunami waves may occur as non-breaking condition where the waves may break upon reaching the shore due to the continuous rise and fall of the sea level. The types of breaking of the waves are greatly induced by the initial waveform, the wavelength, the configuration of the coastline and the width of the ocean floor (Yeh, 2006). A collapsing breaker, occurring on a sloping beach, was shown in Figure 2.3.

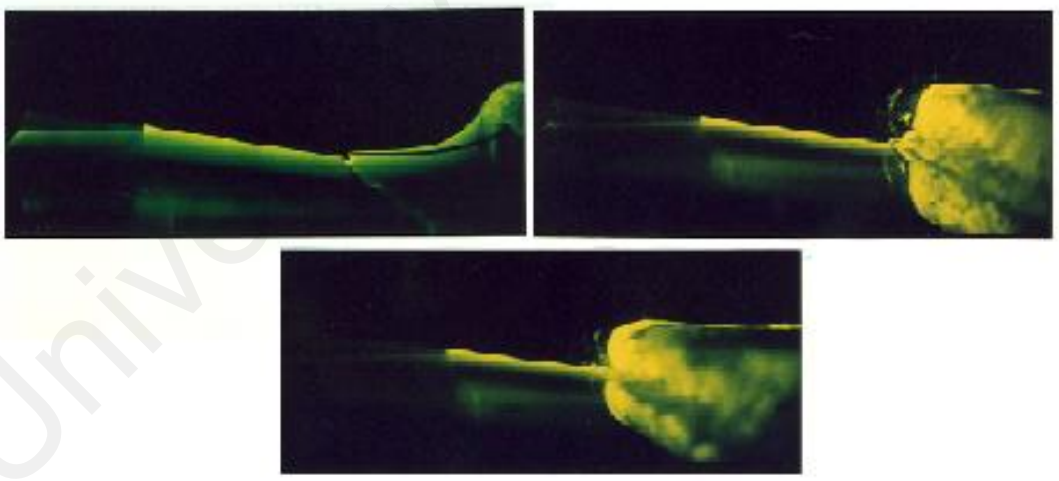

Figure 2.3: A collapsing breaker resulted from an undular bore (Yeh & Mok, 1990).

As the wavelength is more significant than the wave height for the tsunami waves, therefore, shallow water wave theory (i.e., depth-integrated equations of momentum and mass conservation with the assumption of hydrostatic pressure field) could be considered to evaluate the tsunami propagation. Nonetheless, this theory could well describe the characteristics and run-up of the non-breaking waves while the behaviour of the breaking waves showed some discrepancy with this theory. Features of tsunami waves were investigated by Yeh (1991) and Yeh et al. (1989) with two-dimensional dam-break flow. The flow was fully turbulent with high velocity and propagated with considerable oscillation. This phenomenon agreed well with Yeh and Mok (1990). Previous tsunami event witnessed the transmission of the broken waves as hydraulic bore (Cox & Mink, 1963; Palermo et al., 2009; St-Germain et al., 2013; Yeh, 1991). For example, a tsunami-induced hydraulic bore propagating onshore is clearly captured in Figure 2.4. The tsunami-induced bore shown in Figure 2.4 was a highly irregular and turbulent flow, similar in many respects to the flow generated by a dam-break on a dry horizontal bed.

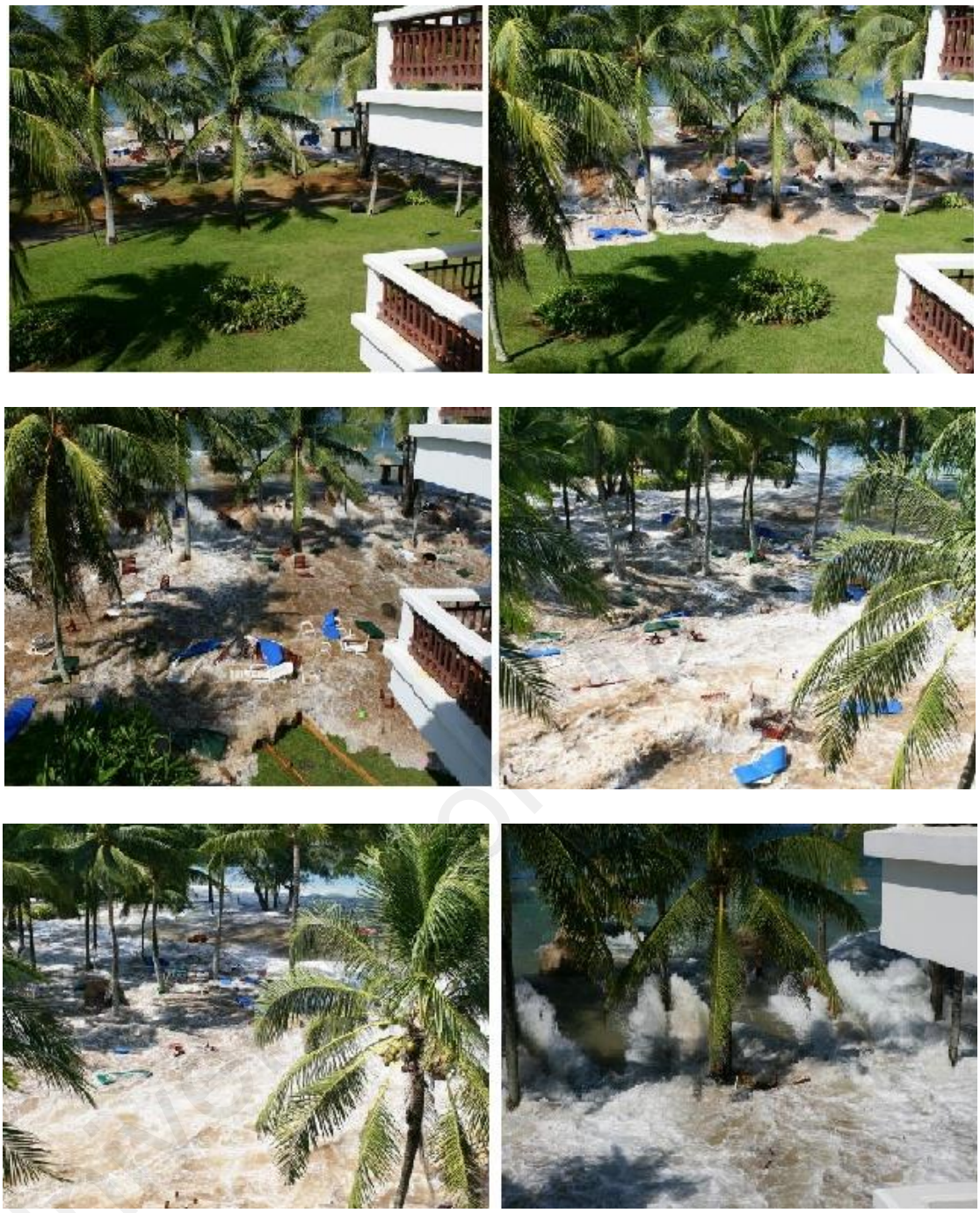

Figure 2.4: Advancing tsunami-induced bore at Phuket Island, Thailand (December 2004 Tsunami) (Pbase, 2007)

It may be assumed that, compared to non-breaking tsunami waves, tsunami-induced broken waves contain less destructive force. This assumption could be based upon the fact that the wave energy will be considerably reduced due to dissipation at breaking. However, the existing evidences from the past tsunamis had proven otherwise: the 1960

Chilean Tsunami caused severe destruction and killed 61 people, according to Cox & Mink, (1963). One hundred fatalities were reported after the 1983 Nihonkai-Chubu Tsunami, where waves carried 4-ton armour units up to 135 m onshore, (Yeh, 1991). As mentioned before, the most devastating effects were caused by the tsunami-induced bores occurring during the Indian Ocean Tsunami in 2004. Tsunami-induced bores in Northern Sumatra and parts of Thailand, such as Khao Lak caused tremendous damages.

2.4 Impacts of Tsunami on Coastal Structures

Post tsunami reconnaissance survey pointed out the violent nature of the tsunami waves by showing the tremendously impacted coastal infrastructures. Structures located near shore region were substantially affected by the tsunami forces. The terrific impacts of 2004 tsunami had raised awareness to the people who live in low-lying coastal area. Wave condition, absence of tsunami criteria in most of the building design, use of localized construction material, and ground condition play significant roles in the pave of the damage scenario. Different wave conditions prevail during the last few tsunami incidents resulting in the complication of making any new rule as to how tsunami impacts the coast and the infrastructures.

2.4.1 Bridge Vulnerabilities to Tsunami Hazards

Bridges are the important lifeline infrastructures to cover immediate rescue activities afterward any tsunami disastrous event. During reconstruction and rehabilitation period, bridges prove their upmost necessities not only for evacuating people but also for transferring first aid to the wounded people and for providing emergency relief to the affected areas. Hence, bridges should be designed with adequate capacity to withstand the tsunami hazards. Damages to bridges by tsunami fall into two categories. These

include damage to the substructure and damage to the superstructure. Bridge substructures are affected by the removal of sediment material from around the pier whereas superstructures are affected by the horizontal and uplift forces resulting in displacement or washing out of the deck or total collapse of the structures.

2.4.2 Field Investigations on Impacts of Tsunami on the Bridges

Dreadful impacts of the tsunami on the coastal infrastructure, communities and economies alert the people about the devastation level. A number of surveys were carried out after each tsunami event to find out the damage scale. Approaching waves take different shapes near coastline forming different types of forces that could attack the coastal infrastructures. Tsunami in 2004 hit north western area of Sumatra Island so tremendously that diminished many houses, bridges and many other coastal structures. According to Unjoh (2007), 81 bridges out of 168, occupying about 250 km road section on the north western coast of Sumatra Island were badly affected. The damage scenario for the bridges during Tohoku tsunami in 2011 was more sever whereas at least 200 bridges in East Japan suffered from serious losses (Kosa, 2012). Kasano et al. (2012) found an interesting result while surveying the damaged bridges in Tohoku area. Concrete bridges remained intact while steel bridges were more likely to be washed away exploring the idea that bridges with substantial weight can defend tsunami forces successfully (Figure 2.5). Another important finding by Kasano et al. (2012) was that bridge with low height superstructure could survive better than those of superstructures made with higher piers while subjected to tsunami waves. Figure 2.6 (a) showed Furukawa Bridge where superstructure was set only about 1 m high from the water level and this bridge survived through the attack of tsunami waves even though it was located just near the seaside. On the other hand, heavy concrete superstructures on high piers were removed by the tsunami waves as shown in Figure 2.6 (b). Another finding of

Iemura et al. (2007) was that a bridge deck located as high as tsunami height was not only affected by the wave force but also by the impact forces of the flowing debris.

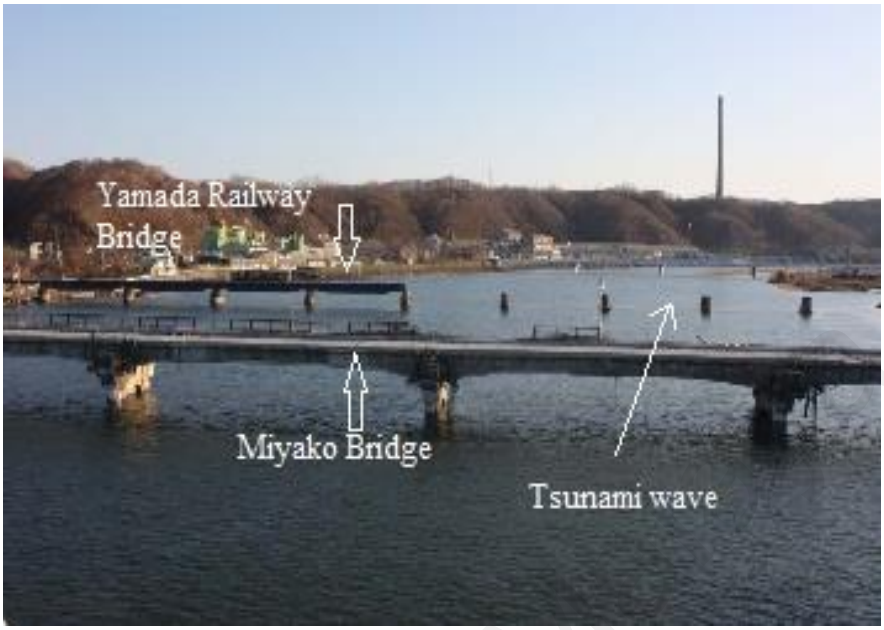

Figure 2.5: Steel Girder Bridge was washed away due to tsunami where Reinforced Concrete Girder Bridge was survived.

Figure 2.6: (a) Bridge with lower height survived from the attack of tsunami; (b) Bridge with higher pier washed away due to the tsunami waves

Evidences on the structural failure of the bridges in Sumatra, Sri Lanka, India and Thailand during the 2004 tsunami event were demonstrated by many researchers. (

Antonios, & Pomonis, 2006; Ballantyne, 2006; H. Iemura et al., 2005; Jain, 2011; Kusakabe et al., 2005; Lukkunaprasit & Ruangrassamee, 2008; Maheshwari et al., 2006; Saatcioglu et al., 2005; Scawthorn et al., 2006; Sheth et al., 2006; Tobita et al., 2006; Unjoh, 2005; Yim, 2005). Damages and failures of these bridges were initiated by either total or partial wash away of deck or excessive scouring of the foundation material. The breakdown of bridges retards the entire transportation system and hampers the rescue and emergency relief efforts.

2.4.3 Tsunami Effects on the Building Structures

Damage studies from the historical tsunami events have provided information on the response of the built environment to the devastating tsunamis and the coastal flooding. Low-height light-framed building structures are the most vulnerable element of the tsunami attack. However, mid to high-rise engineered structures were well managed to survive with little damage during the last two giant tsunami event. The damage level was also greatly affected by the construction type and the tsunami run-up height (Yeh et al., 1995). In contrast to many failures reported as a result of past tsunamis, many structures have been observed to survive tsunami inundation. Figures 2.7, 2.8 and 2.9 showed some of the damaged building constructions.

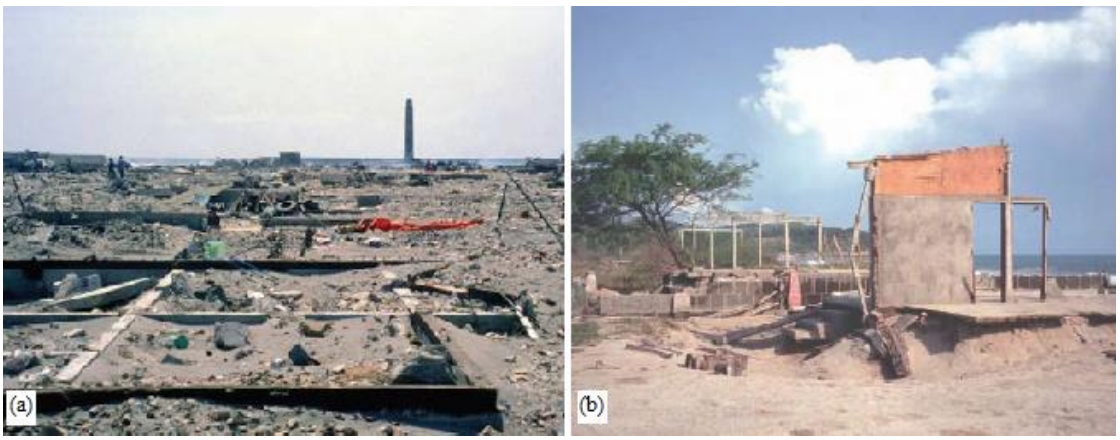

Figure 2.7: (a) Total destruction of a group of wood-frame houses in Aonae Village, Japan (1993 Okushiri Tsunami) (FEMA, 2008); (b) Beach houses with varying levels of damage in El Popoyo, Nicaragua (1992 Nicaragua Tsunami) (FEMA, 2008).

Figure 2.8: (a) Damaged masonry beach house in Devanaanpattinam, India (2004 Indian Ocean Tsunami) (FEMA, 2008); (b) Reinforced concrete building frame structure with shear wall blow-outs (Chock et al., 2011).

Figure 2.9: (a) Examples of reinforced concrete structures that survived the 1993 Okushiri Tsunami: vista house at Cape Inaho (FEMA, 2008); (b) Well-constructed building that survived the earthquake and tsunami.

2.5 Tsunami-Induced Forces

While tsunami waves reach the coast they contained tremendous forces with them. The waves inundate the whole area and affect the structures with terrific forces in their path. Flow depth, speed and direction highly influence the magnitude of these forces. The forces exerted by the tsunami waves are categorized into several types. They are (1) Hydrostatic force, (2) Hydrodynamic (drag) force, (3) Buoyant force, (4) Surge force and (5) Debris impact force. Brief description of these forces is presented below.

2.5.1 Hydrostatic Force

Hydrostatic force is produced by the static or slowly flowing water acting perpendicular to planar surfaces. According to CCH (CCH, 2000) and FEMA 55 (FEMA, 2005), the hydrostatic force per unit width (F_{HS}) is calculated by the Equation 2.1. In this equation, CCH includes velocity head whereas it was assumed to be negligible by FEMA 55.

$$F_{HS} = \frac{1}{2}\rho g\left(d_s + \frac{u^2}{2g}\right)^2 \quad (2.1)$$

Where ρ is the density of water, g is the gravitational acceleration, d_s is the water depth and u is the velocity against a wall. The point of application of the resultant force is located at one third from the base of the triangular hydrostatic pressure distribution. In the case of a broken tsunami wave, the hydrostatic force is significantly smaller than the drag and surge forces. On the other hand, hydrostatic forces are significant when tsunami propagates as rapidly rising tide (Dames & Moore, 1980).

2.5.2 Buoyant Force

During a tsunami, some parts of the structures are submerged by the flowing water and face vertical force at the centre of mass of the submerged part. This force is termed as the buoyant force that is equal to the weight of the volume of water displaced by the submerged part. This force can be calculated using Equation 2.2. Buoyant force is evident while tsunami waves proceed along any coastal area as flooding (Nistor et al., 2006; Saatcioglu et al., 2006a, 2006b). The effect of buoyant force is mostly noticeable in floor slabs of any building.

$$F_B = \rho g V \quad (2.2)$$

Where *V is* the volume of water displaced by the submerged structure.

2.5.3 Hydrodynamic (Drag) Force

As tsunami waves flow inland with moderate to high speed, they try to drag everything in their path. Therefore, structures exposed to their path are subjected to considerable hydrodynamic forces. The following equation (Equation 2.3) is used to estimate the hydrodynamic forces on the structures. Different codes compute different

hydrodynamic force values due to different drag coefficient values (C_D). FEMA 55 (FEMA, 2005) and CCH (CCH, 2000) recommended C_D values 1.0 and 1.2, respectively for circular piles, whereas, for rectangular piles, both FEMA 55 and CCH suggested 2.0 value as drag coefficient.

$$F_D = \frac{\rho C_D A u^2}{2} \quad (2.3)$$

Where F_D is the total drag force acting in the direction of flow, A is the projected area of the body normal to the flow direction and u is the flow velocity. The resultant forces will act on the centroid of the projected area considering the flow to be uniform. From this equation, it is found that the hydrodynamic force is directly proportional to the flow speed.

2.5.4 Surge Force

The surge force is caused due to the rapid advancement of the leading edge of the tsunami waves on any coastal structure. There was significant uncertainty in the calculation of the surge forces on a structure due to limited experimental program on proceeding of the tsunami on shore. Therefore, it becomes more challenging and difficult job to estimate accurately the initial impact force on the structures. CCH proposed the following equation (Equation 2.4) to calculate surge forces (Dames & Moore, 1980).

$$F_S = 4.5\,\rho g a^2 \quad (2.4)$$

Where F_S is the total surge force per unit width of the wall and a is the wave height. The point of application of the resultant surge force is located at a distance z above the base of the wall. The surge force could be estimated from the summation of both hydrostatic and hydrodynamic forces which was presented in Equation 2.5 (Palermo et al., 2009)

$$F_S = \frac{1}{2}\rho g b d_s^2 + \frac{1}{2} C_D \rho A u^2 \quad (2.5)$$

Where C_D is drag coefficient; u is the velocity, A is projected area of interest.

2.5.5 Debris Impact Force

As tsunami wave advances inland with high speed, it could carry different types of debris on its path. Such debris (floating automobiles, floating pieces of buildings, drift wood, as well as boats and ships) could pose additional forces on the structures which may lead to further severe damage or collapse of the structures (Saatcioglu et al., 2006a, 2006b). This force is termed as debris impact force. Equation 2.6 is recommended by both FEMA 55 (FEMA, 2005) and CCH (CCH, 2000) for the calculation of debris impact force.

$$F_i = m_b \frac{d\, u_b}{dt} = m \frac{u_i}{\Delta t} \tag{2.6}$$

Where F_i is the impact force, m is the mass of the body impacting the structure, u_b is the velocity of the impacting body (assumed equal to the flow velocity), u_i is the approach velocity of the impacting body (assumed equal to the flow velocity) and Δt is the impact duration taken equal to the time between the initial contact of the floating body with the building and the instant of maximum impact force.

2.6 Tsunami Wave Velocity

The estimation of tsunami wave velocity is a very crucial parameter as it could influence the exerted forces on the structures. Hydrodynamic forces, as well as debris impact forces are highly dependable on the wave velocity. Therefore, any uncertainty related to the estimation of wave velocity may lead to a larger impact on the amount of the resultant forces. The direction of the tsunami wave plays significant role in the velocity estimation. Most of the current design codes exclude the direction of the velocity as well as the effect of run-up and back wash. It is assumed that the wave with

high velocity hit the structures at a normal angle. Although there are several formulas for the calculation of tsunami wave velocity, the most general form is presented in Equation 2.7.

$$u = C\sqrt{gd_s} \tag{2.7}$$

Where u is the wave velocity, d_s is the inundation depth and C is a constant coefficient. This coefficient could be used to determine Froude number (F_r). Different researchers (Bryant, 2001; Camfield, 1980; CCH, 2000; Dames & Moore, 1980; Iizuka & Matsutom, 2000; Kirkgoz, 1983; Murty, 1977) presented different formulas based on different coefficient values for the calculation of wave velocity (Figure 2.10). The coefficient value significantly depends on the slope and the bed configuration of the inland. Velocities calculated using CCH (CCH, 2000) and FEMA 55 represent a lower and upper boundary, respectively.

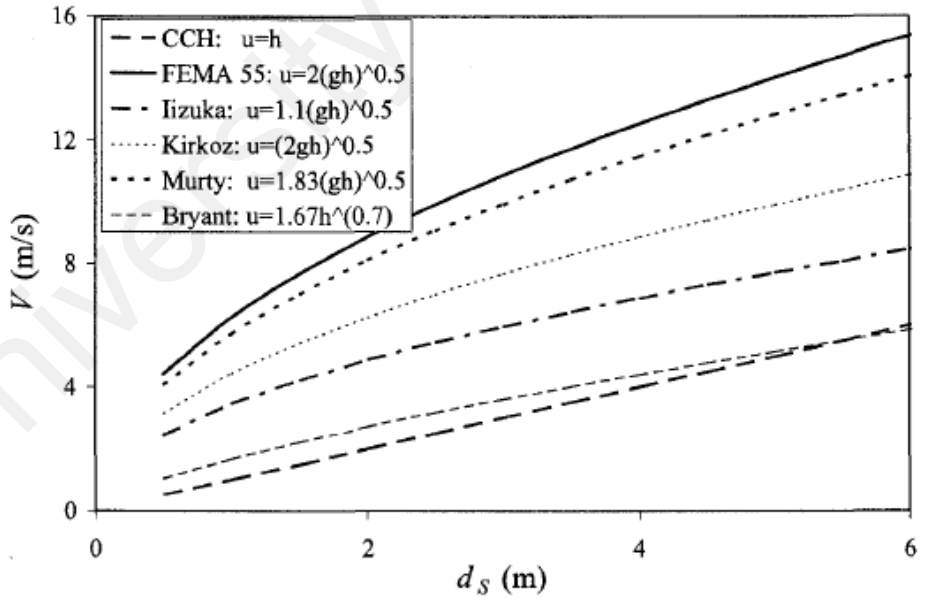

Figure 2.10: Variation of tsunami velocity with inundation depth using different formula (Nouri et al., 2007)

According to Triatmadja & Nurhasanah (2012), the wave velocity generated from dam-break gate could be calculated by the Equation 2.8

$$u = C\sqrt{gh_0} \tag{2.8}$$

Where, h_0 is the reservoir depth, C is the velocity coefficient which depends on the bed friction (Streeter and Wylie, 1975). Chanson (2005) proposed analytical solution (Equation 2.9) to calculate the velocity in the non-zero downstream condition with horizontal bed surface.

$$\sqrt{\frac{h_0}{h_3}} = \frac{1}{2}\frac{u}{\sqrt{gh_3}}\left(1 - \frac{1}{X}\right) + \sqrt{X} \tag{2.9}$$

$$\text{Where } X = \frac{1}{2}\left(\sqrt{1 + 8\,\frac{u^2}{gh_3}} - 1\right) \tag{2.10}$$

and h_3 is the initial downstream depth, with

$$X = \frac{d_s}{h_3} \tag{2.11}$$

According to Chanson (2005, 2006), the wave velocity in a flat dry bed depends on friction coefficient (f) and time (t) and could be formulated by Equation 2.12

$$\frac{8}{3}\frac{1}{f}\frac{\left(1-\frac{1}{2}\frac{u}{\sqrt{gh_3}}\right)^3}{\frac{u^2}{gh_0}} = \sqrt{\frac{g}{h_0}}t \tag{2.12}$$

2.7 Hydraulic Experimental Study on the Vertical Wall

Nevertheless, a number of researches have been done on the formation and propagation of tsunami as well as the interaction between the tsunami and the land structures, still there are rooms for improving the tsunami researches. Tsunami loading impacts on the onshore structures have been extensively studied by many researchers (Arikawa, 2008; Asakura et al., 2002; Chakraborty & Choudhury, 2014; Dias et al., 2005; Ghobarah et al., 2006; Hofland et al., 2011; Nistor et al., 2011; I. Nistor et al., 2009; Nouri et al., 2010; Palermo et al., 2009; Peregrine, 2003; Rahman et al., 2014; Ramsden, 1996;

Thusyanthan & Madabhushi, 2008; Yeh, 2006). Snodgrass et al. (1951) identified that tsunami broken waves induced larger hydrodynamic forces as compared to the waves that broke at the test location. Cumberbatch (1960) presented the impact forces on a vertical wall using Equation 2.13 in which gravity was not included and the dynamics of the impacts was assumed to be occurred before the gravity affected the flow.

$$F = C_F \rho b d_s u^2 \quad (2.13)$$

Where, C_F is the coefficient of forces, ρ is the density of water, b is the width of the wall, d_s is the depth of water and u is the velocity of flow.

Fukui et al. (1963) examined the impacts of the reflected bore by measuring the pressure on a vertical wall. They considered variable bore heights impacting the walls placed at the sloping bed. Cross (1967) proposed formula for small scale tsunami wave pressure considering hydraulic term as well as momentum term. More detailed experimentations on the relationship between the bore and the bed slope with a vertical wall were investigated by Ramsden & Raichlen (1990) and Ramsden (1993, 1996). Ramsden (1996) considered translatory wave impacts on the vertical wall rather than the breaking waves. The measured results could be used to resolve sliding and overturning failures but failed to predict punching type's failure. However, Ramsden (1996) formula could be easily applied to engineering design as it considered bore height and water depth that are easily available from tsunami hazard maps. Moreover, Ramsden (1996) proved that the impact pressure distribution was totally non-hydrostatic. Hence, shallow water equation was not properly applicable for the estimation of the impact pressure and forces on the vertical wall. The experiment also demonstrated that the transition from undular to turbulent bores led to a discontinuous increase in water surface slope, followed by an increase in the measured run-up,

pressure head, and exerted forces and moments. Figure 2.11 showed the difference between a strong turbulent bore (on a wet bed) and a dry-bed surge.

Limited researches were performed on the vertical distribution of force and pressure by the impact of hydraulic bore. Therefore, there is still room for improving the understanding of the bore-structure interaction through more physical experiments. Gomez-Gesteira & Dalrymple (2004) studied the impacts of dam-break wave on a rectangular structure with a dry bed as well as with wet bed. Figure 2.12 showed the vertical distribution of the forces on the rectangular structure. The distribution was given only for one instant and the location of this instant on the total force time-history had not been specified (presumably at the maximum force). This figure showed that in the case of a dry downstream, more than 95 % of the force was exerted on the lower part of the upstream face (up to 0.1 m above the bottom), whereas most of the force was exerted between 0.1 and 0.2 m above the base for the case of a wet bed.

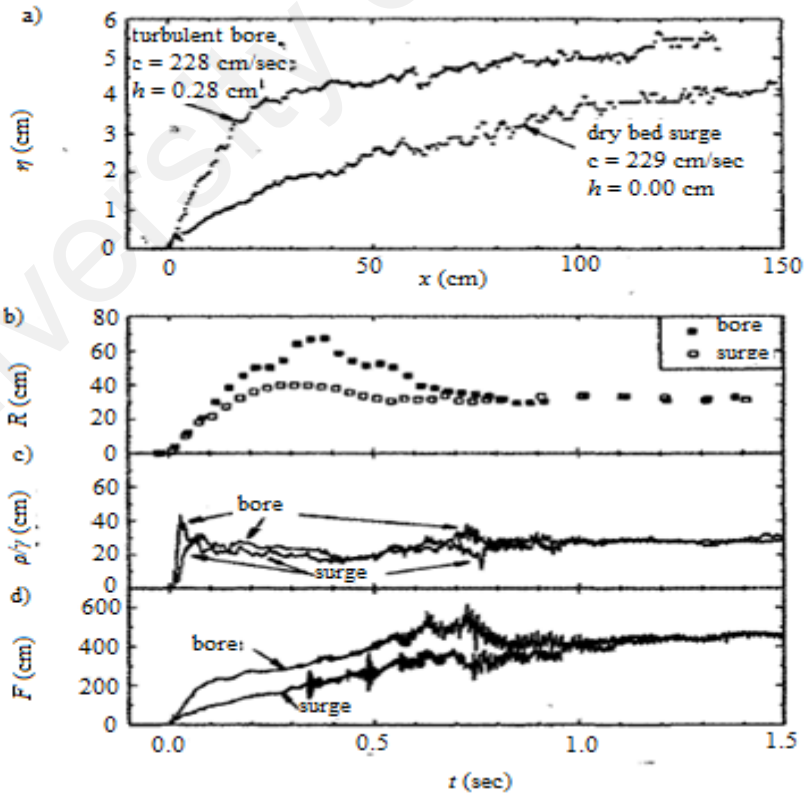

Figure 2.11: Comparison of the experimental (a) wave profile; (b) run-up; (c) pressure head; and (d) force due to a strong turbulent bore and a dry bed surge (Ramsden, 1993).

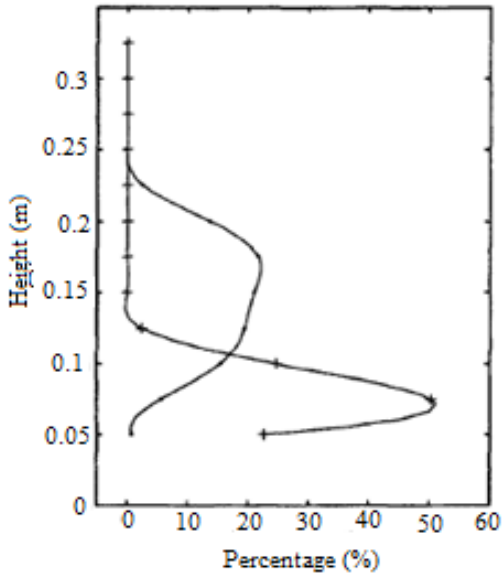

Figure 2.12: Vertical distribution of force exerted on the upstream face of a rectangular structure

Arnason (2005) studied the interaction between different size land structures and hydraulic bore on the dry bed. It was observed that initial impact forces on the square columns were more compared to the hydrodynamic forces for smaller bore height (Figure 2.13). Conversely, this was not evident for the case of larger bore height. For the case with the circular structure, hydrodynamic forces were larger than the initial impact forces (Figure 2.14). Fujima et al. (2009) included both hydrostatic and inertia term in estimating the tsunami forces taking into account the distance of structures from the shore and maximum inundation depth. Thusyanthan and Madabhushi (2008) investigated the impact load on special types of coastal houses. Arikwa (2008) also showed the effects of impact loading on the vertical wall by large scale laboratory experiments. Though most of the design manuals for tsunami risk regions consider hydrostatic formulas, (e.g., City of Honolulu 2003; International Conference of Building Officials 1997; International Code Council 2006; ASCE 2006; FEMA, 2008); there is yet scopes to improve the tsunami formulas for overland flow.

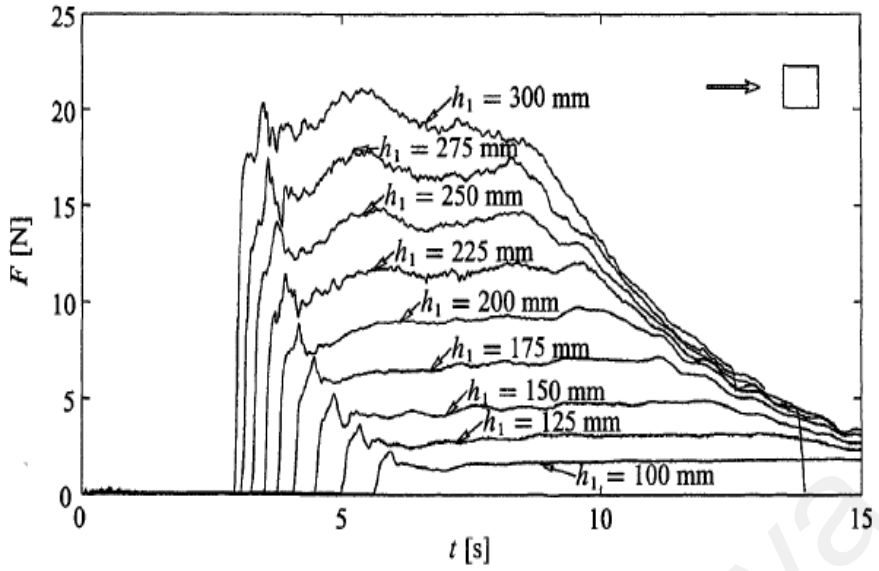

Figure 2.13: Force time history of a square structure with various bore heights.

(Arnason, 2005)

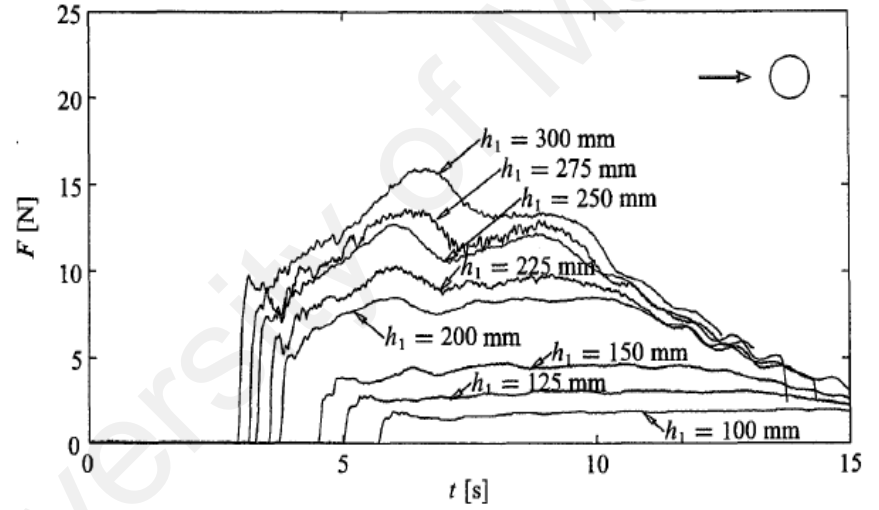

Figure 2.14: Force time history of a circular structure with different bore heights.

(Arnason, 2005).

2.8 Hydraulic Experimental Study on the Bridge Superstructures

A number of researches were performed to investigate the bridge performance during tsunami and to estimate tsunami induced forces on the bridges through physical simulations (Akiyama et al., 2013; Ballantyne, 2006; Lukkunaprasit & Lau, 2011; Maheshwari et al., 2006; Nakao et al., 2009; Scawthorn et al., 2006; Sheth et al., 2006; Shoji et al., 2011). Impacts of tsunami forces on single spanned bridge deck were

evaluated by Kataoka et al. (2006), Shoji & Mori (2006) and Iemura et al. (2007). Iemura et al. (2007) considered I-girder bridge that was placed on the dry bed and identified that, the maximum forces and maximum flow velocity were found to occur practically at the same time. Similar experiments were conducted by Shoji & Mori (2006) and Kataoka et al. (2006), considering box type bridge decks which were placed on a wet bed at certain height of still-water. Sugimoto & Unjoh (2008) proposed the relation between the tsunami wave height and the speed. Shoji et al. (2009) assessed the influence of changes of deck position on the tsunami forces applying similarity law. Nii et al. (2009) compared the results of the horizontal pressure on a water break with Goda (1974) formula. Kataoka et al. (2006) verified Goda's formula by estimating the tsunami forces that affected bridge structures. Nakao et al. (2009) studied results achieved from both laboratory experiments and MPS (Moving Particle Semi-implicit) numerical model and finally demonstrated that the tsunami wave could form flow vortex on a bridge deck. Araki & Deguchi (2009) measured tsunami fluid forces and pressure on the girder bridges used over small rivers and found that wave pressure increased with increase in tsunami height above the bridge model. They also revealed that breaking waves imposed more fluid forces on the bridge girders than those of the post breaking waves. The stability of the bridge girders was inspected using the measured tsunami fluid force. Although the scale effect on the fluid force was not taken into account in the analysis, the critical force for the stability was estimated as the strength of the bolts used in the shoes against shear stress. Araki et al. (2008) demonstrated that the horizontal wave force varies with movement of the bridge deck against tsunami height. Relationship between tsunami inundation height and speed and relationship between tsunami wave force and velocity were established by Sugimoto & Unjoh (2008). According to Pradono et al. (2008), densely populated flexible mangroves were effective in reducing tsunami force as long as the mangrove height was

more than the tsunami flow height. They ran the same test considering breakwaters in front of the bridge model. They found that breakwater was significantly effective in reducing forces on the model only if tsunami depth was lower than the height of the breakwater. Lukkunaprasit and Lau (2011) identified the impacts of hydrodynamic load on piers with the presence of deck through simulation of pier deck combination (Figure 2.15). They revealed that the bridge deck could obstruct the free flowing and topping over the wave before impinging the pier and thus fluid was captured in front of the piers creating larger pressure on them. Araki et al. (2010) investigated the attributes of the tsunami fluid force acting on the bridge girder and declared that wave pressure on bridge girder was greatly influenced by the tsunami height. Thus, considering shocking powers of tsunami, it is evident that damages of the bridges by tsunami forces should be encountered in the design provision and effective remedial measures should be developed to withstand against these devastating forces.

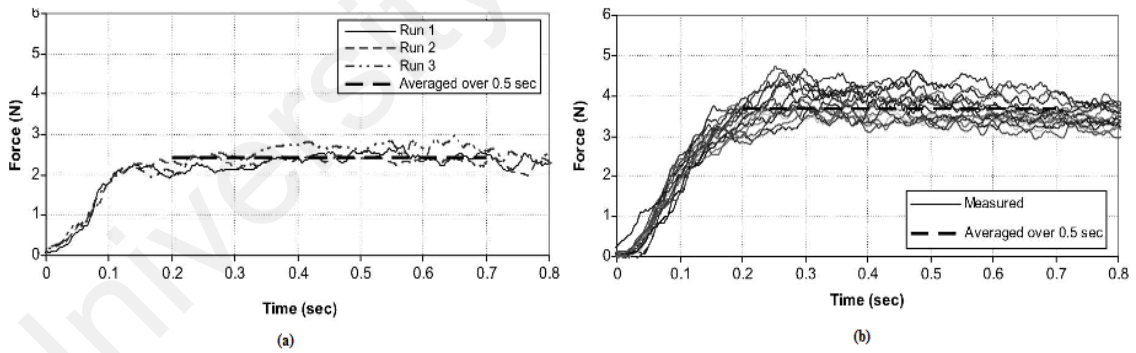

Figure 2.15: Total force time histories on: (a) Stand-alone piers model; (b) The complete pier-deck model (Lukkunaprasit & Lau, 2011)

2.9 Tsunami in Malaysia

Malaysia is surrounded by two of the most seismically active plate boundaries namely the plate boundary between the India Plate which is part of the huge Indian-Australian Plate that underlies the Indian Ocean and the Bay of Bengal and the Burma Plate that is part of the Eurasian Plate on the west at the Sunda Trench off Sumatra and the plate boundary between Eurasian and Philippines Plates on the east (Figure 2.16). Large earthquakes originating from in and around these boundaries have resulted in tremors being felt in Malaysia. Therefore, Malaysia will be expected to be affected by high earthquake arising from the Sumatra and Andaman fault. Such great earthquake may impose larger possibilities of tsunami in the coastal region. During the 2004 Indian Ocean tsunami, several areas including Penang Island, Langkawi Island and Kedah, were badly affected by the tsunami waves. Figure 2.17 showed the most affected areas in Malaysia during 2004 tsunami. The surveyed tsunami run-up heights along the beaches in Penang vary between 2.3 m and 4.0 m while those in Langkawi were between 2.2 m and 3.7 m. For the state of Kedah excluding Langkawi, the run-up heights were observed to vary between 0.38 m and 3.8 m exhibiting significant scattering. All these incidental information reveal the necessity of introducing detailed study on tsunami waves on a regional basis for the accurate prediction of different aspects of tsunami along the coastal belts. In Malaysia, structural engineers thus have begun to consider some seismic design considerations ever since tremor effects were felt on the local bridge structures.

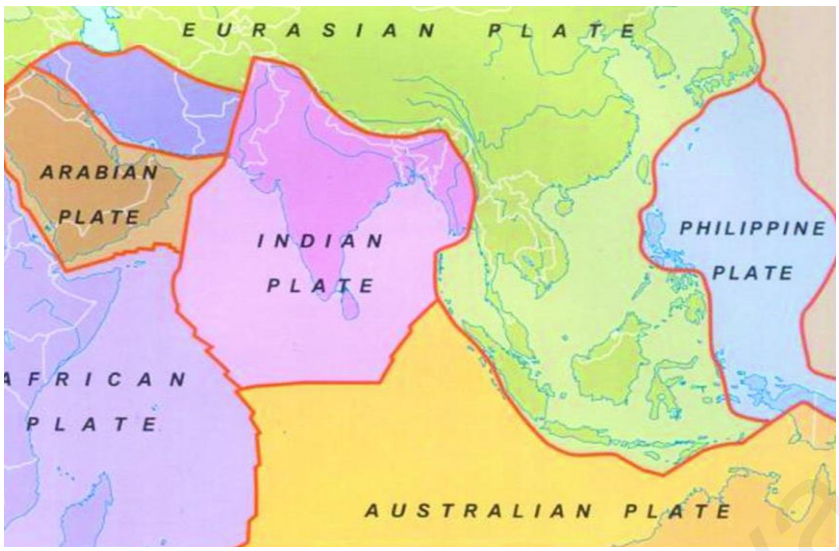

Figure 2.16: Plate boundaries

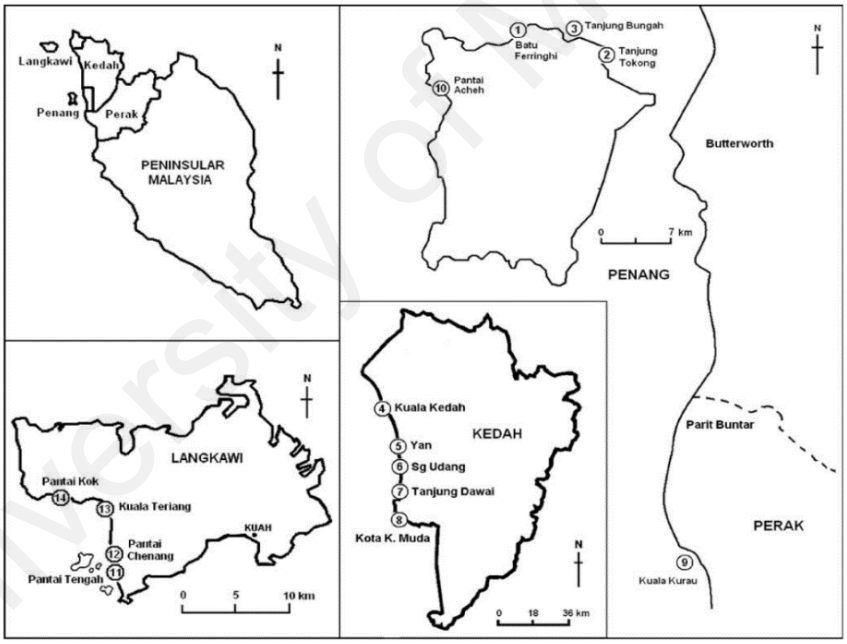

Figure 2.17: Impacted areas in peninsular Malaysia during 2004 tsunami

2.10 Conclusion

Tsunami is a natural complex phenomenon. Due to the adverse effects, tsunami has originated hazard prevention studies focusing on the behavior of the tsunamis both along the coastal line and the seaward. The effects of the tsunami on the coastal

structures are experimentally evaluated in a number of studies. The present study aims to focus on the damage mechanism of the tsunami wave loading. Therefore, any technique that could be introduced in mitigating the tsunami impacts will also be suggested. In the future, this type of study will be more useful on the clear understanding of the damage pattern of the coastal structures by the tsunami waves that might be a threat to structural stability of any coastal structures (FEMA, 2008).

CHAPTER 3

METHODOLOGY

3.1 Introduction

In this chapter, the experimental facilities, the preparations and making of the model structures, the measurement of the variables and the data recording systems have been summarized. All of the experiments were conducted in the Hydrology and Hydraulics laboratory at the University of Gadjah Mada, Indonesia. Previous tsunami incident disclosed that, in most of the cases tsunami waves break adjacent the shoreline where their height becomes almost equal to the local water depth. In that case, the waves travel toward the shore as a hydraulic bore with a sharp turbulent leading edge. Video footages taken during 2004 tsunami agreed well with these phenomena, where tsunami waves took the form of hydraulic bores near the shore. The waves maintained substantially high velocity while propagating the onshore (Nouri et al., 2010). Studies showed that waves, produced by the dam-break mechanisms could exhibit the characteristics of tsunami bore as well. Although a number of researches were performed on dam-break waves, more extensive laboratory experiments are required to explore the clear understanding of the analogous between a tsunami induced bore and a dam-break wave (Chanson, 2006). In this present study, complex interaction between the impacted structures and the tsunami waves was described where waves were generated through the dam-break mechanism.

3.2 Experimental Set up

3.2.1 Facilities

Physical experiments were conducted in a wave flume of 17.5 m long, 0.60 m wide and 0.45 m high. The flume was divided into two parts with the upstream section served as a reservoir for generating tsunami, while the downstream section was used to simulate the tsunami propagation along the flume. The reservoir (approximately 6.25 meters long) could hold reasonably large volume of water behind the gate. The maximum depth of water inside the reservoir was about 0.43 m from the bottom. The gate that separated the flume was equipped with quick release mechanism. The experimental set up in this research was similar that was used by Triatmadja and Nurhasanah (2012) and Arnason et al. (2009). Figures 3.1 (a, b) showed schematic illustrations of the experimental setup and Figure 3.2 showed the photograph of the flume.

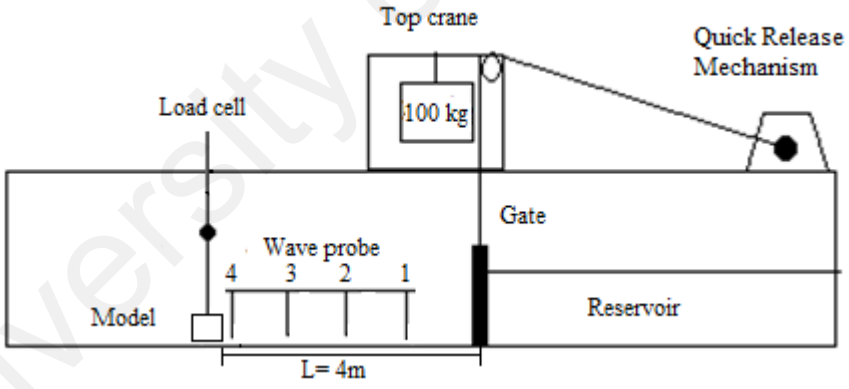

Figure 3.1: (a) Experimental set up (Elevation View)

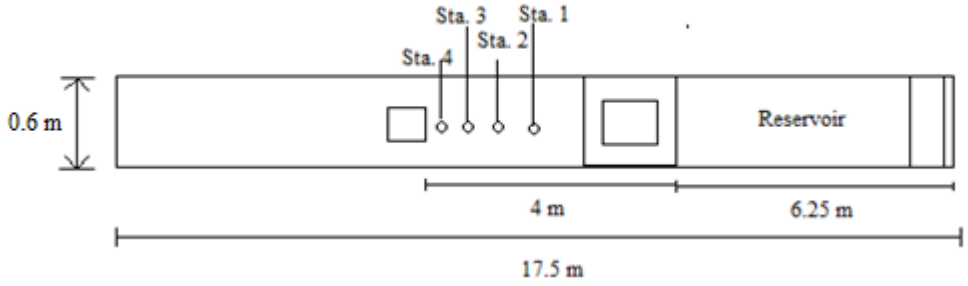

Figure 3.1: (b) Experimental set up (Plan View)

Figure 3.2: Photograph of the flume

The bottom of the flume was made of stainless steel plates. Thus, the bed friction was considered small. Sidewalls of the flume were made of glasses along both sides of its full length in order to facilitate the visual observations. A wooden part with a length of 5 m was placed downstream from the gate. During the simulation, models were placed over this wooden part at a distance 4 m from of the dam-break gate so that the flows around the model structures could be measured optically from the underneath. According to Wilkinson (2005), during 2004 tsunami, waves got broken prior reaching the shoreline, where each lower height wave was followed by the subsequent high waves. Therefore, the coastal area was inundated initially before coming of the main tsunami wavefront. In this study, a 0. 5 cm downstream water depth was considered in order to simulate such preliminary flood incident.

A simple yet reliable quick-release mechanism was used for the rapid opening of the gate. A 100-kg weight and a winch with strings were connected to the gate. The weight was released and the gate was lifted up instantaneously by pulling down a handle

connected to the weight. Within a very short period viz. 0.2 sec to 0.3 sec or depending on the reservoir depths, the gate was completely opened. Thus, the abrupt opening of the gate produced dam-break waves that propagated downstream like the tsunami wavefronts. Figure 3.3 showed the dam-break mechanism for simulating the tsunami waves. The speed of the gate opening mechanism resembled Arnason et al. (2009) experimental procedure. Rubber gaskets were installed to minimize the leakages when the gate was closed. The flume was also equipped with a pump to fill the reservoir and an outlet to drain the downstream part of the flume after each simulation. Figure 3.4 showed the preparation of the flume and the gate.

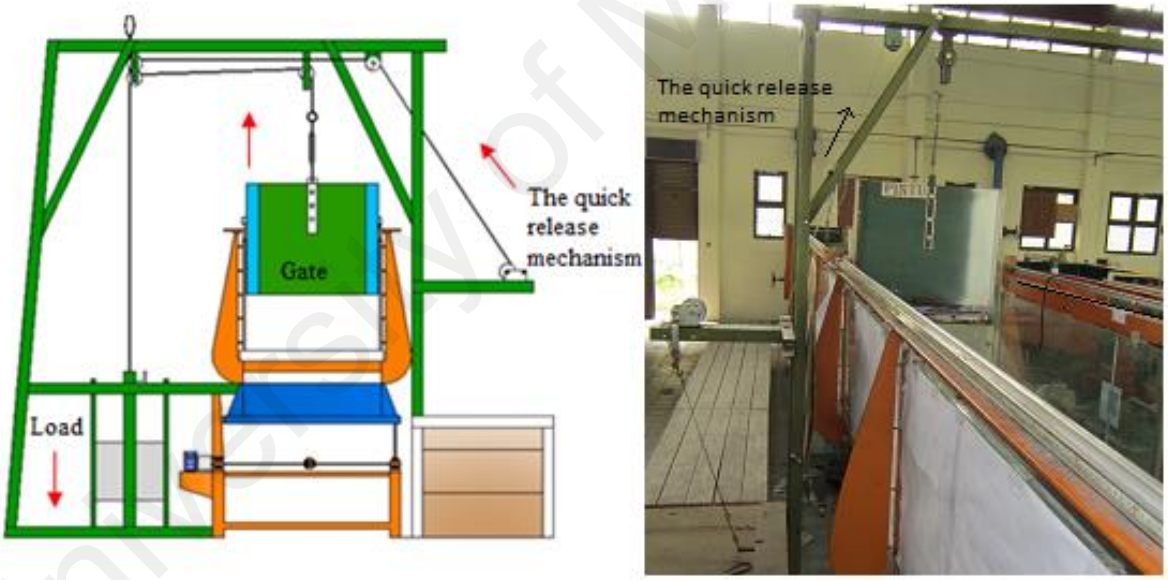

Figure 3.3: Dam-break mechanism

Figure 3.4: The high discharge flume: (a) Preparation of the flume and the gate; (b) The flume and the gate in operation.

A wooden frame was installed on the top of the flume across the longitudinal axis of the flume. A larger size vertical steel rod with a diameter of 2.54 cm was attached to this frame. All the models were fixed with this vertical rod. The steel rod was stiff enough due to its size. Therefore, it did not affect the recorded forces. There was a space of about 5 mm between the model and the bed to avoid any types of contact between them. The rod could swing freely on a hinge located at a distance l_a from the center of the model. A small pin was connected to the top of the rod that pressed a capacitive load cell when the tsunami hit the model. Thus, the forces were recorded in the load cell. Recorded values were adjusted by the load cell calibration factor and the handling factor in order to get the exact forces. The distance between the hinge and the centre point of the load cell was denoted by l_b. Loadstar Sensors DQ-4000 4-Channel Frequency to USB module was used along with the load cells to convert the outputs from the load cells into a PC friendly USB digital output. Figure 3.5 (a) showed the arrangement of the model structure connected to the load cell, while the data acquisition

system was shown in Figure 3.5 (b). Water that was splashing over the model structures produced some additional forces on the rod. However, after experiments it was found that this rod assigned only 2~3 % of forces on the model structures and could be assumed to be insignificant.

With the above arrangements of the reservoir and the quick gate opening system, a dam-break wave might be generated that could imitate a tsunami surge. This type of action was carried out by opening the gate vertically. In order to measure the flow velocity and the water levels at various locations throughout the experiment, a series of wave probes were installed at the selected stations (Sta) (Figure 3.6). The distance between the model and the nearby wave gauge was 0.15 m and the subsequent distances among the wave gauges were about 0.95 m. The wave gauge at station 1 was 1 meter distance from the gate (Figure 3.1). Each wave probe consisted of a wire (approximately 0.8 m long) and a head containing electronic components connected to the data acquisition system. The accuracy of the wave probes was of the order of millimeters. The wave probes were attached with a wooden frame that was installed inside the flume. The installations of the wave probes were prepared in such a way that they remained approximately 1 cm above the bottom of the flume. Therefore, they could start to measure the water level approximately 1 cm above the bottom of the flume.

Figure 3.5: (a) Bridge model connected to the load cell; (b) Four channel frequency to USB interface

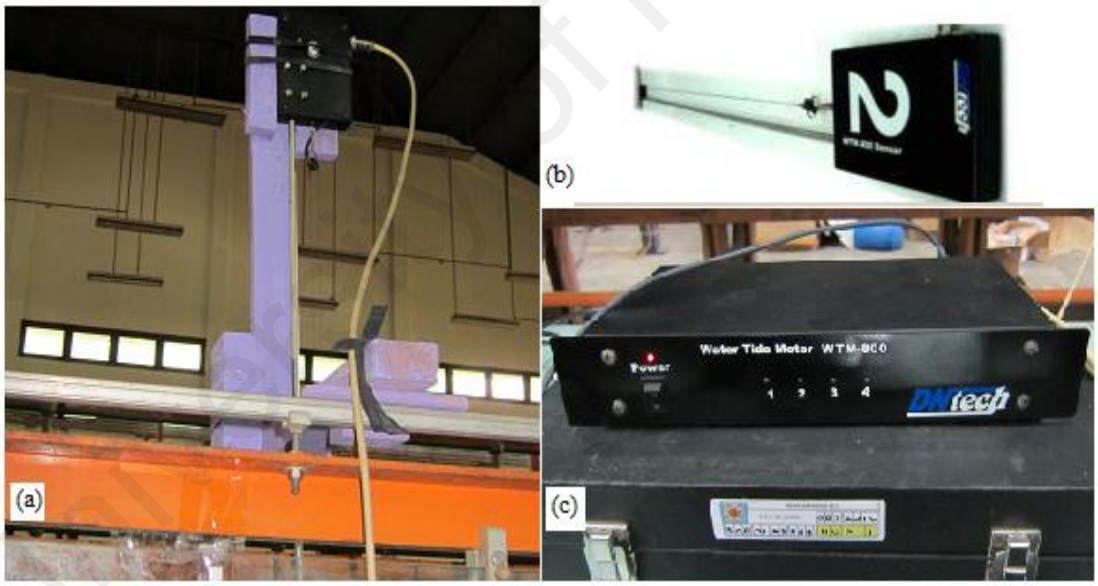

Figure 3.6: Wave gauges: (a) Fitted with a wooden frame; (b) Head and a wire; (c) Data acquisition system

In the present experiments, debris loading was not considered. Previous experimentations on the tsunami loading demonstrated that the presence of the debris may reduce the wave velocity, as a result, may affect the tsunami forces. Nevertheless, such debris carried by the tsunami flow may increase the density of the water, which in

turn increases the forces. According to FEMA 646 (FEMA, 2008), density of the water would be increased by approximately 20 % as the debris loading is considered in the flow. Wilkinson (2005) proposed to double the measured velocity in order to estimate the tsunami forces when the flow carried debris with it.

3.2.2 Load Cell Calibration

Forces on the model structures were recorded through the recording instruments or the measurement tools. However, the results obtained in the tool cannot be used or analysed before the data are adjusted with the calibration results. Therefore, implementation of the calibrations was done before and after each testing. The calibration of the load cell is described below (Figure 3.7).

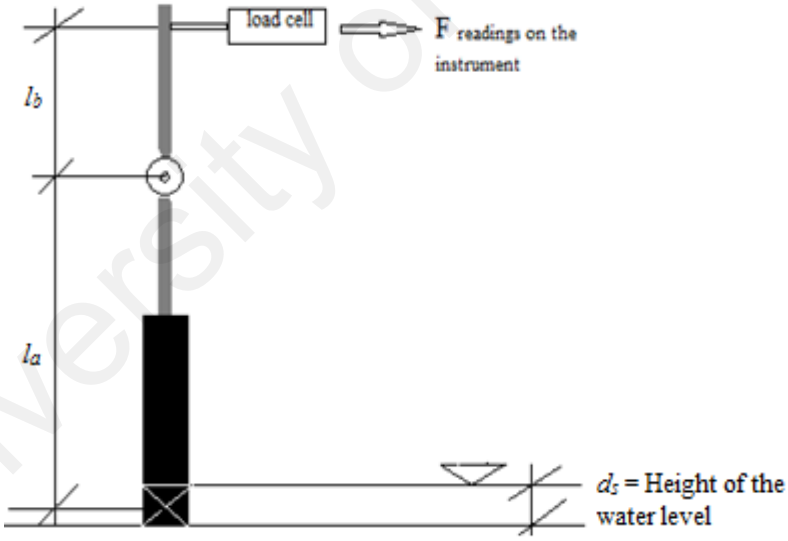

Figure 3.7: Illustration of the load cell calibration

Note:

l_a = Distance between the center of the model to the hinge (cm)

l_b = Distance between the hinge to the centre point of load cell (cm)

$F_{(\text{readings on the instrument})}$ = Force on the load cell device (N)

d_s = Height of the water level (cm)

So, Calibration becomes: $F_{(\text{calibration})} = \frac{l_b}{l_a} \text{ x } F_{(\text{reading on the tool})}$

3.3 Model Structures

The present investigation was focused on analyzing the tsunami forces on the coastal structures. Hereafter, bridge and building structures were selected for the purposes of evaluating the forces. Forces exerted by the tsunami flows were measured under different wave conditions.

Bridge models and some of the building models were prepared from 5 mm thick Perspex material to ensure sufficient rigidity. A 1/100 scale bridge model with three girders was placed inside the wave flume. Two bridge configurations were investigated as shown in Figures 3.8 (a) and 3.8 (b) viz. the first one was solid girder bridge and the second one was with approximately 16 % perforations in its girder. Figures 3.9 and 3.10 showed the graphical representation of the solid girder bridge model and the perforated girder bridge model, respectively. In the perforated girder model, perforations were provided with the aim of reducing the forces on the girder. Table 3.1 denoted the properties of the test bridge models.

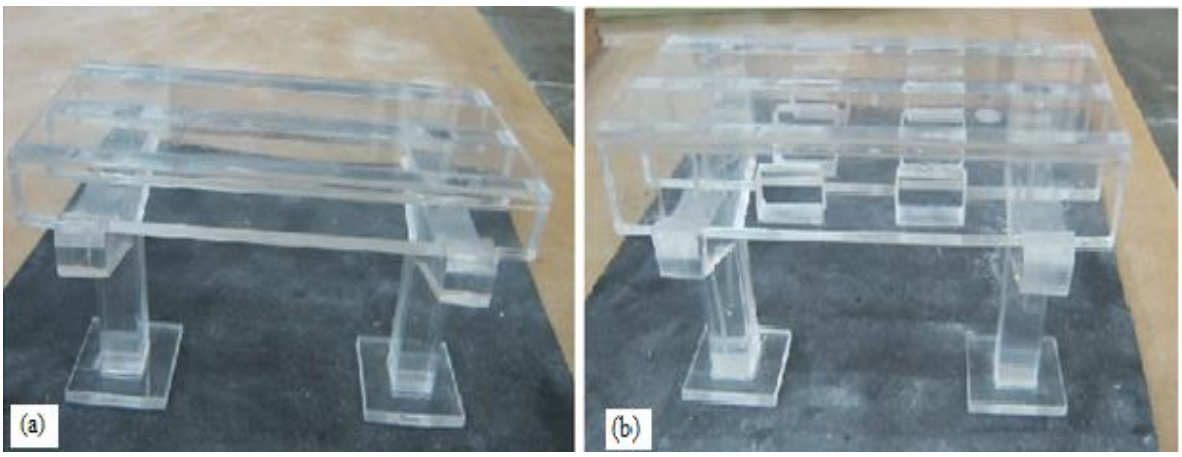

Figure 3.8: Photograph of the Bridge Model: (a) Solid girder bridge; (b) Perforated girder bridge

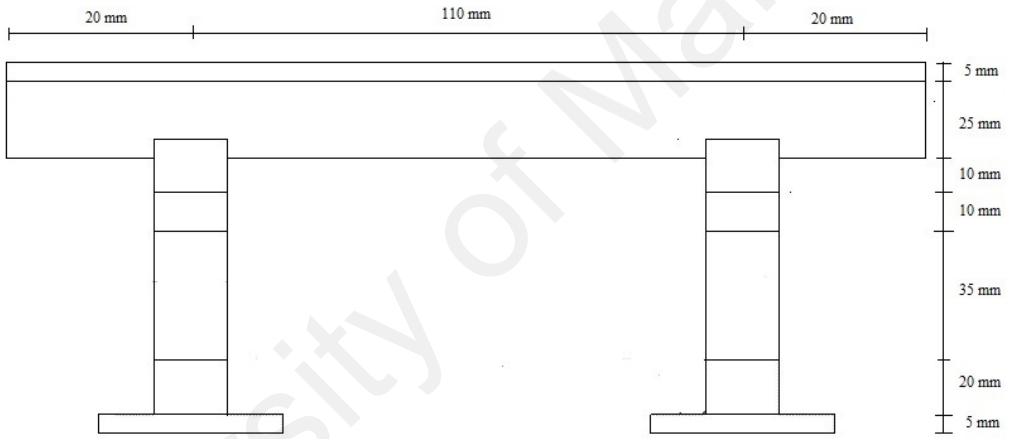

Figure 3.9: A Schematic view of the solid girder bridge

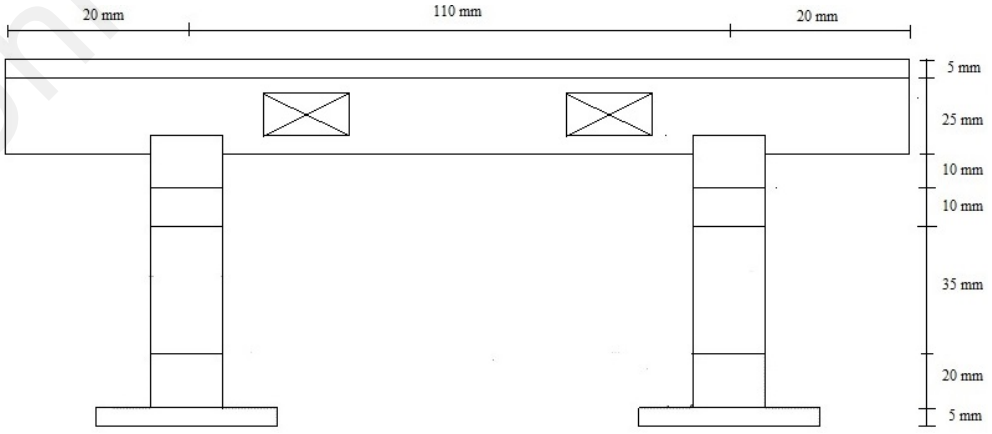

Figure 3.10: A Schematic view of the perforated girder bridge

Table 3.1: Details of the bridge girder

Girder Models	Solid	Perforated
Vertical projection area of each girder (mm^2)	3750 mm^2	3750 mm^2
Vertical projection area of the slab(mm^2)	750 mm^2	750 mm^2
Perforation area (percentage) in girders	0 mm^2 (0)	600 mm^2 (16 %)

The girder of the bridge model was pinned with a steel frame that was attached with the vertical steel rod. When the dam-break tsunami flows propagated, a small pin that was attached to the top of the steel rod, pressed the load cell and thus, load was recorded in the load cell. Figure 3.11 showed the installation of the bridge model inside the flume. Observations showed that most of the waves generated by the dam-break mechanism broke 3 m downstream from the gate. After that, the waves converted into the bore and hit the model as a hydraulic bore. Figures 3.12 and 3.13 depicted the sequences of the simulated tsunami waves (broken and unbroken, respectively) that were approaching as hydraulic bores along the flume.

Figure 3.11: Installation of model structure inside the flume

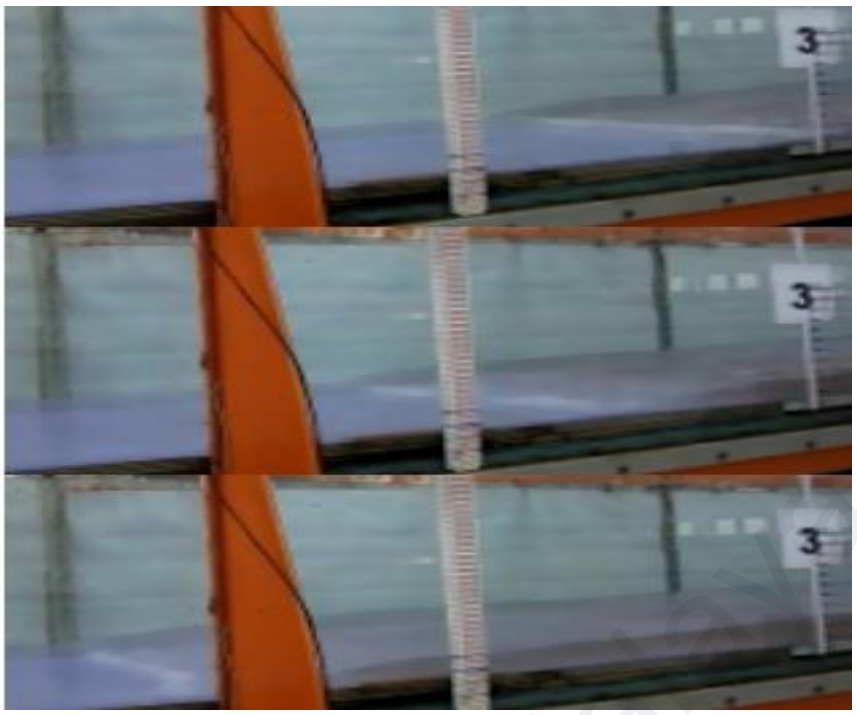

Figure 3.12: Simulated tsunami waves (broken)

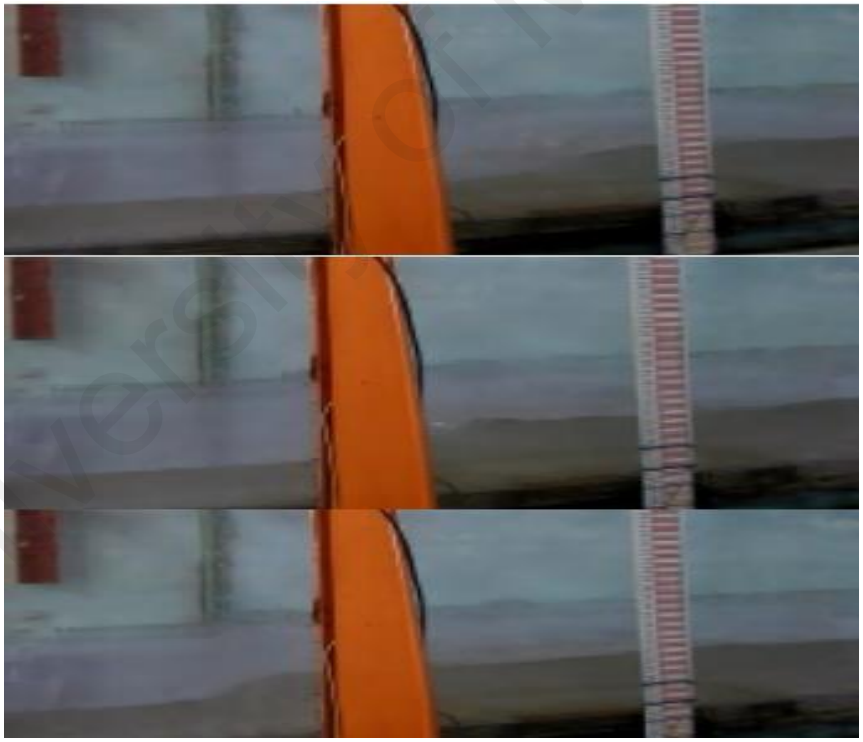

Figure 3.13: Sequences of the approaching unbroken tsunami waves

Both the broken and unbroken waves were simulated by varying the static water depth (length between the bottoms of the flume bed and the static water level). Various girder heights (the distance between the static water level and the girder lower panel) were

achieved by different static water depths. In order to identify the effects of breakwater, two different heights (5 cm and 10 cm) armoured breakwaters were used. Horizontal forces were measured on the bridge model with different upstream reservoir depths. In this experiment, tsunami wave height was referred as the utmost rise of the water surface near the model and varied between 3.75 cm to 7.5 cm. The measurements of the forces and the wave heights were made simultaneously with a sampling duration of 90 seconds so that the complete inundation phase could be accomplished properly.

The evaluations of the horizontal forces exerted by the tsunami waves on the building structures were performed with solid box model with a dimension of (length, width and height) 8 cm x 8 cm x 8 cm at a scale of 1/35. The model was made of plywood and placed 4 m from the gate. Using the selected scale, the distance between the shore and the model became 140 m, which was considered as a general distance between the shore and any building structure in a coastal area. To study the effects of the opening on the building structures, box models with holes were used. Two different openings were considered that were 30 % opening and 60 % opening (Figure 3.14). Another research was done with the building model fronted by the seawalls. The seawalls used in this experiment were made up of plywood with two different heights, (wall 1, W_1 = 4 cm high; wall 2, W_2 = 8 cm high). The length and width for the seawall models were 60 cm and 3.8 cm, respectively. These walls were placed in front of the building model on four different positions. At a scale of 1:35, the wall heights (4 cm and 8 cm) became 1.4 m and 2.8 m, respectively, which could represent the real wall heights that are more common to any coastal area. The coordinate system used in these experiments was x = 0 m from the gate and positive onshore in the direction of the flow. The wall positions were chosen over the distance $2 < x < 3.75$ m from the gate. The dimensionless ratio, x/L was measured to discover the appropriate location that showed better wall

performance as a protection measure. Here, L was the distance from the gate to the model. With the above arrangements, all of the waves were observed as broken and advanced along the downstream of the flume. For some of the cases, subsequent overtopping was observed when the wall height was smaller than the maximum run up heights. The wave height was taken as the height of the instant water level in the inundation area. Four different reservoir depths were considered that produced different flow depths near the model. Finally, the results obtained from using higher solid wall (wall 2, W_2 = 8 cm, high) were compared with the wall of modified configuration containing 26 % perforations (Figure 3.15). These experiments were performed to examine the effectiveness of using perforated wall relative to a solid wall in the force reduction as the construction of the perforated wall is less expensive than that of a solid wall.

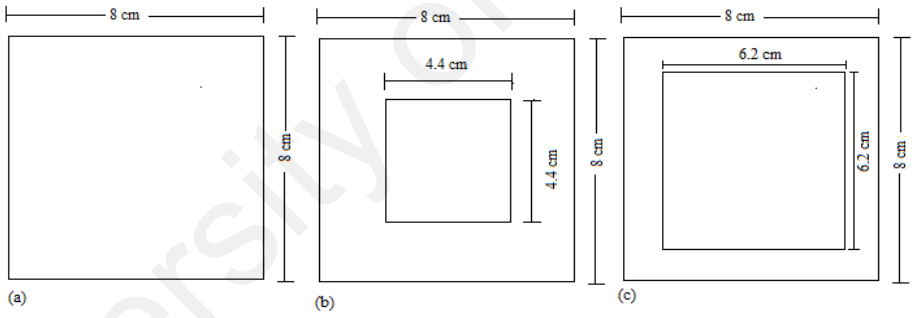

Figure 3.14: Building Model: (a) Solid building; (b) Building with 30 % opening; (c) Building with 60 % opening

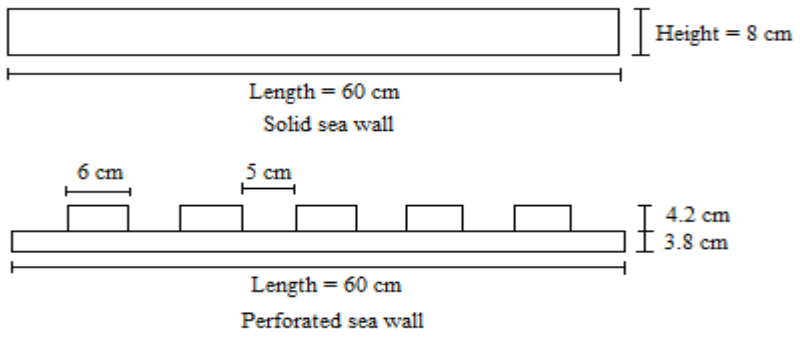

Figure 3.15: Seawalls (solid and perforated)

Another building model with smaller size was used with different barriers placed in front of the building model. These were done in order to idealize the full impact of the barriers. The selection of such small model size was based on the size of the flume. In this simulation therefore, a smaller model size (box width to flume width ratio was 0.133) was utilized to avoid the side wall effect. It was expected that the effect of the side walls would be much smaller and could be neglected. In that case, the dimension of the building model was (length, width, height) 20 mm × 20 mm × 40 mm. The model was made of 5 mm thick acrylic Perspex material. The scale of preparing the model was 1/150. Hence, the distance from the shoreline to building structures became 600 m, which could also be considered as a common distance between the shoreline and any coastal building. In reality, these barriers could be considered as higher building that could front a lower height building. The effects of such barriers were evaluated through their performance in the reduction of the forces on the building model. Barriers with different lengths were placed in front of the building model. The schematic of the building model fronted by the barriers was illustrated in Figure 3.16. The dimension (length, width, height) of barrier 1 was (40 mm x 20 mm x 80 mm), barrier 2 was (20 mm x 20 mm x 80 mm) and barrier 3 was (40 mm x 20 mm x 80 mm). The distances from the rear wall of the barrier to the front wall of the building models were denoted as d_1 = 5 cm, d_2 = 10 cm and d_3 = 15 cm. It was expected that the position, their length along the flow direction and the distance between the barrier and the building were important factors that affected the forces on the building. A photograph of the building model and the barriers was given in Figure 3.17. Building model that was installed inside the flume with different barriers was shown in Figure 3.18.

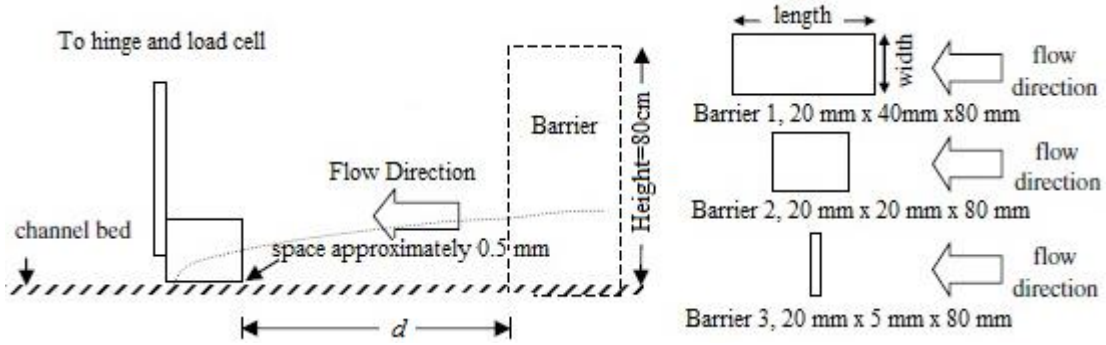

Figure 3.16: Schematic view of the building model and the barriers

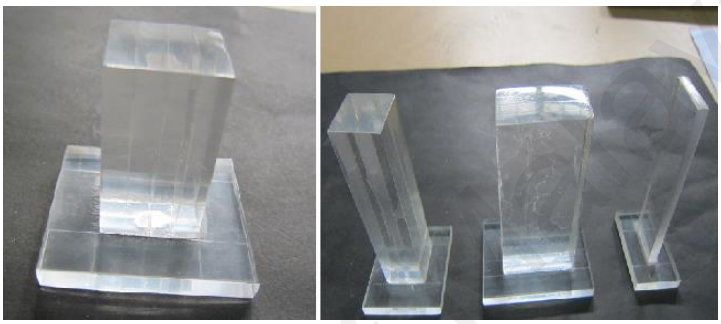

Figure 3.17: Photograph of the building model and different types of barriers.

Figure 3.18: Building model with the barriers installed inside the flume

3.4 General Experimental Procedure

In each of the cases, execution of the test was performed following few steps. At first, the model structures and the measurement devices were placed at the stated locations. In the same time, the gate was closed and locked and the reservoir (approximately 6.25 m long and 0.6 m wide) was allowed to fill with water up to the specified level using the

pump. It was to be noted that, the water level should be approximately constant behind the gate at the instant when the gate was opened quickly. Before opening the gate, all the measurement devices (data acquisition system of both the load cell and the wave probe) were turned on so that they could start recording from the moment of opening the gate. As the reservoir filled up to the desired level of water, the handle released the weight suddenly and the gate was opened quickly. Water rushed to the downstream abruptly and produced tsunami like waves. Data were recorded while waves were passing the model structures.

The experiments were divided into three different categories which were identified as test program 1, 2 and 3, respectively. Tables 3.2, 3.3 and 3.4 showed the details of the test conditions with different types of model structures. Tests were performed with different types of reservoir depths. The reservoir depths were selected on the basis of the maximum inundation height that would occur at the location of interest without the presence of the model structures. In this experiment, this maximum inundation height near the model structures was referred as the wave height. All of the tests were repeated for at least two times and the repeatability of the tests agreed well enough with the results.

3.4.1 Test program 1: Bridge Model

In this test program, Bridge model was placed at L = 4 m from the gate inside the flume. Table 3.2 showed the experimental conditions with bridge models. For this investigation, different reservoir depths were chosen based on the maximum flow depth that could occur near the bridge location in the absence of the model. The experimental set up was shown in Figure 3.19.

Table 3.2: Test conditions with the bridge model

Structure type	Reservoir Depth (h_0, cm)	Static water level (h, cm)
Solid girder bridge	30, 25, 20	N/A
Perforated girder bridge	30, 25, 20	N/A
Solid girder bridge	30, 25, 20,15	3, 4, 5.5, 7

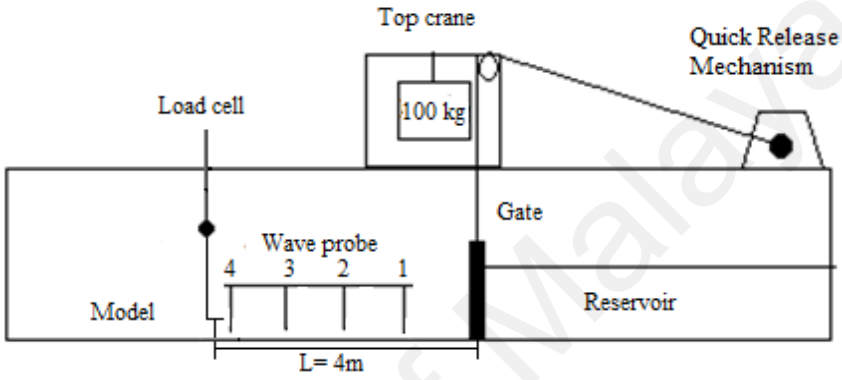

Figure 3.19: Experimental set up with bridge model

3.4.2 Test Program 2: Building Model (Solid and Open) and Building Model with Seawall

For this test program, Building model was placed at 4 m from the gate (similar to test program 1). Building with 30 % and 60 % opening was placed one by one to observe the effectiveness of using the opening in the building model. The details of the test program were demonstrated in Table 3.3. Similar tests were performed with the building model fronted by different seawalls. The experimental set up was shown in Figure 3.20. The location of the seawalls were presented in Table 3.4.

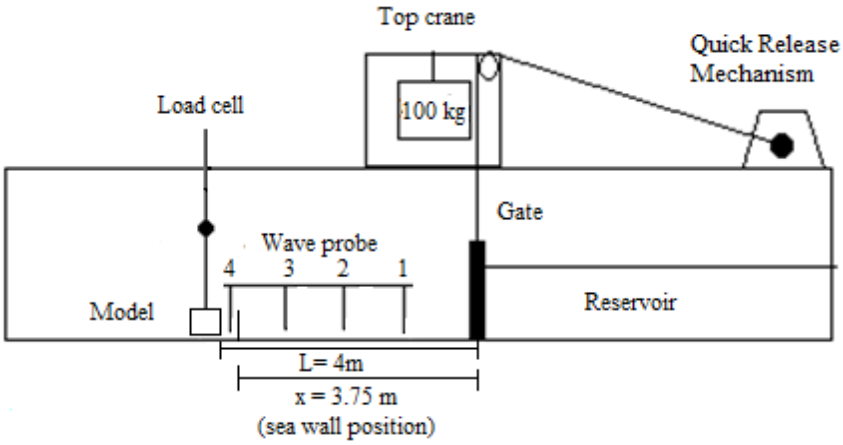

Figure 3.20: Experimental set up with building model fronted by the seawalls

Table 3.3: Summary of test program using building of various configurations

Structure type	Reservoir depth (h_0, cm)
Solid building	30, 25, 20, 15
Building with 30 % opening	30, 25, 20, 15
Building with 60 % opening	30, 25, 20, 15

Table 3.4: Wall positions with corresponding reservoir depths

Wall position	*L* (Distance from gate to model) (m)	*x* (Distance from the gate) (m)	*x/L*	Reservoir depth (h_0, cm)
1	4	3.75	0.9375	30, 25, 20, 15
2	4	3.5	0.875	30, 25, 20, 15
3	4	3	0.75	30, 25, 20, 15
4	4	2	0.5	30, 25, 20, 15

3.4.3 Test program 3: Small Building Model with Barrier

This test program was customized with building model having smaller size. The effects of different barriers on the measured forces were evaluated. The test condition was presented in Table 3.5.

Table 3.5: Summary of test program considering building with the barriers

Structure type	Reservoir depth (h_0, cm)	Distance between rear face of the barrier to the front face of the building (d, cm)
Solid building	15, 12.5, 10	5, 10, 15
Solid building with barrier 1	15, 12.5, 10	5, 10, 15
Solid building with barrier 2	15, 12.5, 10	5, 10, 15
Solid building with barrier 3	15, 12.5, 10	5, 10, 15

CHAPTER 4

RESULTS AND DISCUSSIONS

4.1 Introduction

The basic aim of the present research program was to explore the influences of tsunami-induced forces on the coastal structures. In this chapter, tsunami forces imparted on the coastal structures were quantified and then evaluated based on several experimental conditions. This research comprises of physical assessment of tsunami forces on two different types of coastal structures, such as- bridges and buildings. A number of test programs were performed to compute the exerted tsunami forces on the physical models under different wave conditions. Forces and wave heights were measured using the load cell and wave probe, respectively. Visualization of tsunami propagation, generated by the quick opening of the dam-break gate, was captured by a video camera.

4.2 Characteristics of Waves

In the present experimental process, wave velocities were calculated based on the water elevation time history measured by different wave probes placed at four separate locations. The velocity was estimated using the following Equation (4.1).

$$u = \frac{\Delta t}{\Delta s} \tag{4.1}$$

Where Δt is the time variance between the arrival times of the wave at two adjacent stations and Δs is the distance between the stations. The calculated values of wave velocity were validated with the values obtained from the video images. The variations of velocities with distances from the upstream gate along the flume were depicted in Figure 4.1. These variations were observed for different reservoir depths (h_0). From the

Figure 4.1, it was found that the velocity remained almost constant with the distances. However, the changes of velocities with distance were more apparent with larger reservoir depths than those of smaller reservoir depths. Previous experiments showed that the front velocity of the waves was larger when the wave height was comparatively small (Lukkunaprasit et al., 2009). Velocity became slower as the wave height increased. The water surface of the leading edge of the wave changes quickly to a maximum value. As in the present case, velocity was calculated based on the arrival time of the wave leading edge, so the calculated velocity was considered as the maximum velocity. Figure 4.2 showed the comparison between the observed values of velocity with Chanson (2005) analytical equation (Equation 2.12) using $f = 0.03$, where f is the friction coefficient. This figure illustrated the position of the leading edge of the wave with respect to time. The graph also revealed that the observed values of velocity of the wavefront agreed well enough with Chanson (2005) analytical solution. According to Lukkunaprasit et al. (2009), the maximum wave velocity does not coincide with the maximum wave height and at maximum wave height the velocity is approximately 65 % of the maximum value.

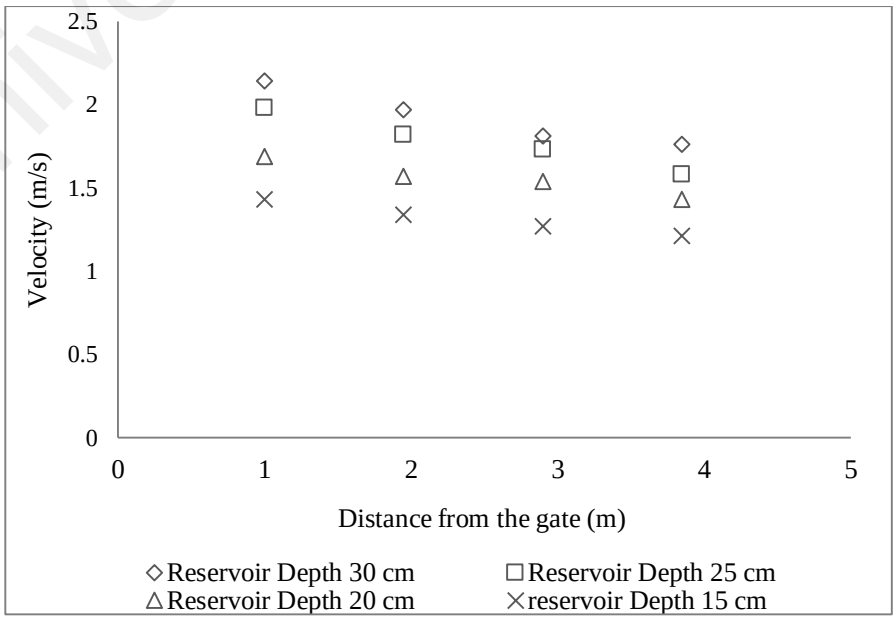

Figure 4.1: Variations of velocity with the distances

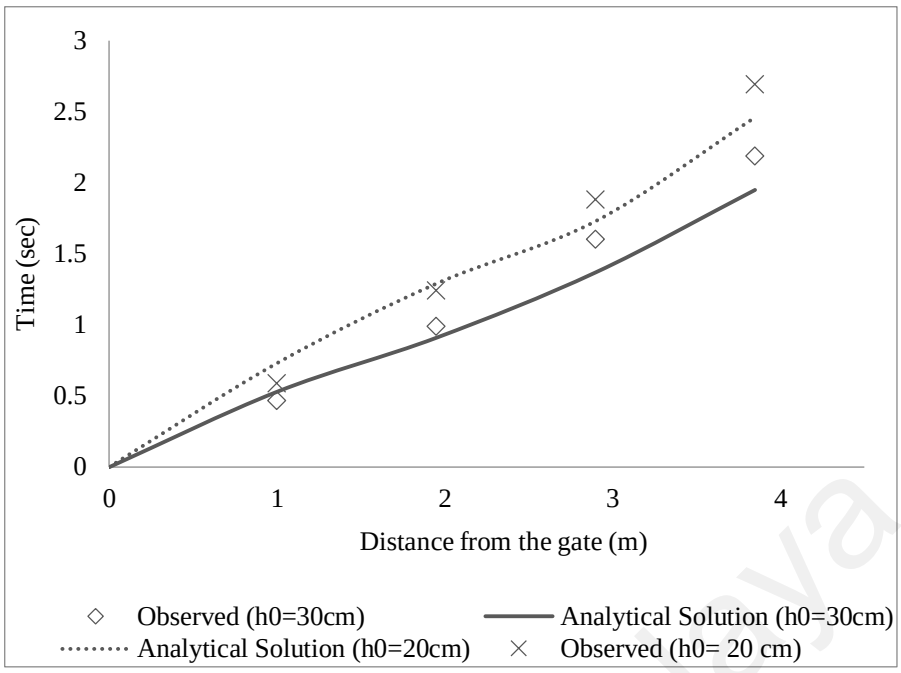

Figure 4.2: Observed and calculated position of wavefront with respect to time

Wave heights were measured by the wave probe located at four different stations (as shown in Figure 3.1). Wave probe placed at station 4 was very much close to the model structures and measured the approximate values of water level that hit the model. Figure 4.3 showed the typical wave profiles that propagated downstream of the flume. In this figure, the water surface elevations from station 1 to station 4 (near the model location) for 30 cm reservoir depth were illustrated. Wave profiles were characterized through the measured data. Two sets of experiments were performed and the closeness of the data pair indicated the reliability of the tests. In order to make comparisons among the wave heights, the starting times of the plots were adjusted in such a way that the waves reached any specific station at the same period. From this figure, it was found that the initial water level during the first few seconds of measurement were almost same among the stations 1, 2 and 3, However, there was a sudden escalation of water of approximately 17 cm above the model at station 4. This happened due to the back water effect that caused this additional rise of water.

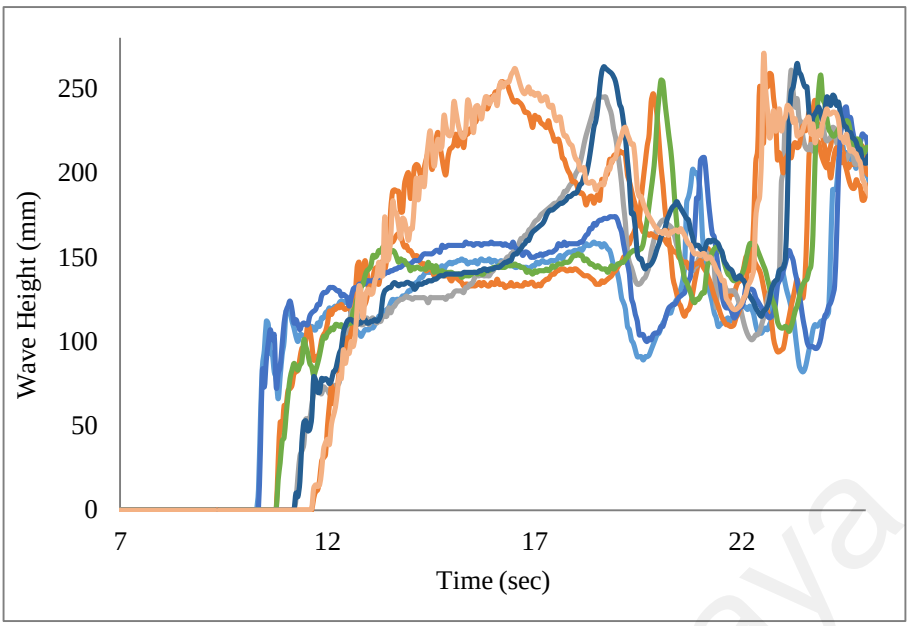

Figure 4.3: Typical wave profiles at different stations along the flume with 30 cm reservoir depth

The velocity of the wavefront and the water level history near the model location (at station 4) was compared with the equations given by Chanson (2005). Table 4.1 revealed the properties of the wavefront at station 4 for different reservoir depths. The observed velocities as well as the measured wave heights near the location of interest, where the model was placed, were agreed well enough with the calculated values from Chanson equations (Chanson, 2005). The average Froude number varied among 2.13 to 2.26 for the present study. According to Lukkanaprasit (2009), maximum forces did not occur by the maximum wave height. Triatmadja and Nurhasanah (2012) demonstrated that the leading edge of the wave did not contribute to the maximum forces rather the wave height at about 0.3 s to 0.6 s after hitting the model was considered to produce the maximum forces. These considerations were adopted in this present study where the presented values of wave height produced the maximum forces.

Table 4.1: Wave properties at station 4 for various reservoir depths

Reservoir depth (h_0, cm)	Avg. Wave height (cm) (experiment)	Avg. Wave velocities (m/s) (experiment)	Calculated wave height (cm) (Chanson, 2005)	Calculated wave velocities (m/s) (Chanson, 2005)	Average F_r
30	7.36	1.92	5.88	1.87	2.26
25	6.41	1.78	5.4	1.74	2.24
20	5.21	1.56	4.7	1.6	2.18
15	3.87	1.31	3.9	1.35	2.13

As the experiments were performed in a flume of limited width, the measured values might be affected by the side walls. The effects of side walls might influence the result. Therefore, analyses were performed keeping in mind about this influence of the walls. The duration between the impact forces and the maximum forces was smaller than the time required by the reflected waves travelled from the model to the side walls and then returned to the model. This result revealed that the measured values were not influenced by the side walls.

4.3 Quantitative Analysis of the Wave-Structure Interaction

The purpose of this section is to represent the quantitative and qualitative analysis of the tsunami wave impacts on different coastal structures. In order to do that, study on the exerted forces and the wave height data were evaluated to identify the characteristics of the wave-structure interactions. Different reservoir depths were considered behind the gate that could produce different wave heights along the flume.

4.3.1 Bridge Structures

4.3.1.1 Evaluation of Tsunami Forces on the Bridge Girders

In order to quantify the tsunami forces on the bridge girder, a number of tests were performed considering different static water depths (h) under several reservoir depth conditions (h_0). Figure 4.4 showed the snapshots that were taken during the simulation process. The images showed the sequences of the approaching waves that hit the girder model. Each image was documented with the time when the waves reached any specific location. This time was measured after opening of the dam-break gate.

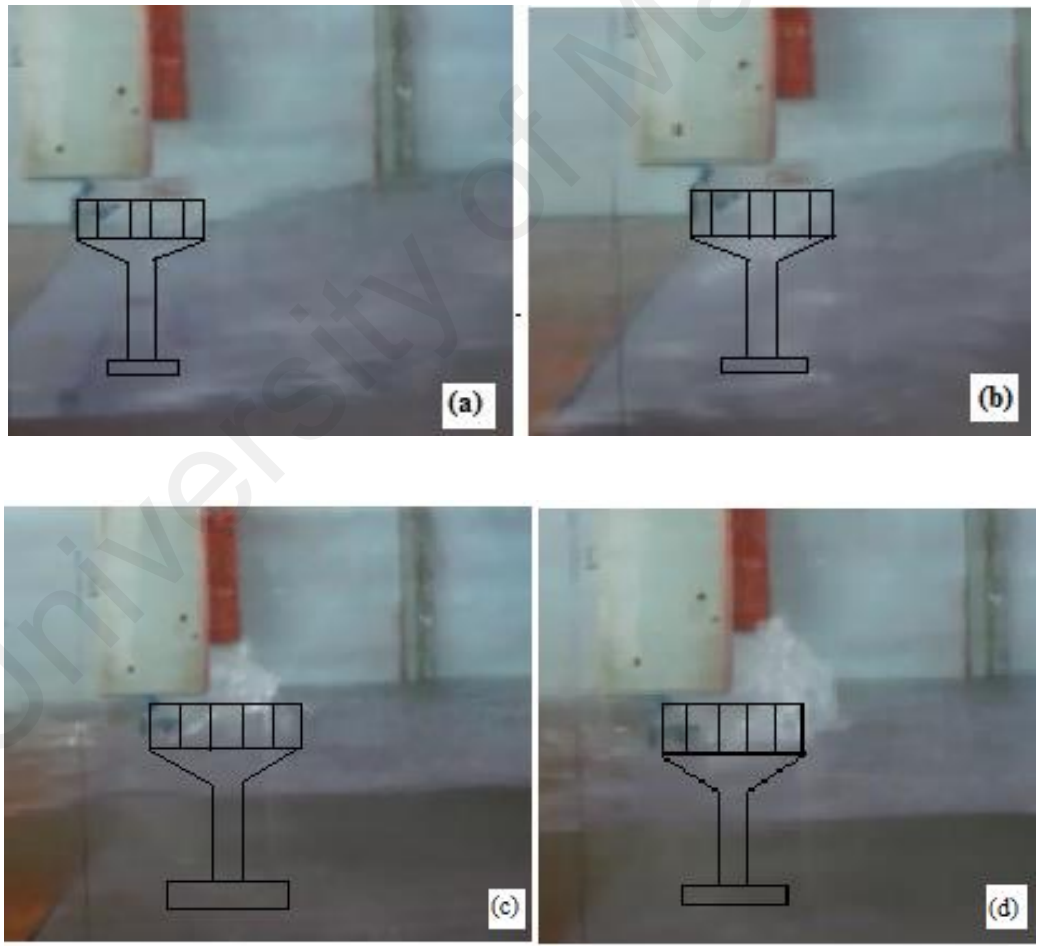

Figure 4.4: Sequences of waves attacking the bridge girder model

The present section included the experimental modeling of the wave forces acting on the bridge girder struck by a tsunami. The simulated tsunami waves propagated from the right side to the left side of the bridge model. Reservoir depths in cooperation with static water depth conditions were adjusted in such a way that could produce broken as well as unbroken waves for the analysis purposes. In the case with larger reservoir depths, all of the waves broke in advance of hitting the bridge model. The simulated waves containing tremendous forces reached the girder site promptly and collided with the girder lower panel. Waves readily splashed upward and collapsed at the girder site (Figure 4.4). Finally, these waves overtopped the girder. The wave heights recorded while overtopping the girder were almost two times the incoming wave heights. For smaller reservoir depths, waves remained unbroken still after colliding with the bridge model. It was observed that oscillations exist in the measured time history of the force prior to the wave impact. These oscillations were caused by the vibration of the wooden plate which was not rigidly attached to the underlying flume bottom. As the wave impacted the structure and passed over the plate, these vibrations were attenuated and their effects became small.

The typical force time histories with two different reservoir depths (25 cm and 15 cm) considering static water depth, h = 5.5 cm were portrayed in Figures 4.5 and 4.6, respectively. Broken waves along with unbroken waves were observed with these reservoir depths (Figure 4.5- broken waves that hit the model just after being broken, Figure 4.6- unbroken waves that hit the model and then broke). From these figures, it was found that the horizontal forces of broken waves produced from larger reservoir depths were more apparent than those of the unbroken waves created by smaller reservoir depths. Peak forces measured along the entire time history were considered as the maximum forces (Figures 4.5 and 4.6). The initial sharp rise in the force time

history characterized the impact force (surge force). The magnitude of this impact force was greater; however, the duration was short. This peak value was followed by the continuous turbulent flow. With larger reservoir depths, these initial impact forces were higher than the hydrodynamic forces that corresponded to the continuous turbulent flow. According to Ramsden (1996), the variation of forces was highly dependable on the types of slope of the wavefront. Larger reservoir depths contributed to produce higher initial impact force due to the steep wavefront whereas smaller reservoir depths contained almost mild slope. In that case, hydrodynamic forces governed and were more noticeable than the initial impact forces. For the unbroken waves (produced from 15 cm reservoir depth), the fluctuations of forces were not as much evident as the broken waves (produced from 25 cm reservoir depth).

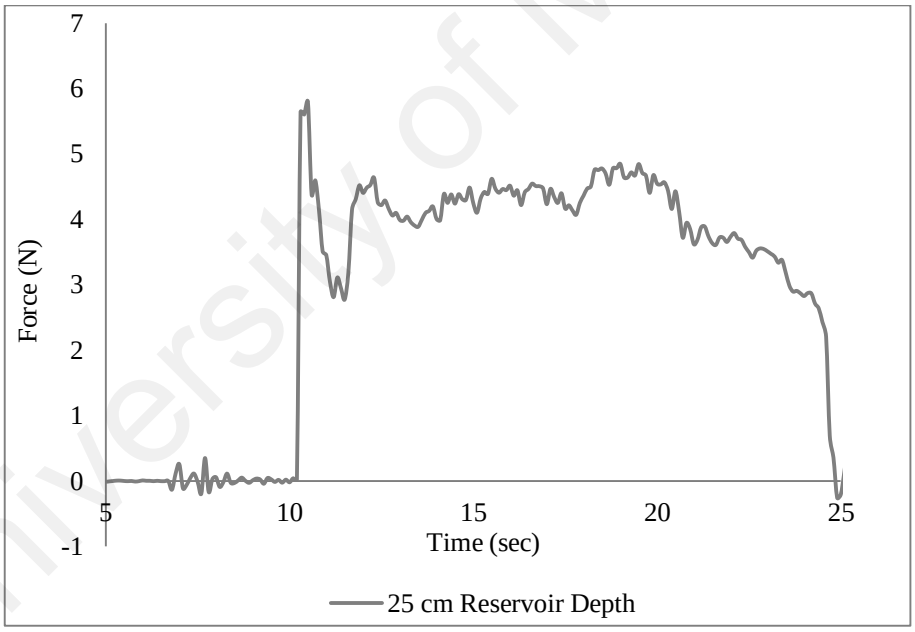

Figure 4.5: Force time history for the waves with 25 cm reservoir depth (h_0 = 25 cm)

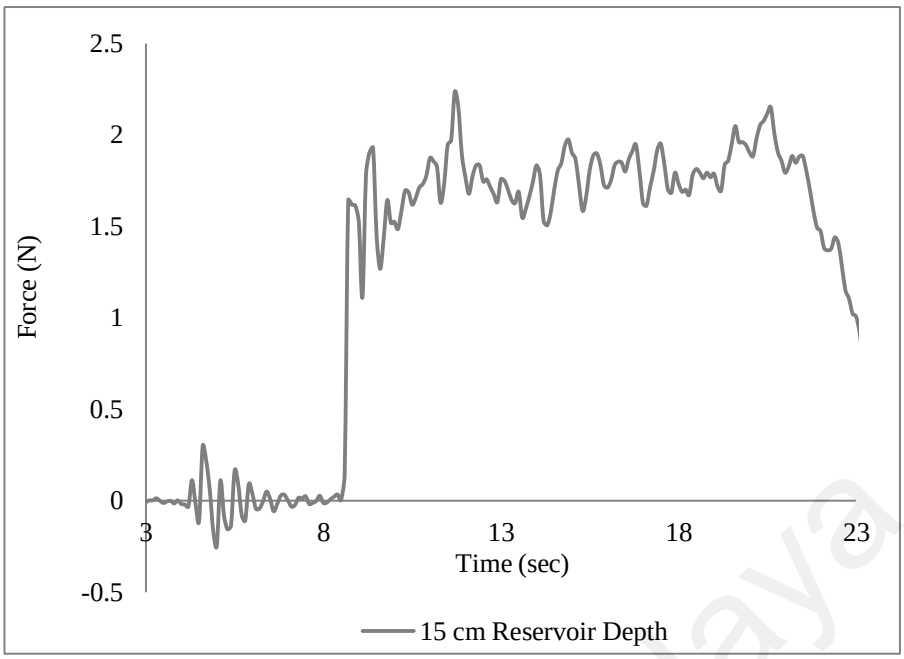

Figure 4.6: Force time history for the waves with 15 cm reservoir depth (h_0 = 15 cm)

The variations of the wave heights measured at wave probe 4 (W4) near the bridge model were evaluated with the force time history data set in Figures 4.7 and 4.8. The measured tsunami wave heights near the model were 6.41 cm and 3.87 cm, respectively. It was to be noted that the front edge of the wave hit the base of the bridge pier model with high velocity and attained the peak value of the forces instantaneously with relatively smaller water surface elevation. The wave height became high when the velocity, as well as the forces started declining. This observable fact, indeed agreed well with the result of Lukkunaprasit et al. (2009). The similar trends were observed for all of the cases regardless of the reservoir depths. Among all the combinations of reservoir depths and static water depths, the force observed with reservoir depth of 30 cm and static water depth of 4 cm achieved maximum magnitude. At that moment, the wave was breaking with a higher impulsive force having shorter duration.

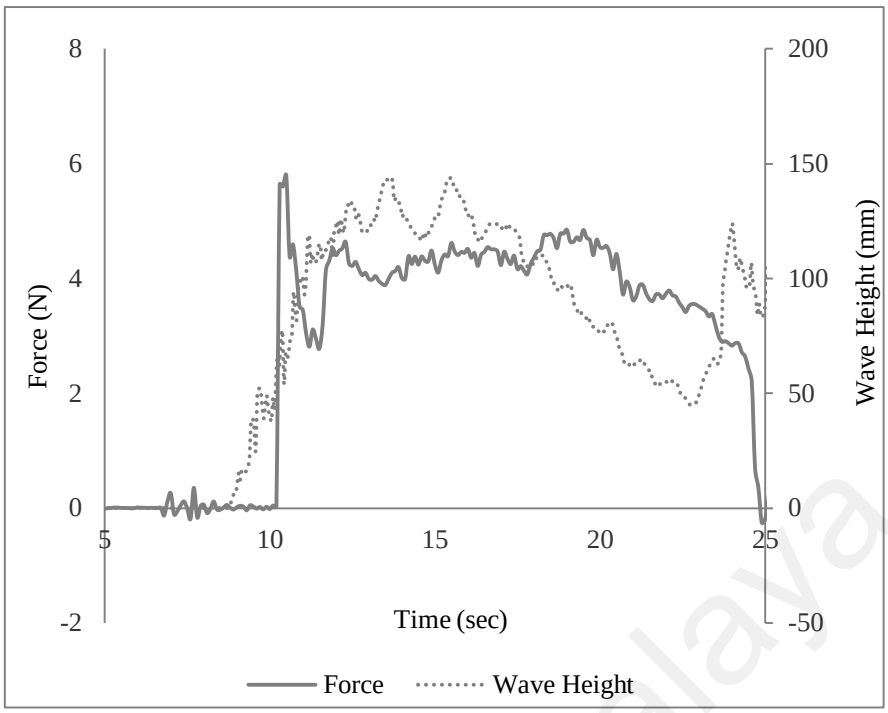

Figure 4.7: Time history of force and wave height with 25 cm reservoir depth (h_0 = 25cm)

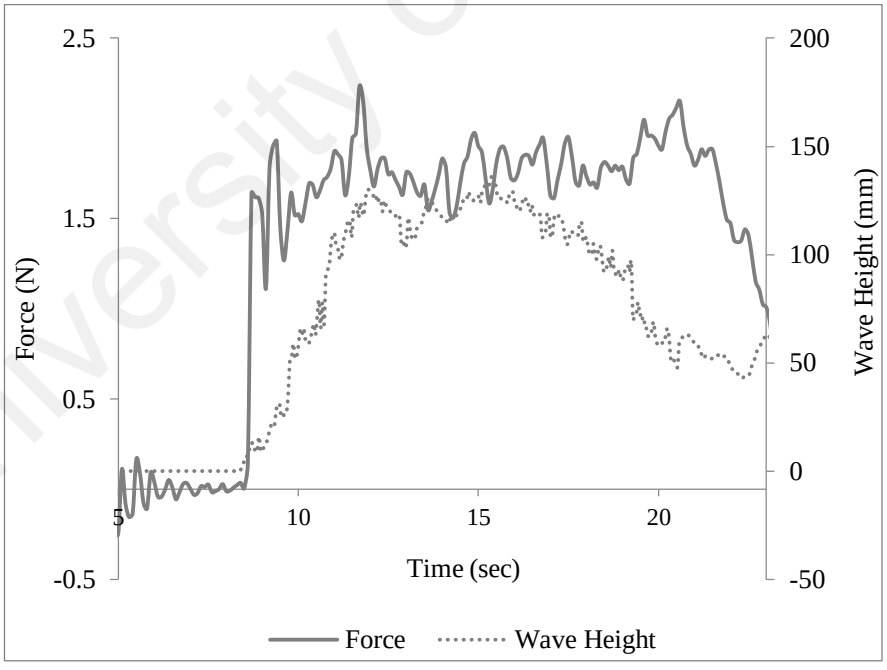

Figure 4.8: Time history of force and wave height with 15 cm reservoir depth (h_0 = 15 cm)

Figure 4.9 showed the maximum value of horizontal forces obtained from different experimental cases. The vertical axis represented the dimensionless ratio of the girder height to the tsunami wave height that was characterized by δ. Forces were evaluated through this dimensionless ratio.

$$\delta = \frac{Z}{a} \tag{4.2}$$

Z is the girder height (distance between the static water level and the girder lower panel) and a is tsunami wave height.

In this experiment, girder height was controlled by changing the static water depth (h). It was seen that the maximum value of forces were obtained at higher girder height (lower static water level) for all of the selected reservoir depths. Forces were increasing significantly with increasing tsunami wave height at lower static water depth which represented the case of the broken waves. The escalation rate of the forces for the unbroken waves with increasing tsunami wave height was lower than those of the broken waves. It was to be noted that, at higher tsunami wave height, girder position subsequently affected the fluctuation of forces whereas; at lower tsunami wave height these variations of forces were not so much noticeable. From this figure, it was also found that horizontal forces were larger for the broken waves than those of the unbroken waves. In the case, when the bridge girder was located at a higher position, upper part of tsunami waves containing tremendous energy attacked the girder with high velocity and caused severe damages. From these results, it could be said that, larger height bridges are more vulnerable to tsunami destruction compared to the bridges that are located at lower height near the ground level.

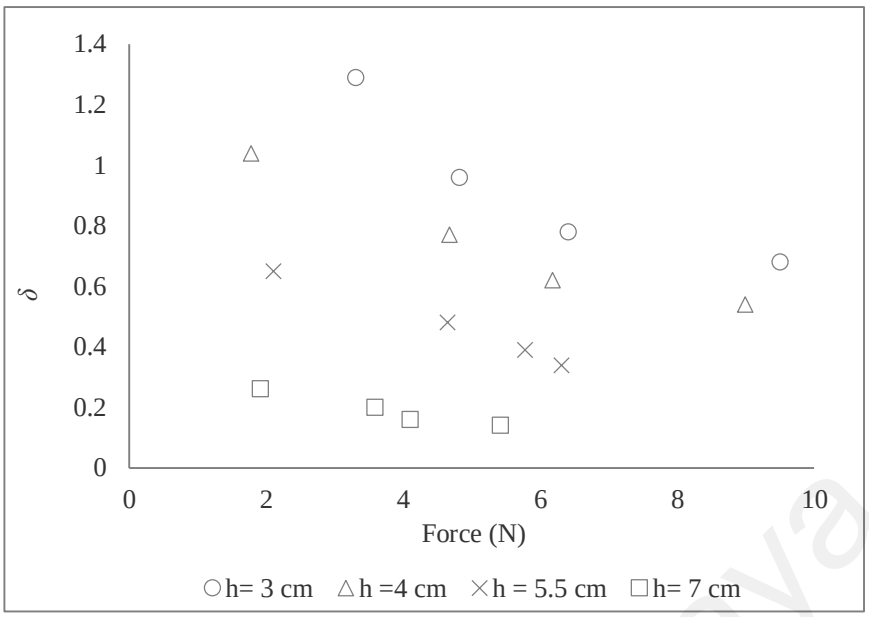

Figure 4.9: Relationship between δ and measured forces

The present research was concentrated on the elaborate analysis of tsunami forces on the bridge girder. The changes of forces were also discussed evidently in terms of pressure, considering another different parameter. This parameter was defined by κ that was obtained by dividing the maximum measured forces by the possible area of wave attack on the girder's side plan and static water pressure against the tsunami wave height.

$$\kappa = \frac{F/A}{\rho g a} \tag{4.3}$$

F is the horizontal wave forces, A is the possible area of wave attack on girder's side plan, a is the tsunami wave height, ρ is the density of water, g is the gravitational acceleration

An inclusive relationship was developed between δ and κ in Figure 4.10. The vertical axis showed the ratio of the girder height to the tsunami wave height, δ and the horizontal axis showed the maximum measured forces normalized by the possible area of wave attack on the girder's side plan and the static water pressure against the tsunami

wave height, which was identified as κ. At lower girder position (in the case with 7 cm static water depth), the increase of κ value was not much significant with decrease of δ due to the increase of wave height, a. In this situation, lower part of tsunami waves touched the bridge girder resulting in lower forces than those of the other cases. The changes of κ value with the declination of δ (with the increase of tsunami wave height) were much evident in the case with lower static water depth where bridge girder was located in a higher place. In this case, upward part of tsunami waves hit the girder with high energy and velocity, resulting in higher forces. The experimental results agreed well enough with Shoji et al. (2011). With the results obtained from the Figure 4.10, wave pressure could be evaluated through the parameter κ.

$$q = \kappa * \rho g a \tag{4.4}$$

Based on this result, approximate linear line was drawn for 3 cm static water depth. From this linear line, horizontal wave pressure (q) was assessed. The linear equation can be written as:

$$\delta = -0.34\kappa + 2.105 \tag{4.5}$$

$$\frac{Z}{a} = -0.34\ \frac{q}{\rho g a} + 2.105 \tag{4.6}$$

After simplification, it becomes

$$q = \rho g \left(6.18\, a - \frac{1}{0.34}\, Z\right) \tag{4.7}$$

The Equation 4.7 represented the pressure distribution due to the horizontal forces. If the tsunami wave height and girder position relative to the static water depth are known, the wave pressure in the horizontal direction can be measured by following the above equation.

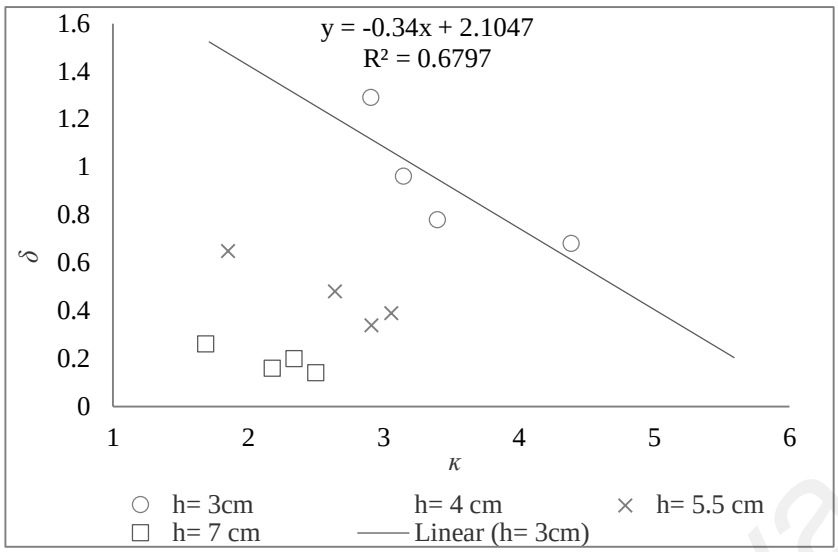

Figure 4.10: Relationship between δ and κ

4.3.1.2 Bridge Structures with Perforations in Girder

This section demonstrated the performance of a bridge girder with perforations under tsunami wave loading. The effectiveness of providing perforations in bridge girder was evaluated through the reduction of tsunami forces on the bridge girder. The details of perforation sizes were discussed in chapter 3. Approximately 16 % perforations were considered within the girder model. The time histories of the forces for both solid and perforated girder bridge were presented in Figure 4.11. The peak forces were taken as the maximum forces from the force time history. From the Figure 4.11, it was found that the substantial amount of force reduction was observed due to the use of perforations in the girder. This force reduction was experienced not only in peak force but also throughout the whole time history. Table 4.2 provided the results obtained from using solid and perforated girder bridge. Another finding was that, the time to attain the peak forces was less for perforated girder bridge than that of solid girder bridge (Table 4.3).

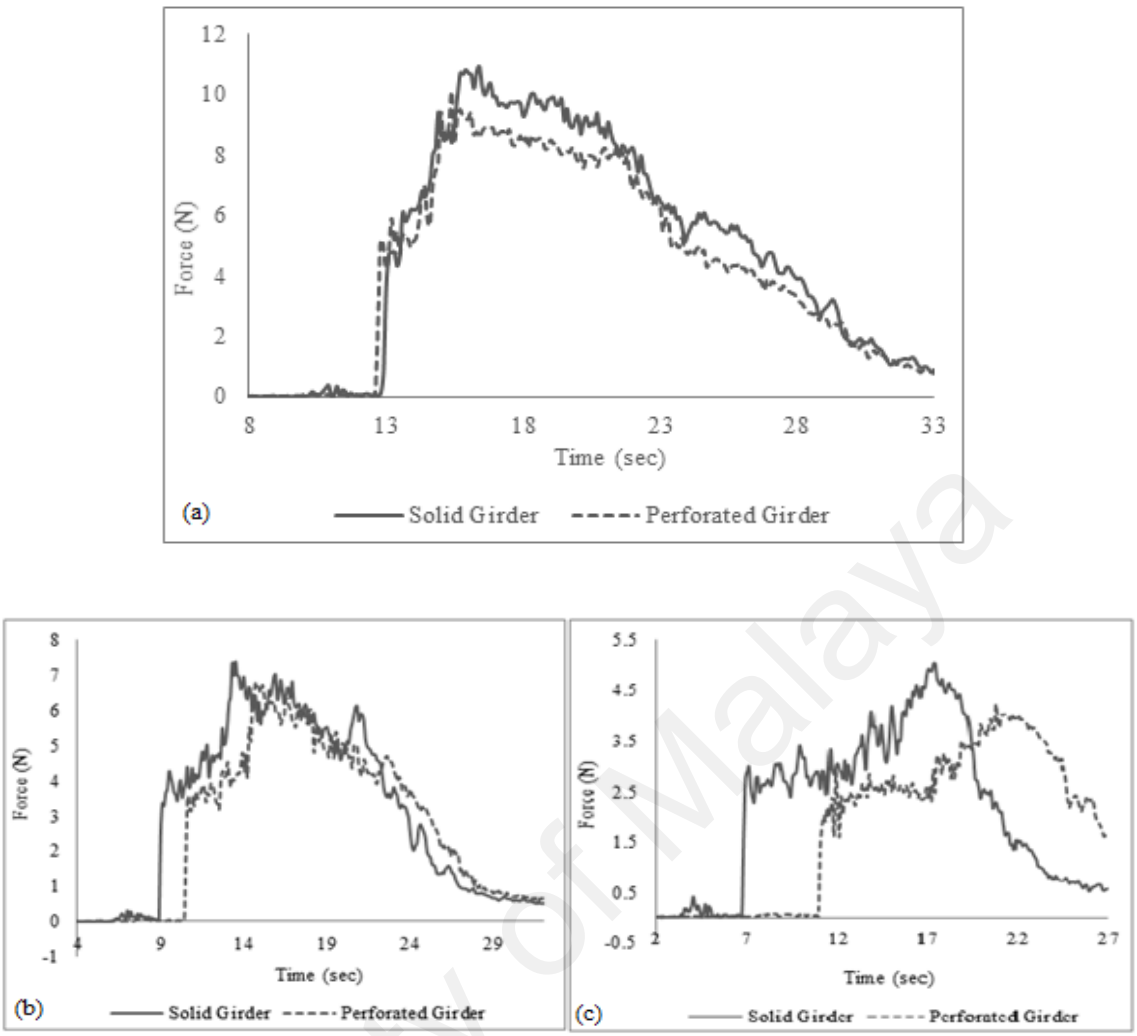

Figure 4.11: Force time histories for both solid and perforated girder bridge for: (a) 30 cm reservoir depth; (b) 25 cm reservoir depth; (c) 20 cm reservoir depth

Table 4.2: Force reductions by perforations in girder

Reservoir Depth (h_0, cm)	Peak forces in Solid Girder Bridge (N)	Peak forces in Perforated Girder Bridge (N)	Reductions in forces
30	11.075	9.97	10 %
25	7.9	6.464	13 %
20	4.67	3.8	18 %

Table 4.3: Time to reach peak value

Reservoir Depth (cm)	Wave Height (cm)	Time to attain peak force (sec)	
		Solid girder Bridge	Perforated girder Bridge
30	7.36	3.6	2.3
25	6.41	4.5	4.2
20	5.21	11.1	7.4

Tests were performed with perforations in the girder to detect the bridge performance under the tsunami attack. For all of the selected reservoir depths, substantial reductions were found due to the presence of perforations in the girder. The force time histories for solid and perforated girder bridge with different reservoir depths were illustrated in Figures 4.12 (a) and 4.12 (b), respectively. The reductions in the total forces due to the presence of the perforations were given in Table 4.2. For 20 cm reservoir depth, the percentage of reduction was higher compared to the reductions observed during 30 cm and 25 cm reservoir depths. From Table 4.2, it was found that the peak force reductions were 10 %, 13 % and 18 % for reservoir depths of 30 cm, 25 cm and 20 cm, respectively. The presence of the perforations in the girder minimized the attacking area of the waves and consequently became responsible for the force reductions in the girder. Perforations in the girder allowed some amount of flowing water to pass through the perforations, created counteracting forces in the perforations and thus contributed in the force reduction. Moreover, with decreasing reservoir depth, reductions in the forces were increasing. This fact indicated that the reductions in forces were more apparent for smaller wave heights.

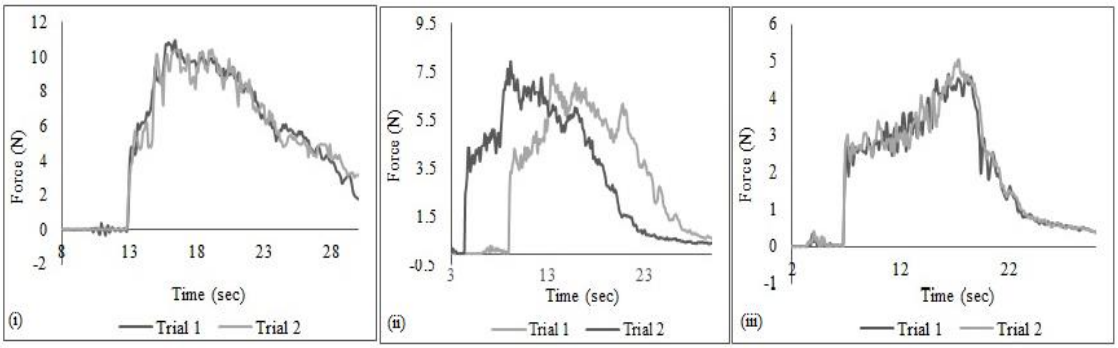

Figure 4.12: (a) Time history of tsunami forces on the solid girder bridge: (i) 30 cm reservoir depth; (ii) 25 cm reservoir depth; (iii) 20 cm reservoir depth

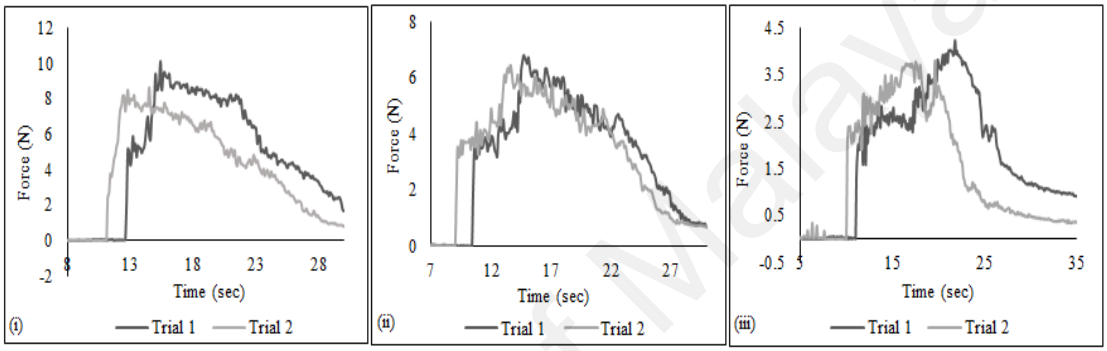

Figure 4.12: (b) Time history of tsunami forces on the perforated girder bridge: (i) 30 cm reservoir depth; (ii) 25 cm reservoir depth; (iii) 20 cm reservoir depth

4.3.1.3 Bridge Structures Fronted by Breakwater

The next stage of these experiments was based on the experimentation of using of two different heights armored breakwater in front of the bridge model (Figure 4.13). The effectiveness of introducing breakwater in reducing the impact of the tsunami forces was investigated. For the experimental purposes, 5 cm and 10 cm armored breakwaters were used. Total forces on the girder were recorded for three different wave heights produced from three different reservoir depths (h_0). Both solid and perforated girder bridges were considered for this study. Figure 4.14 showed the effects of the presence of 5 cm and 10 cm armored breakwaters in front of the solid girder bridge at h_0 = 20 cm. During the whole time history, the value of the forces with 10 cm breakwater was lower

than the forces with no breakwater condition. This finding indicated that the presence of breakwater reduced the forces during its complete travel period. However, the impact of using 5 cm breakwater was not much significant in reducing the forces. The main reason lied behind that the wave height was more than the breakwater height in the case with 5 cm breakwater. Therefore, their contribution in the force reduction was minimal in amount. The reduction of the forces with 10 cm breakwater was about 7 %, whereas for 5 cm breakwater it seemed to be only 1 % at h_0 = 30 cm. The trends of reduction of the forces were almost similar for other reservoir depths. The force reductions for 10 cm and 5 cm breakwater were about 7 % and 1.6 %, respectively at h_0 = 25 cm. For the case with 20 cm reservoir depths, the reduction for 10 cm breakwater was great in magnitude with a value of 11 %, whereas it was about 3 % with 5 cm breakwater. All these scenarios revealed that the total forces exerted on the bridge model was declined with the use of the breakwater as long as the height of the breakwater was more than the wave height. However, when the wave height was more than the breakwater height, the effectiveness became quite insignificant in the force reduction.

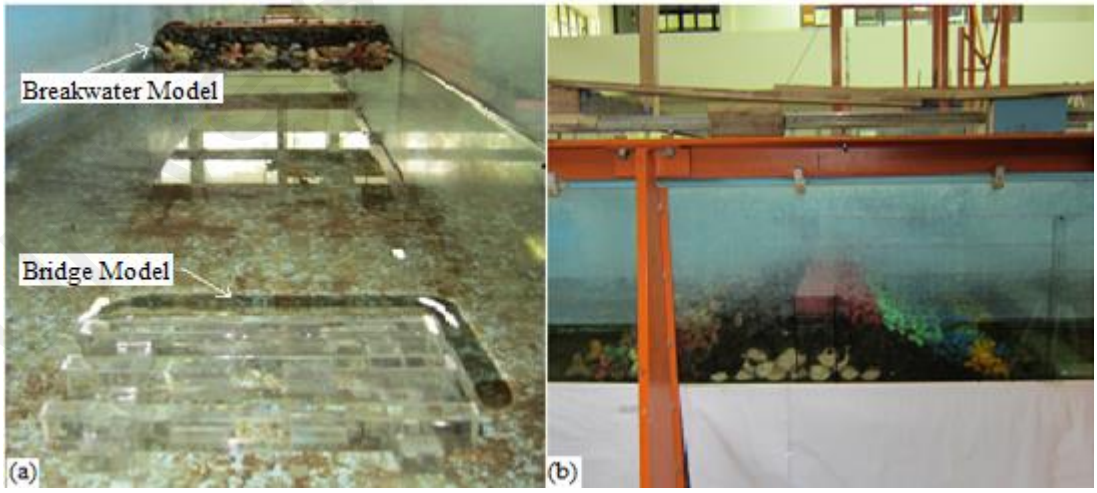

Figure 4.13: Breakwater model in front of the Bridge model

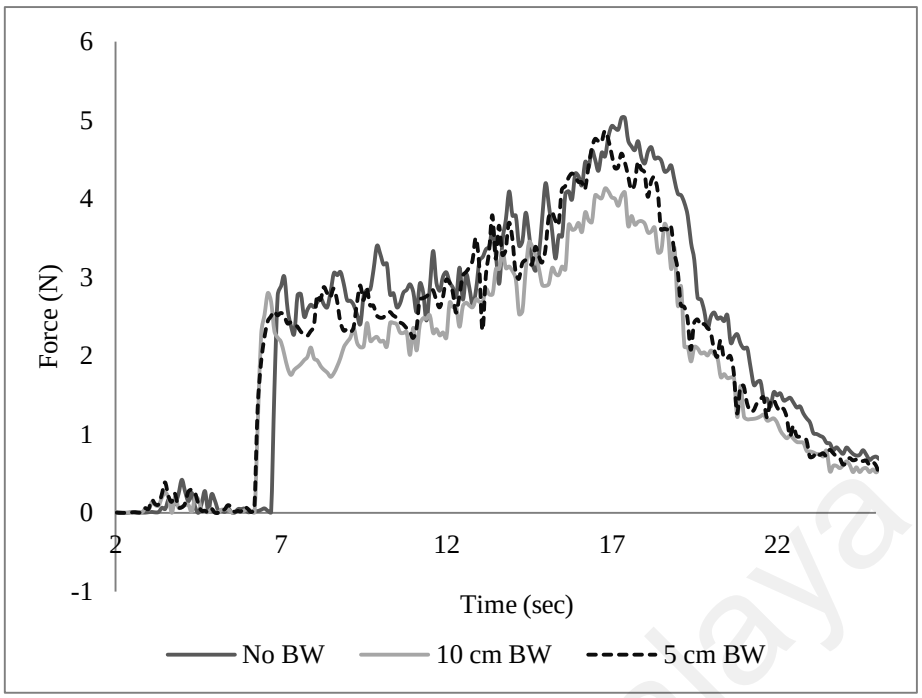

Figure 4.14: Comparison of forces in the solid girder bridge with 5 cm and 10 cm breakwater (h_0 = 20 cm)

Another set of tests was performed with the bridge model having perforations in the girder. The amount of force reductions in the perforated bridge girder for both 10 and 5 cm breakwater was more than those of the solid girder bridge. Results indicated that the perforations in the girder exhibit better performance than the solid girder bridge. The presence of the breakwater showed the similar result in controlling the tsunami forces on the perforated bridge girder as that of the solid girder where 10 cm breakwater was more effective in reducing the forces than that of 5 cm breakwater. Figure 4.15 showed the force time history of the perforated bridge girder at h_0 = 20 cm. In this case, about 16 % and 7 % forces were reduced with 10 cm and 5 cm breakwater, respectively. In a similar way, forces were declined at 25 cm and 30 cm reservoir depths with both types of breakwater. Table 4.4 showed the amounts of force reductions due to the presence of the breakwater.

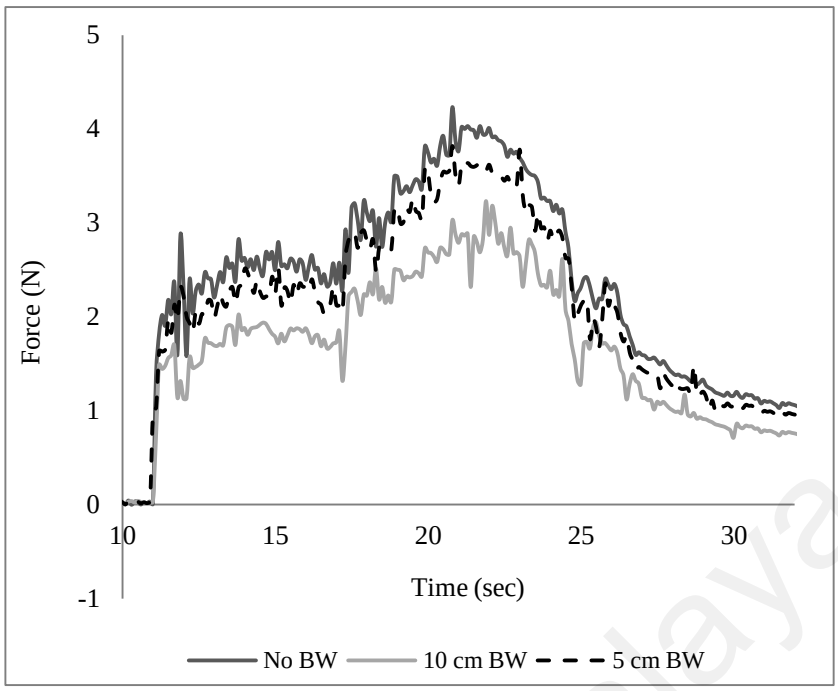

Figure 4.15: Comparison of forces in the perforated girder bridge with 5 cm and 10 cm breakwater (h_0 = 20 cm)

Table 4.4: Reduction of forces due to the presence of the breakwater

Reservoir Depth (h_0, cm)	Girder type	Force reduction with 10 cm BW (%)	Force reduction with 5 cm BW (%)
30	Solid	6.82	1.27
25		7.06	1.57
20		11.13	3.3
30	Perforated	9.28	2.99
25		13.7	3.46
20		16.17	7.21

4.3.2 Building Structures

4.3.2.1 Analysis of Tsunami Forces on the Building Structures

The horizontal forces exerted on the building model in the direction of the flow were measured using the load cell. The force time histories for various upstream reservoir depths (h_0 = 30 cm, 25 cm, 20 cm, 15 cm) were portrayed in Figures 4.16 and 4.17. It was to be noted that reservoir depths were denoted by h_0 in these figures. There was a sharp increase in force at the instant when the waves hit the upstream face of the model structure. This type of situation was observed with each of the cases having different reservoir depths. This abrupt rise of the force in the force time history could be termed as surge force or the initial impact force. The measured surge forces were 15 N, 13 N, 6.2 N and 4.5 N with reservoir depths of 30 cm, 25 cm, 20 cm, and 15 cm, respectively. After that, this initial impact force reduced to a certain level and then it again started increasing up to nearly constant value. The reduction of initial impact forces ranged from 54 % to 70 % for h_0 = 30 cm, 25 cm, and 20 cm. However, for h_0 = 15 cm, this drop of force was approximately 29 %. The approximate constant value in the force time history corresponded to the quasi-steady state of the flow when the wave had surrounded the model structure. This form of flow could be matched with turbulent flow situation and the associated force could be termed as hydrodynamic (drag) force. For the evaluation of the tsunami forces on the structures, the most important unknown is the surge forces, whereas hydrodynamic force could be estimated from the turbulent flow regions. From the Figures 4.16 and 4.17, it was found that surge forces due to the initial impact of the waves were more than the hydrodynamic forces which were caused due to the passing flow with reservoir depths of 30 cm, 25 cm and 20 cm, respectively. Nevertheless, the opposite was true for smaller reservoir depth (h_0 = 15 cm). The steeper slope of the wavefront made surge force value higher than the hydrodynamic force value. This situation was agreed well enough by Ramsden (1993). Therefore, it could be

said that, for a square structure, hydrodynamic forces are crucial for smaller water depths, however, surge forces become more critical as the water depths increases. It should be noted that, the present experimental program was conducted with limited reservoir depths. Additional testing with larger reservoir depths will provide a better understanding of the tsunami force components on the structures.

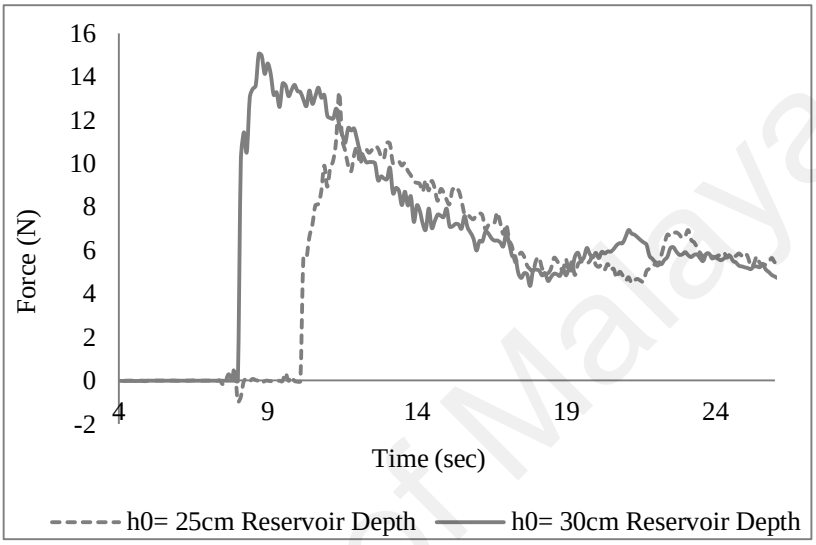

Figure 4.16: Time history of forces exerted on the building structures with 30 cm and 25 cm reservoir depths

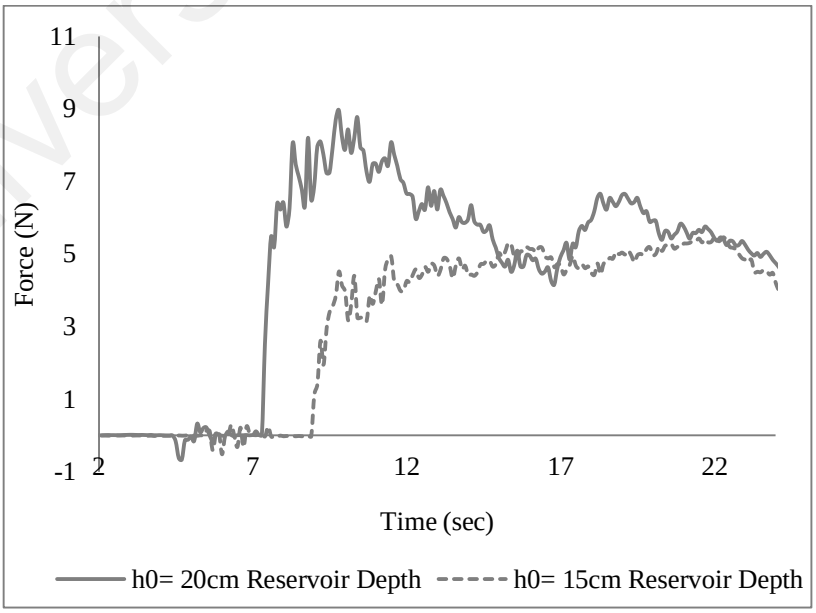

Figure 4.17: Time history of forces exerted on the building structures with 20 cm and 15 cm reservoir depths

Figure 4.18 represented the time history of forces and wave heights with h_0 = 15 cm. Here, the measured surge forces were compared with the calculated values obtained from Equation 2.4. Using the wave height value at the instant when the water flow hit the model and the width of the model, the surge force was about 9.55 N. This value overestimated the recorded value of the surge force of 4.5 N. Another approach of estimating surge forces was done using the Equation 2.5 where surge forces were considered as the combination of hydrostatic and hydrodynamic forces (Palermo et al., 2009). Velocity *u* was calculated using Equation 2.7. The Coefficient value *C*, was taken as 2 according to FEMA 646 (FEMA, 2008). Using equation 2.5, the surge value came 8.49 N, which correspondingly overestimated the recorded value. Here, the hydrodynamic force component was very much larger than the hydrostatic force component. Such enlarges divergence occurred mainly due to the high velocity of the front edge of the wave (Yeh et al., 2005). Nonetheless, the both equations still overestimated the documented value; they gave improved guidelines and predictions on estimating the surge forces.

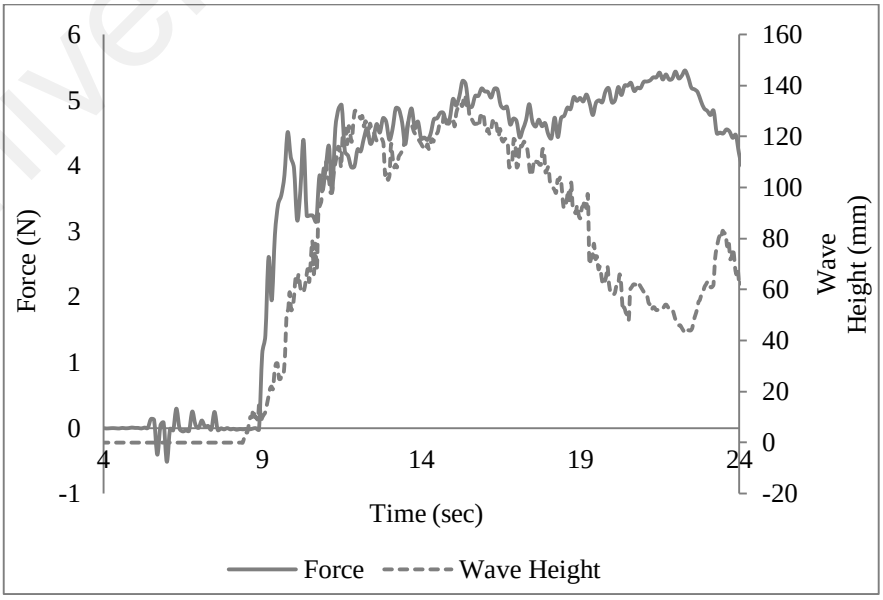

Figure 4.18: Time history of force and wave height with reservoir depth of 15 cm

The evaluation of hydrodynamic forces using Equation 2.3 provided useful recommendations for the estimation of velocity of the flow while they were passing around the building model. Several approaches were identified that investigated the velocity measurement during the quasi-steady state of flow condition. These are FEMA 55 (FEMA, 2005), FEMA 646 (FEMA, 2008), CCH (CCH, 2000). All of the methods considered Equation 2.7 to compute velocity of the turbulent flow with different coefficient values. According to FEMA 55 and FEMA 646, the recommended C_D (drag coefficient) values for calculating hydrodynamic forces were 1.25 and 2, respectively. Figure 4.19 showed the comparisons of the recorded wave forces with values obtained from FEMA 55 and FEMA 646 methods.

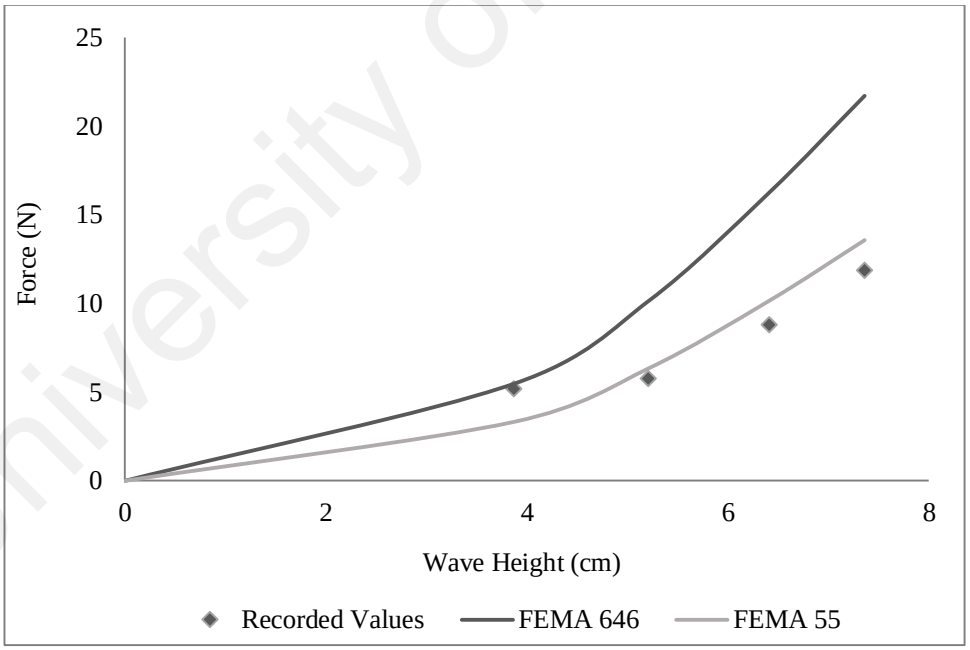

Figure 4.19: Tsunami forces on the building model with different wave heights

The measured hydrodynamic forces were 11.85 N, 8.77 N, 5.76 N and 5.19 N with 30 cm, 25 cm, 20 cm, and 15 cm reservoir depths, respectively. Using the recorded force

values and corresponding wave height values (7.36 cm, 6.41 cm, 5.21 cm, 3.87 cm), in Equation 2.3, the values of drag coefficient (C_D) were found to be 1.09, 1.08, 1.23, and 1.95, respectively. The average C_D value was 1.31 which was very close to FEMA 55 (FEMA, 2005) suggested value; however, it was much lower than FEMA 646 (FEMA, 2008) value. This was portrayed in Figure 4.19. The main reason for the small value of C_D was due to the limited height of the building model. This smaller height model was easily overtopped by the waves, thus it was difficult to idealize the full impacts of the waves during the turbulent flow condition. The overflowing waves did not contribute to the force measurement. In order to examine the effect of full wall height, it could be recommended that model height should be 3 to 4 times the water depth near the area of interest. In that case, model structures will be slightly overtopped by the waves and the full phase of the hydrodynamic condition could be captured subsequently. Triatmadja and Nurhasanah (2012) adopted another different bulk coefficient (C_f) in measuring the average forces exerted on the building model. They combined the component of both impact and drag forces in Equation 4.8.

$$F = C_f \rho A u^2 \tag{4.8}$$

In the present experimental program, estimated C_f values were 0.55, 0.54, 0.57, and 0.976 for the reservoir depths of 30 cm, 25cm, 20 cm, and 15 cm, respectively. A higher ratio between the building heights to wave heights leads to higher C_f value where the full impact of the waves could be realized.

The experimental results were compared with the predicted values determined from different formulas in Figure 4.20. The graph showed that the experimental results conformed to Triatmadja and Nurhasanah (2012) formula and as the F_r increased, there was no significant difference between the experimental data and the values obtained from the formula. According to FEMA 646 formula, with increasing F_r value, the ratio

between F_{Exp} and $F_{Formula}$ reduced, which indicated that recorded forces became lower as compared to the calculated values. The almost similar trend was observed for FEMA 55 formula, except at lower reservoir depths. Nonetheless, FEMA 55 and FEMA 646 formulas over predicted the experimental data; at smaller wave height FEMA 55 under predicted the experimental value.

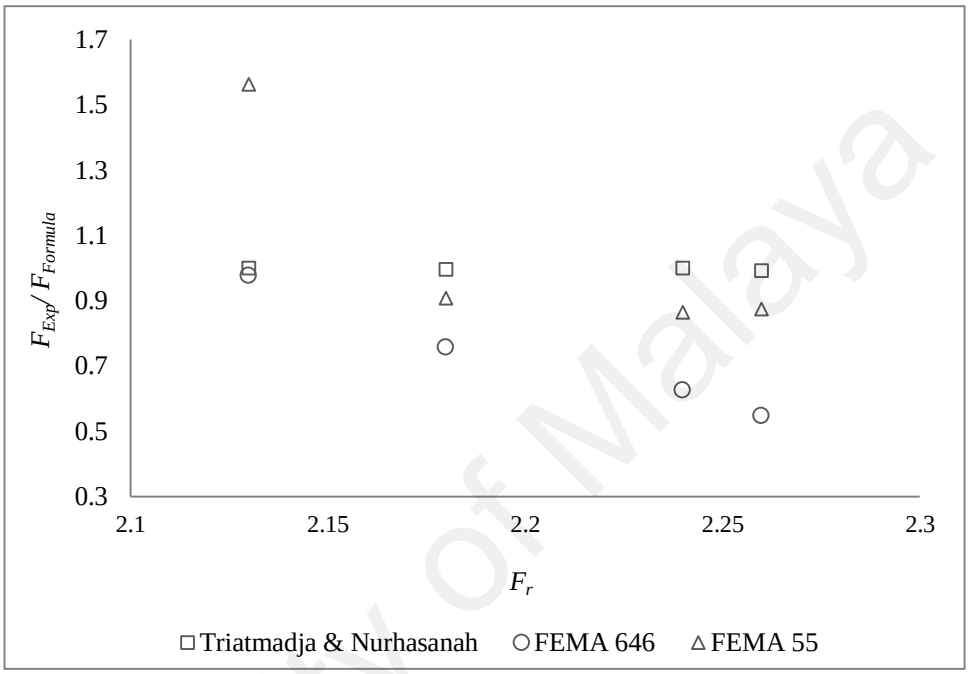

Figure 4.20: Comparison of observed force values with other formula values

4.3.2.2 Effects of Openings in the Building Structures

The effects of various openings present in the building structures were evaluated with the consideration of different size holes in the model structures. Practical buildings always have openings (windows, doors etc.) in their shape that may affect the magnitude of the tsunami forces exerted on the building structures. Size of such opening in the building has a high influence on the exerted forces of the tsunami flows. In the present experimental cases, openings were adjusted to symmetrical on both the front and rear face of the building model in the direction of the tsunami flow. The amounts of openings were identified by the following Equation (4.9).

$$\eta = \frac{A_0}{A} \tag{4.9}$$

Where A_0 is the area of the opening and A is the area of the front face of the building model. Two different opening sizes were considered, viz. 30 % and 60 %. Measured forces were compared with the baseline conditions where building model was considered without any opening. Results showed that subsequent reductions in the forces were achieved with the presence of the openings. Approximately 10 % to 42 % of forces were reduced with 30 % opening, whereas 22 % to 65 % declinations of forces were obtained from 60 % opening. Table 4.5 showed the results obtained from different reservoir depths. From Table 4.5, it was found that forces were reduced more significantly with 60 % opening than that of 30 % opening. Therefore, opening size plays an important role in the reduction of the tsunami forces. Thus, larger openings in the building model provide more safeguard against the tsunami forces in the coastal region. The benefit of using the opening in the building structure considering their contribution in the force reduction was illustrated in Figure 4.21. The presence of the opening allows water to pass through the opening, thus creating counteracting forces inside the building and contributes in the force reduction.

Table 4.5: Reduction of forces on building model with different configuration

Reservoir Depth	Force (N) with 0 % Opening)	Force (N) with 30 % Opening	Force (N) with 60 % Opening	Force Reduction in 30 % Opening	Force Reduction in 60 % Opening
30	9.94	5.74	3.45	42.25	65.29
25	5.37	4.74	2.59	21.04	51.77
20	4.51	3.42	2.21	16.63	50.99
15	2.43	2.42	1.9	10.29	21.81

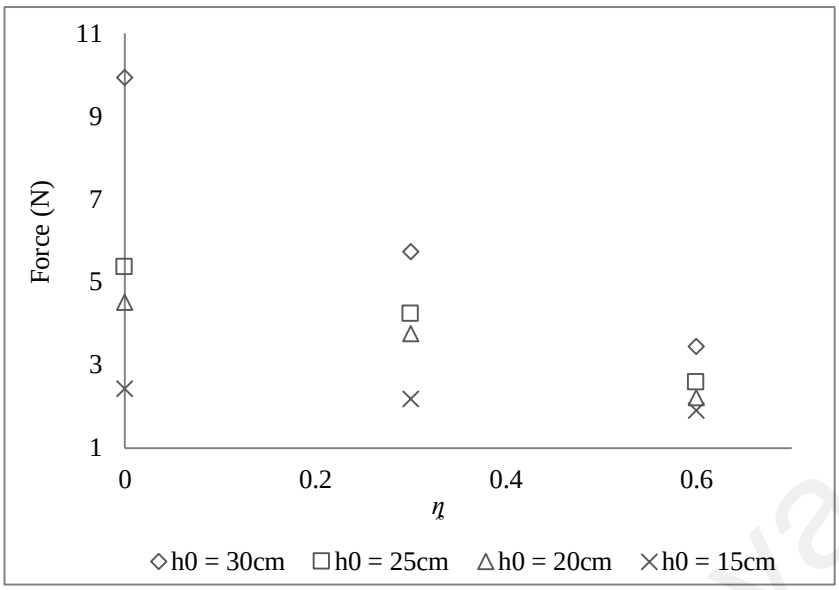

Figure 4.21: Force reduction with different opening sizes.

The sequences of wave impacting the building model with opening were illustrated in Figure 4.22. During experiments, it was observed that when the waves hit the building model, they strongly splashed from the front face of the model. The splashing was stronger for a smaller opening than that of larger opening. The waves entered the building model through the opening and went out from the rear face as a jet. The velocity of flowing water through the opening was substantially smaller than the velocity of the flow passing beside the building model. From visual observation, it was found that the jet flowed out from the back side of the model and reached about 7 to 8 cm distance behind the model for 30 % opening, whereas, the waves passing beside the model reached about 16 cm behind the model. A similar trend was observed for 60 % opening. In this case, the distance that the jet reached behind the building model was more in magnitude. With 60 % opening, the splashing of waves on the model was considerably low; however, the speed of the water was as same as the flow passing beside the model. At smaller opening (η), there was a noteworthy change in momentum when the waves hit the model. At larger opening (η), the change in momentum was comparatively less, thus resulting in lower forces inside the model.

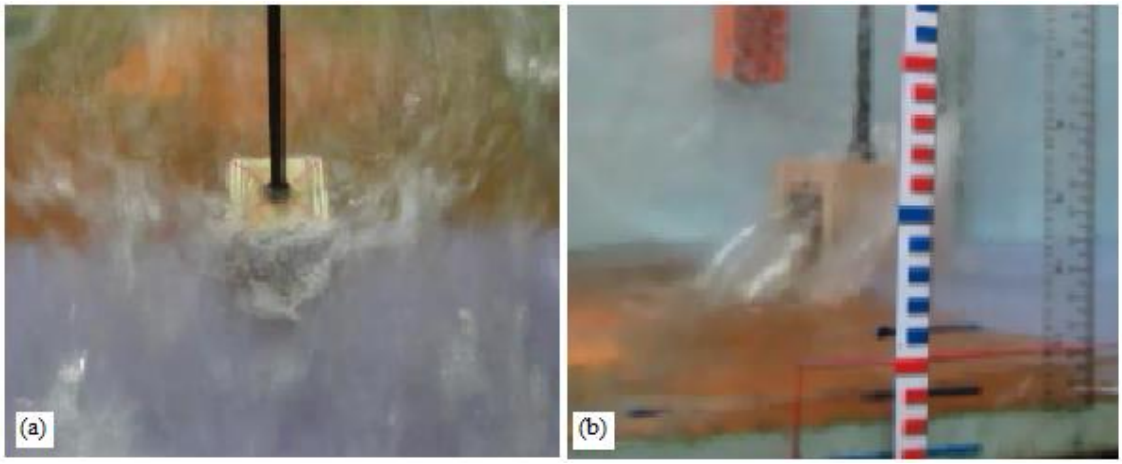

Figure 4.22: Tsunami waves hit the building model: (a) front side; (b) back side

The results of the present experimental cases were compared with Lukkunaprasit et al. (2009) and Triatmadja & Nurhasanah (2012) values, as the model used by them were almost similar in shape with the present experimental case. Lukkunaprasit et al. (2009) considered 25 % and 50 % opening, whereas Triatmadja & Nurhasanah (2012) used box models with various opening sizes ranged from 7.5 % to 80 %. The results were showed in Figure 4.23. In all of the cases, forces were reduced due to the increase of the size of the opening (η). Figure 4.23 also illustrated that the reductions of forces (Δ) were not linearly related to the opening size (η). At lower opening (η), force reductions (Δ) were lower; with increasing opening size (η), force reductions (Δ) also increased. The results from the present experimental cases agreed well enough with the trends of reductions observed by Lukkunaprasit et al. (2009) and Triatmadja & Nurhasanah (2012). Several tests were performed in order to identify the effects of the partition wall on the exerted forces that was placed inside the building model. The width and height of the wall was 4 cm and 8 cm respectively. Experimental results revealed that the presence of the partition wall significantly reduced the effectiveness of the openings. The flowing water entered the building model through the opening, and then deflected by the partition wall. This occurrence created additional forces on the model. Therefore, it can be said

that, partition wall in any coastal building should be designed in such a way that it would not create any hindrance to the effectiveness of the opening and could be easily washed away by the tsunami flow.

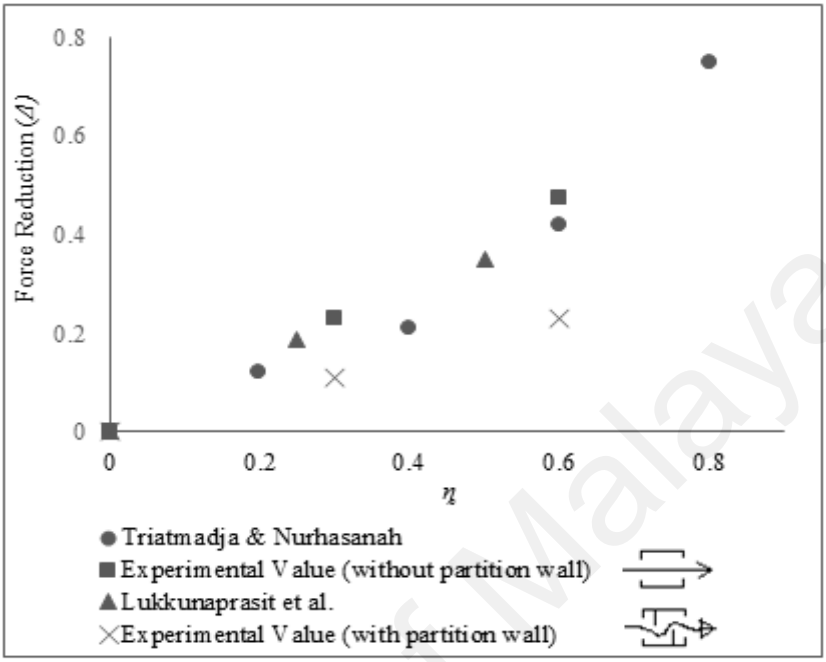

Figure 4.23: Reduction of forces with different openings

4.3.2.3. The Coefficient of Drag Forces on Building with and without Opening

The coefficient of drag (hydrodynamic) forces C_D, of tsunami waves on any building structures is highly influenced by the percentage of opening present in the building structures. Table 4.6 represented the values of C_D, where higher C_D values were found for solid building model (without any opening). Due to the presence of the opening, water passed through it and the speed of the flow inside the opening was not as large as the surrounding waves and hence, the exerted forces were also lower. Thus, lower forces resulted in lower C_D values.

Table 4.6: C_D values on building model with different configurations

Building Model	C_D
0 %	1.09-1.68
30 % opening	0.68-0.89
60 % opening	0.48-0.59

4.3.2.4 Evaluation of Tsunami Forces on Building Model Fronted by Seawall

The experiments were performed to quantify the reductions of the forces on a solid building fronted by a small seawall. Seawall height, wall position, seawall configuration and reservoir depths were varied throughout the experimental period. Tsunami like waves were produced from dam-break mechanism which propagated abruptly along the flume (Chanson, 2006). An experimental time series data set measured at wave probe 4 (W4) with walls of two different heights in position 1 (x = 3.75 m from the gate) considering h_0 = 30 cm, were presented in Figure 4.24. Waves were transmitted over the seawall (solid-wall 1 and dotted- wall 2) and data were recorded by the wave probe. From this figure, it was found that as the seawall height was increased, the wave height near the building model decreased. Another experiments were performed by placing these walls in position 2 (x = 3.50 m from the gate). The decreasing trends of the wave height corresponding to wall height were similar to Figure 4.24, however, the wave height reduction rates for both of the walls were smaller relative to position 1.

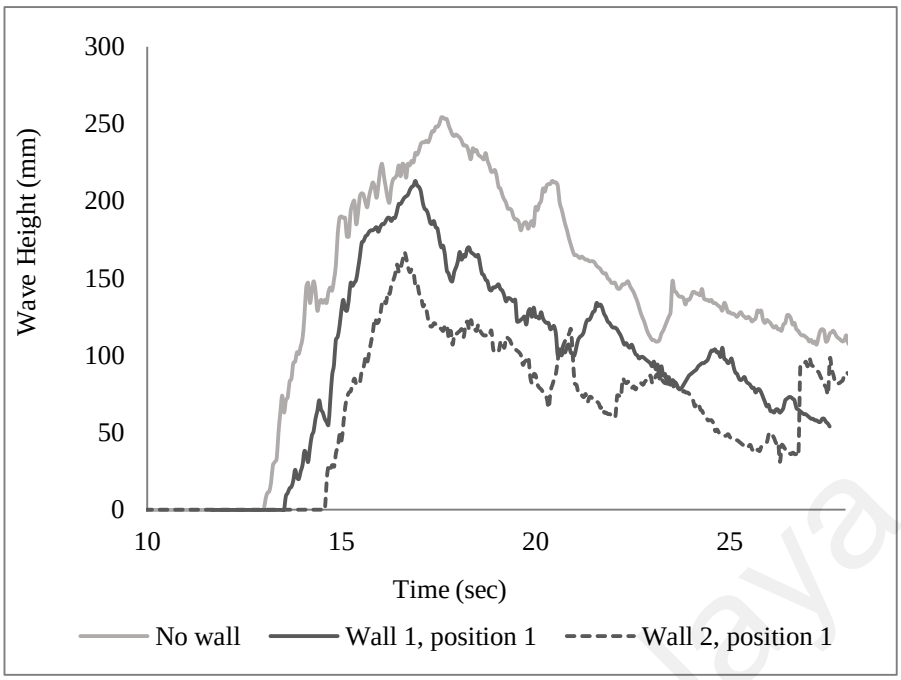

Figure 4.24: Time series of wave height for wall 1 and wall 2 in position 1 (x = 3.75 m from the gate)

Figures 4.25 and 4.26 showed the horizontal force time histories measured by the load cell attached to the building model at a reservoir depth of 30 cm. The graphs showed that there were sharp rises of forces resulting from the initial impact of the wavefront. This force was termed as surge force (initial impact force) and followed by a quasi-steady force. This fact was agreed well with the previous researches (Fujima et al., 2009; Oshnack et al., 2009; Thomas & Cox, 2011). These initial impact forces (surge force) were higher than the hydrodynamic forces for both no wall and seawall conditions at higher reservoir depth. Steeper slope of the wavefront was mainly responsible for this higher value as the exerted forces were highly dependable on the front slope (Ramsden, 1993). With decreasing reservoir depths, hydrodynamic force could overshoot the initial impact forces for all of the cases. The effectiveness of using the seawall was also presented by Figures 4.25 and 4.26. In general, results showed that the presence of the seawall reduced the forces significantly on the model. Nonetheless,

wall height was an important parameter in computing the force reductions. For both positions, forces were decreased with increasing seawall height, however, the reduction rate was more apparent for position 1 (seawall that was placed closer to the building model) than that of position 2. Figure 4.25 showed that maximum force for wall 2 in position 1 was about 59 % of the total force measured with no wall condition. Thus, 41 % of the total forces were declined by wall 2. The reduction of forces for wall 1 showed a similar trend as that of wall 2 whereas maximum reduction was about 27 %. In addition, Figure 4.25 showed that wall 1 exhibited sharp peak force while this was not significant for wall 2. The results revealed that higher the seawall height, lower was the forces on the model as well (Figure 4.27). Besides force reduction, seawall also caused reflection of the incoming waves over the tested wave conditions. The more the height of the seawall, higher the reflection of the waves. Though wave heights as well as forces were reduced in the presence of the seawall, the reduction was not proportional between them. The changes of the forces with seawall relative to no wall conditions were more apparent than those of the reductions of wave height near building structure comparable to no wall condition. Therefore, it could be said that wave height near to a structure fronted by a seawall could not be a good predictor of tsunami forces.

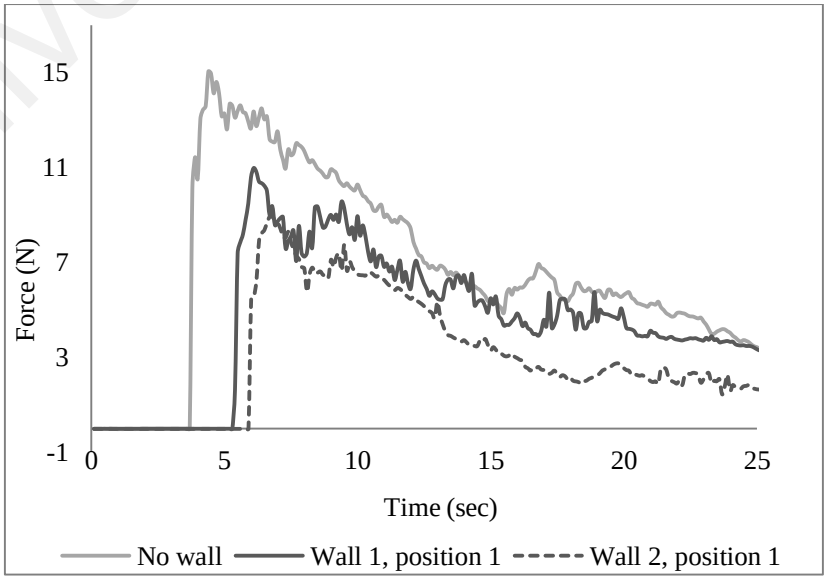

Figure 4.25: Force time history with seawall 1 and seawall 2 placed in position 1

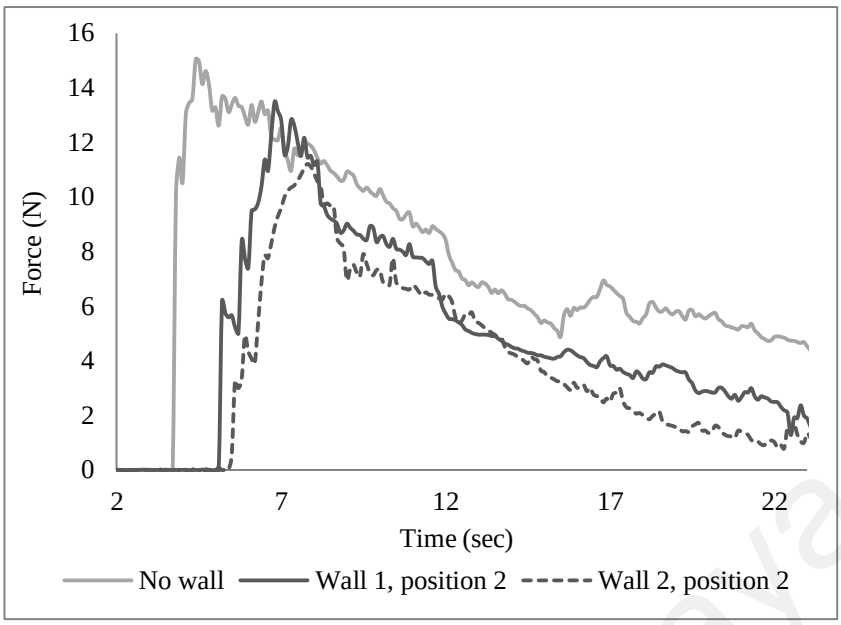

Figure 4.26: Force time history with seawall 1 and seawall 2 placed in position 2

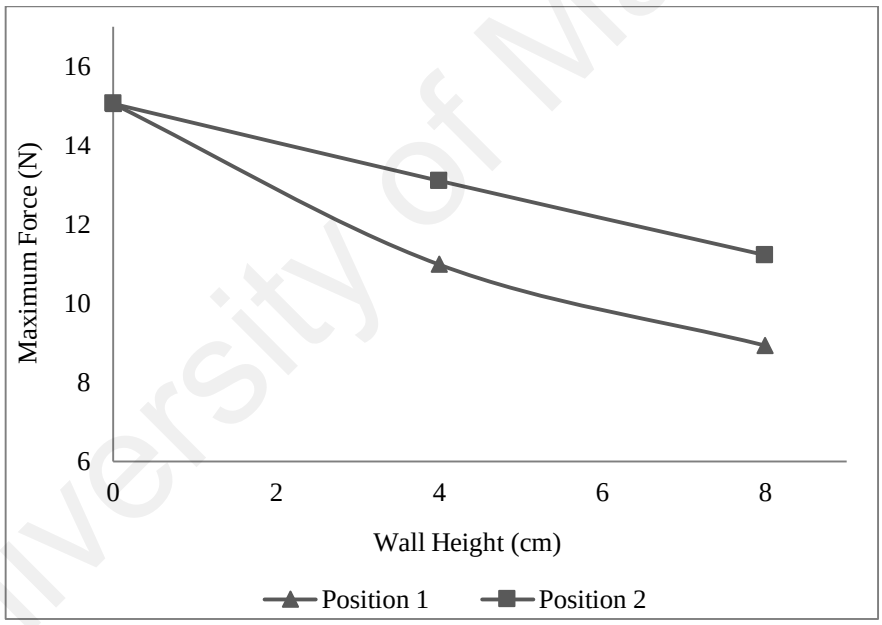

Figure 4.27: Changes of maximum forces with seawall height

Another set of tests was performed placing wall 1 and wall 2 in position 2 (Figure 4.26). The results showed that the trends of lessening of the forces were almost similar as that of position 1, whereas values in position 2 were smaller than that of position 1. The values of force reductions were 13 % and 25 % for wall 1 and 2, respectively. This fact indicated that a seawall at position 1, which was closer to the model was more effective

in reducing the forces. The result could be approximated clearly by Figure 4.28 where variation of the maximum forces with wall 1 and wall 2, relative to no wall condition were presented as a function of dimensionless ratio *x/L*. The graph showed that the forces reduced as the wall height increased over the range $0.5 < x/L < 0.9375$ m at h_0 = 30 cm. As the walls moved closer to the model, forces were decreased. The almost same trends were found with other wave conditions. This was indeed more evident with larger seawall i.e. for the case with wall 1 (larger seawall) where the reduction factor ranged from 0.95 (5 % reduction), when the wall was located far away from the building model to 0.59 (41 % reduction), when the wall was placed very close to the model. Therefore, seawall with adequate height locating in proximity to a structure was proved to be effective in the force reduction and could provide more protection. On the other hand, if the wall height is small and placed much closer to the structure, there might have detrimental effects on the upper floor of the structure due to the localized force and large reflection. This study requires further investigation.

Figure 4.29 showed the changes of the forces with respect to the variety of wave heights. As expected, forces were increased due to the increase in the wave height. This escalation of forces was more significant in no wall condition than those of conditions with wall 1 and wall 2. Higher seawall subsequently reduced the forces over all of the tested wave height conditions.

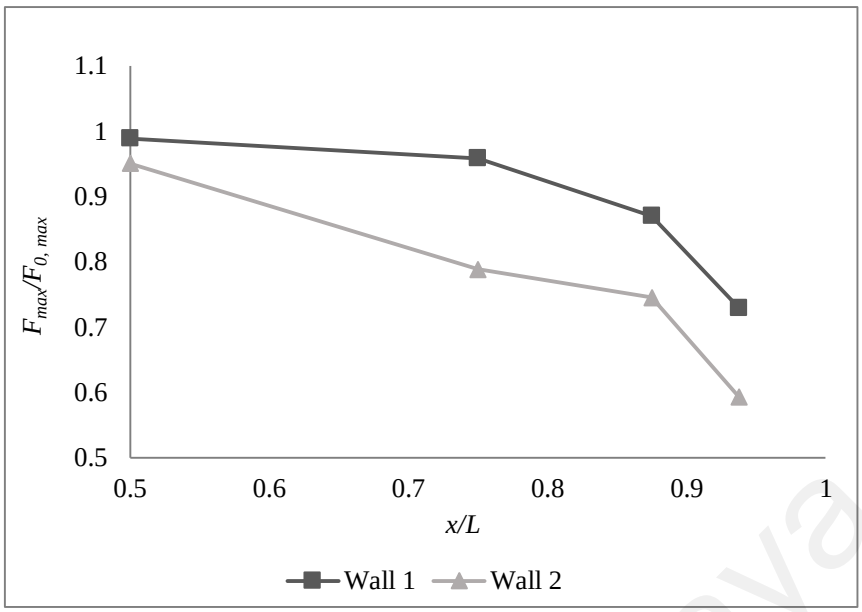

Figure 4.28: Force reductions by seawalls

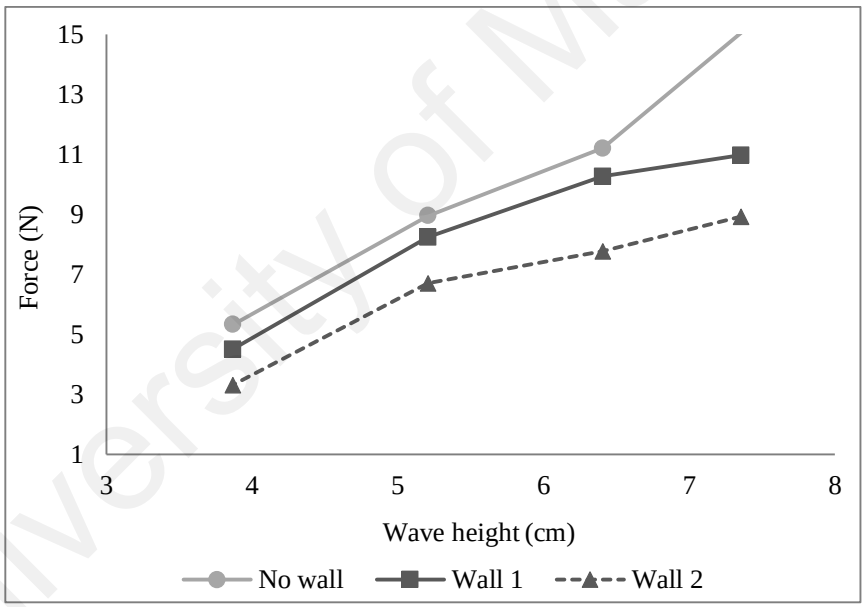

Figure 4.29: Maximum force as a function of the wave height

Another set of experiments was performed with perforated seawall placed in position 1 (x = 3.75 m from the gate). The results from this arrangement were compared to no wall condition and wall 2 condition. In comparison to the solid wall, perforated wall is inexpensive to construct. Moreover, in case of solid seawall, when overtopping of the wave occurs, receding water cannot directly go back to the sea and remains stuck

behind the solid wall that creates additional forces to any structure located nearby. In that case, perforated wall performs well as it could allow a significant amount of water to recede through the perforations. This study included the verification of the efficiency of the perforated wall in the force reduction relative to the solid wall. The contribution of the perforated wall was almost similar to a solid wall and hence, perforated wall could replace the solid one successfully. Wave height along with the force time histories were considered for comparison purposes. Figure 4.30 showed the comparison of the wave height time history data set between two different configuration walls (solid and perforated) relative to no wall condition. The trend of changes in wave height with time was somewhat similar between the solid wall and the perforated wall condition with few exceptions. In both cases, the measured wave heights were smaller than no wall condition. This statement indicated that the presence of the seawall decreased the wave height monotonically near the model whereas the reduction rate of the perforated wall was as satisfactory as the solid wall. The variations of force time histories with solid and perforated seawall was presented in Figure 4.31. In general, solid and perforated seawall provides subsequent protection compared to no wall condition. The graph (Figure 4.31) showed that the perforated wall did not exhibit any sharp rise in the force time history as that of a solid wall (both are placed in position 1) and the initial impact force was more than the hydrodynamic forces. The maximum force with the perforated wall was 65 % of the total forces. Hence, 35 % of force reduction was achieved when the perforated seawall was placed in position 1 instead of the solid wall which provided 41 % of the force reduction. Comparing the amount of force reduction, the perforated wall provided nearly similar protection as that of a solid wall over the tested wave conditions at position 1. Thus, it could be stated that for this particular test conditions, the perforated wall could be proved to be as successful as the solid wall. Perforated seawall is preferred to be used in lieu of a solid wall owing to the cost effectiveness.

Moreover, perforated wall allowed easy declining of water that go back to the sea, while solid wall trapped the coming water behind and thus, creating additional forces on the building. As the performances of both walls were quite satisfactory, lower construction cost enables the researchers to develop the perforated wall rather than a solid wall as the tsunami protection structures. It should be noted that the results of this study were appropriate for this particular type of setup as the distance between the seawalls and the building structures plays a very crucial role in the declination of the forces.

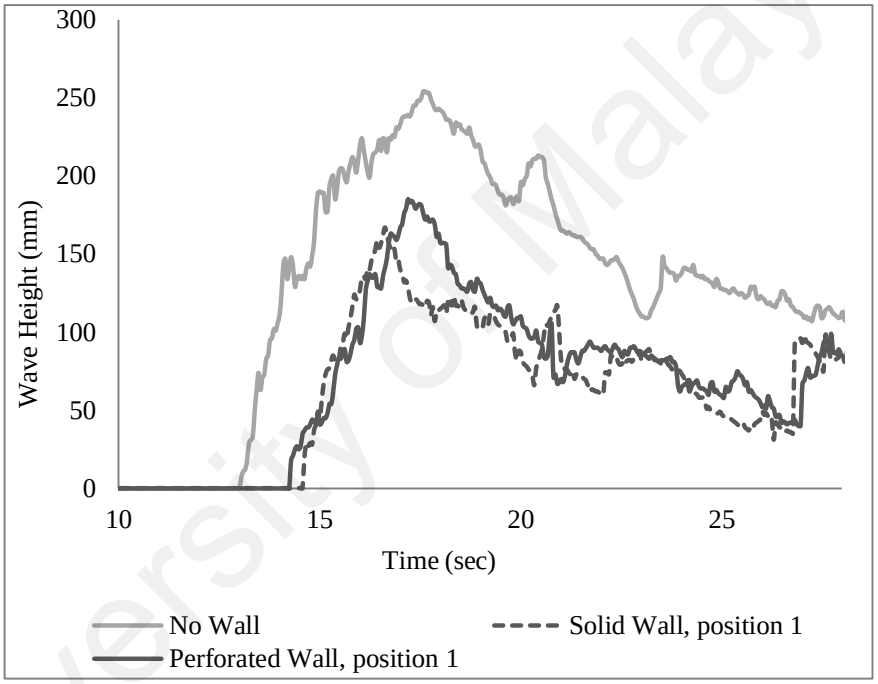

Figure 4.30: Comparison of wave height time history data set of solid and perforated seawall in position 1 with no wall condition

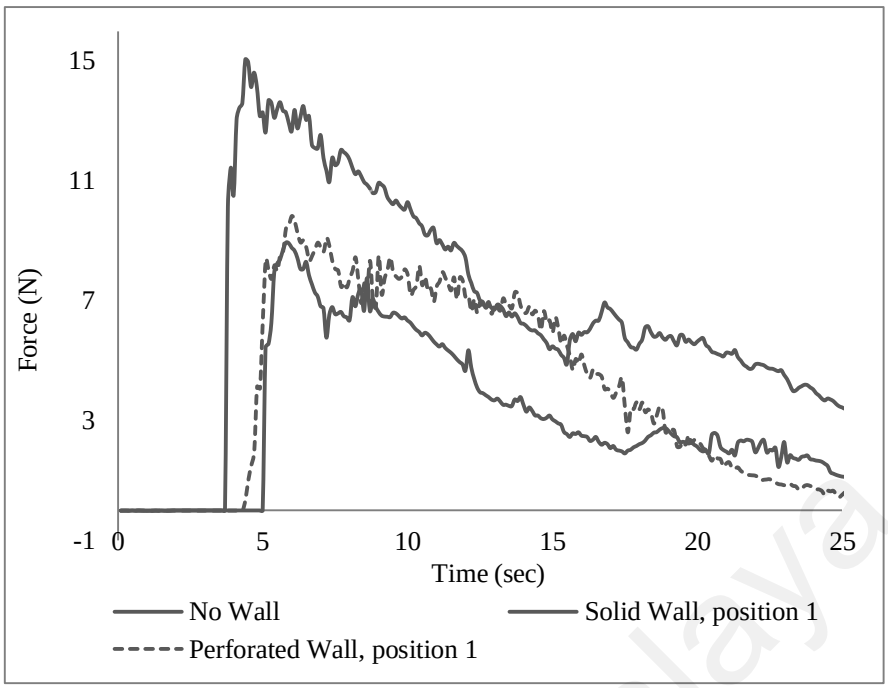

Figure 4.31: Comparison of force time history data set of solid and perforated seawall in position 1 with no wall condition

4.3.2.5 Effects of Different Size Upstream Barriers on the Building Model

The present section evaluated the experimental results of the effects of the barriers on the tsunami forces exerted on the building model. In order to quantify the effects of the barriers, three different size barriers were placed one by one at three different locations in front of the building model, viz., position 1, d_1 = 5 cm (d = Distance from the rear wall of the barrier to the front wall of the building); position 2, d_2 = 10 cm and position 3, d_3 = 15 cm. The barriers were moved along the centerline of the flume upstream of the building model. In each case, the tsunami forces were measured in the horizontal direction. The effectiveness of using the barriers was analyzed through their contribution in the reduction of the forces exerted on the building model. This section demonstrated the amount of protection achieved by the barriers. The benefits of the barriers highly depend on their shape, their length along the flow direction and the distance between the barrier and the building.

The time histories of the forces with and without different barriers placed in position 1 (d_1 = 5 cm) and position 2 (d_2 = 10 cm) with a reservoir depth of 15 cm (h_0 = 15 cm) were shown in Figures 4.32 and 4.33, respectively. Comparisons were made among the building with no barrier and the building with different barrier conditions. The general trend of the time variation of the measured forces under different barrier conditions remained almost constant (Figures 4.32 and 4.33). From Figure 4.32, it was found that a substantial amount of the forces were reduced with the presence of the barrier in front of the building model. In this case, barriers were placed very close to the model building (d_1 = 5 cm). The force reductions, for different barriers placed alternately in position 1 (d_1 = 5 cm), ranged from 20 % to 52 % and the highest amount of reduction in the forces were achieved from the barrier 3 placed in position 1. This graph also pointed out that there was an abrupt rise of the forces without the barrier condition due to the sudden impact of the wavefront. However, this was less significant with the barrier conditions, as the wavefront was faced by the barrier initially and then hit the building model. As the presence of the upstream barriers affected the leading edge of the approaching wave, the changes in the forces on the building model were more obvious at the initial impact. Figure 4.33 showed the force time histories with barriers placed in position 2 (d_2 = 10cm). This graph showed that, a significant amount of the forces were reduced by installing the barrier in front of the building model. However, the reductions of the forces with the barrier located in the position 2 (d_2) were less noteworthy compared to the barriers placed in the position 1 (d_1). This information indicated that the barrier with sufficient size and shape placed closer to the building model is more effective to provide sufficient protection against the tsunami forces. The reduction of the forces with the barriers located in position 2 varied from 28 % to 47 %. Similar to the barriers located in position 1, the highest reduction in position 2 was attained by the barrier 3. Therefore, results showed that, a rectangular barrier with

adequate height, placed closer to any building structure maintaining the thinner side along the flow direction gives better performance during any tsunami event.

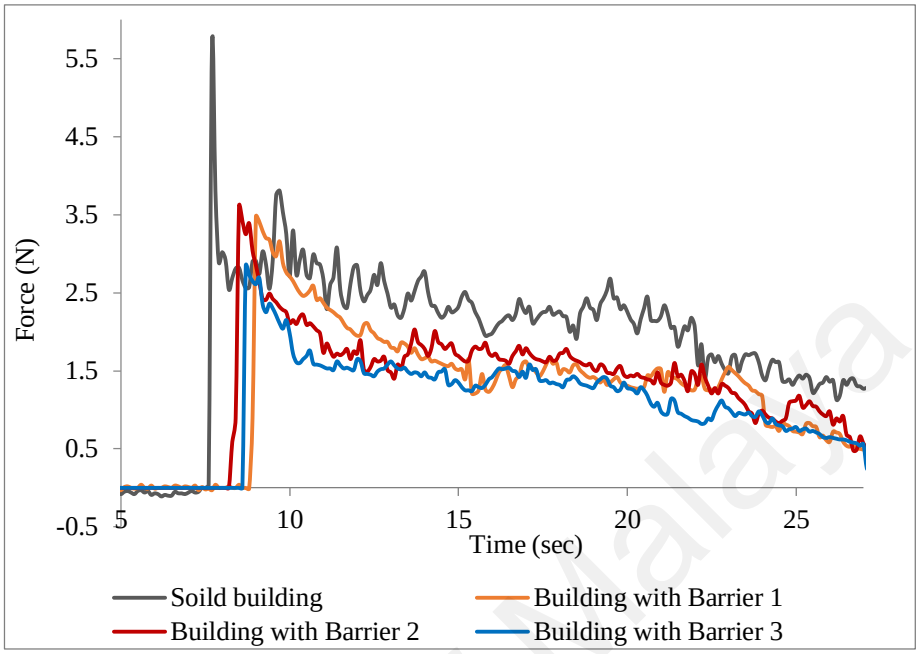

Figure 4.32: Time history of measured forces with barriers placed in position 1 (d_1 = 5 cm) for h_0 = 15 cm

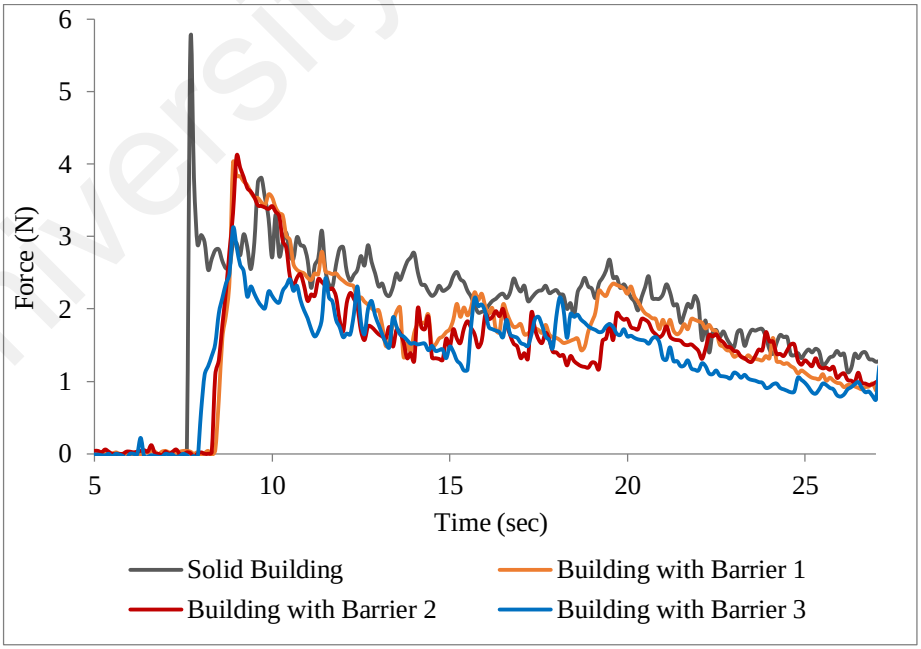

Figure 4.33: Time history of measured forces with barriers placed in position 2 (d_2 = 10 cm) for h_0 = 15 cm

During the experiment, significant amount of deflection of the incoming waves was observed by the sideways of the barriers. Reflection of the waves from the flume wall and deflection from the barrier's side wall made the flow uneven, especially in high reservoir depth. When longer barrier is placed close to the building model maintaining its longer side in the flow direction, reflection from the waves would be more. This phenomenon eventually would affect the forces on the building model. Therefore, length of the barrier played a crucial role in measuring the forces on the model with higher reservoir depths. At a higher reservoir depth and barrier placed close to the model, thinner barrier performed well enough than other types of barrier. This fact was also agreed well with the Figures 4.32 and 4.33. For all of the cases, the barrier 3 performed well enough to reduce the exerted forces on the model compared to other types of barriers. This finding had been characterized in Figure 4.34, in which forces on the building model fronted by the barriers relative to no barrier condition were evaluated as a function of distance between the building model and the barrier. This figure showed that, forces were increased as the distance between the barrier and the model increased. The increment of forces was observed for all of the cases; however, the increase rate of force was slower for the thinner barrier (barrier 3) than those of the barrier 1 and the barrier 2.

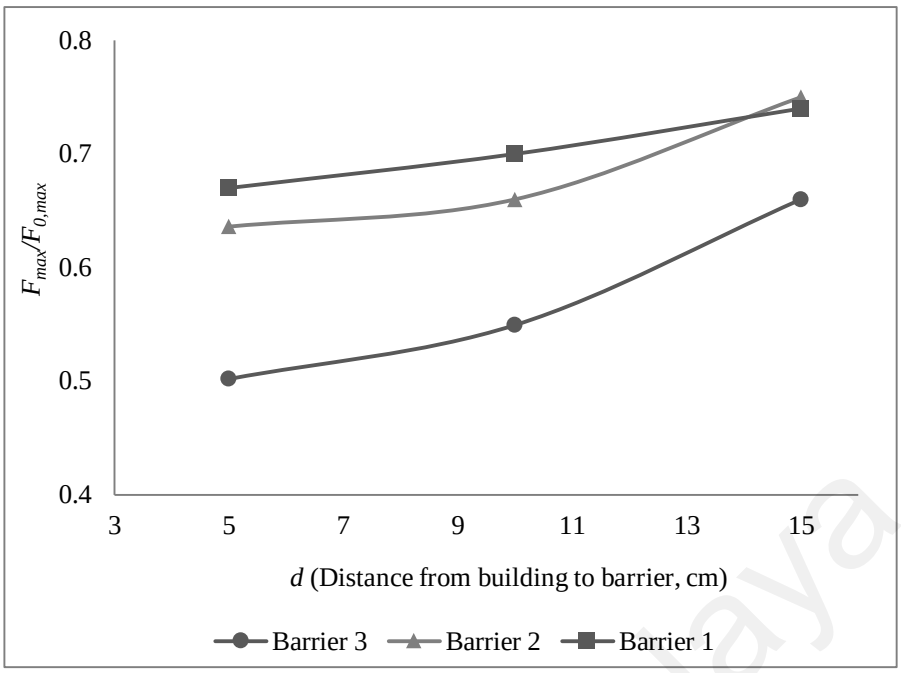

Figure 4.34: Force reductions by the barriers

Figure 4.35 showed the variation of the forces on the building model with and without the barrier conditions as a function of wave height. As expected, forces were increased with the increase of the wave heights. The rate of escalation of the forces on the unprotected building was much significant than those of the protected buildings. However, the rate of force increment of the building fronted by the barrier 3 was slower than those of the other cases with the barrier 1 and the barrier 2.

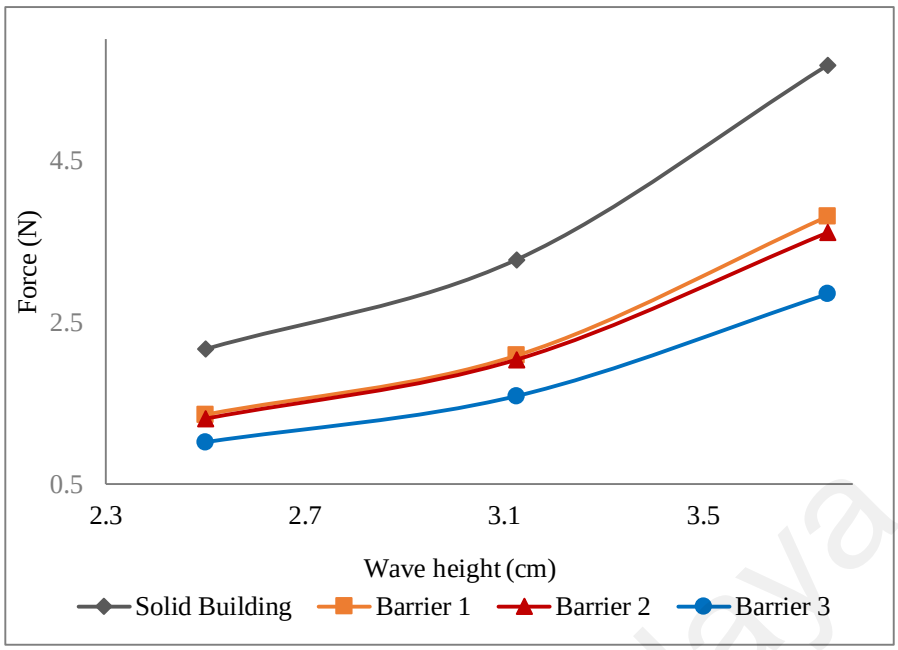

Figure 4.35: Variation of forces with wave height

In the present section, the building and the barrier models were smaller in size. The model width to flume width ratio was 3.33 %. Therefore, it was expected that the experimental results would be free from the boundary effects. Previous research results revealed that the maximum forces occurred approximately 0.3 sec to 0.4 sec after the wave hit the model (Triatmadja & Nurhasanah, 2012). Nevertheless, the maximum forces might be affected by the boundary wall and this criterion should have to be considered during the analysis of the maximum forces on the protected building model.

As the wave propagated along the flume, the presence of the barrier created some wave disturbances. Visual observations showed that, these disturbances reached the flume side walls approximately 0.5 sec after the wave hit the barrier. Then waves reflected from the flume wall and came back to the barrier site. The returning time of the reflected waves was assumed to be as same as the time required by the waves to reach the side walls. Therefore, the measurement of maximum forces on the building model should be performed at $t < 1$ sec, where t is the instantaneous time when waves hit the

building model. At $t > 1$ sec, the reflected waves increased the water level in front of the model and slowed the flow. As a result, forces on the building model were significantly influenced by the increased water level at $t > 1$ sec. In the present experiments, measurement of forces were made in t < 1 second after hitting the model. Therefore, the results were assumed to be free from the boundary affects.

Figure 4.36 showed the variation of maximum forces on the building model protected by the barrier 3 relative to the building without any protection. This force variation was evaluated as a function of the barrier distance normalized by the wave height (d/a). Data presented in the Figure 4.36 were taken at $t < 1$ sec and assuming that they were free from the boundary effects because of the use of smaller size model. The vertical axis represented the forces on the building model protected by the barrier 3 and the horizontal axis corresponded to the ratio of the distance (the space between the building and the barrier) to the wave height, which was denoted by σ.

$$\sigma = \frac{d}{a} \tag{4.10}$$

It was seen from the graph that the forces were reduced when the barrier was placed close to the building model (position 1, d_1 = 5 cm). The reduction of the forces was more significant with the barrier placed at position 1 (d_1) than those of position 2 (d_2) and position 3 (d_3). Nonetheless, the forces were decreased with increasing σ due to the decreasing of the wave height for all of the cases, the declining rate of the forces with decreasing wave height was more significant with barrier at location 1 (d_1) than those of location 2 (d_2) and location 3 (d_3). This situation indicated that the barrier located close to the building model provided better safeguard against tsunami as compared to the barrier located at the far away from the building model. The similar analysis was shown in Figures 4.37 and 4.38 for the barrier 1 and the barrier 2, respectively. In Figure 4.37,

forces were reduced due to the presence of the barrier 1 in front of the building model. However, the reduction was smaller than the case with the barrier 3. In a similar way, forces were reduced with increasing σ due to the decreasing of the wave height. The same trend was also observed with the barrier 2, whereas the reduction was not as significant as that of the barrier 3. Overall case studies indicated that a thinner barrier located near the building model provided a better protection to any coastal building at smaller wave heights.

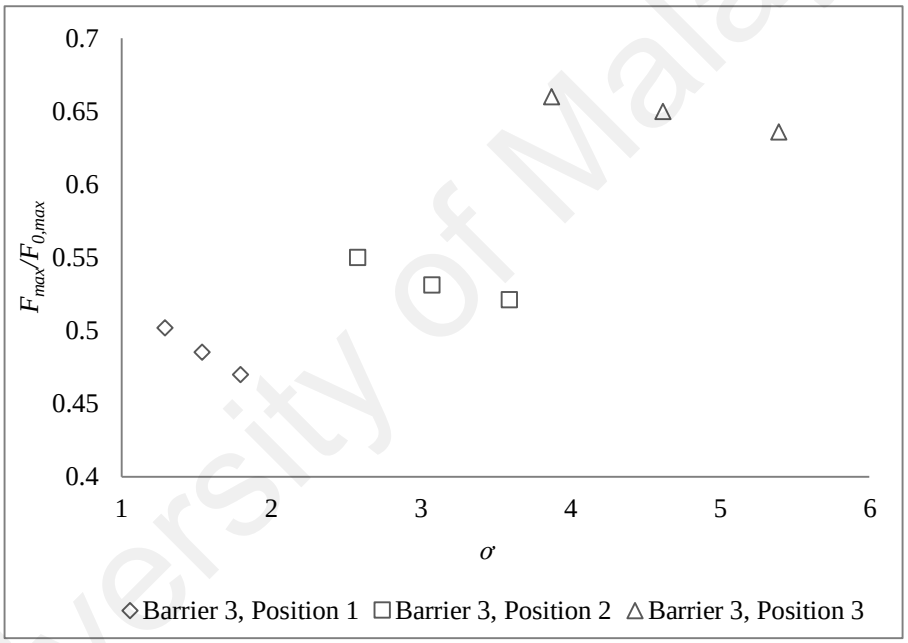

Figure 4.36: Variation of the forces with the changes of the position of the barrier 3

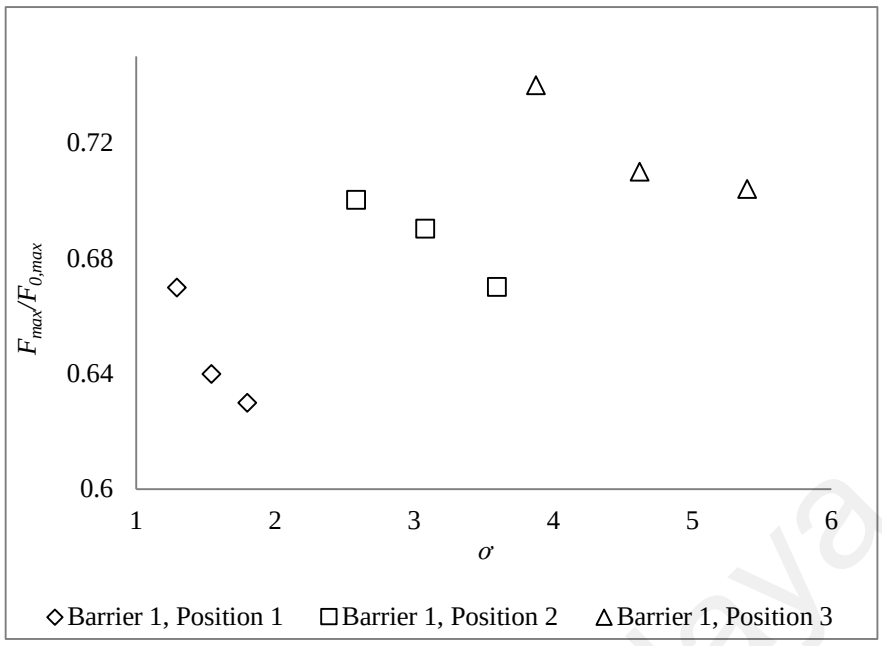

Figure 4.37: Variation of the forces with the changes of the position of the barrier 1

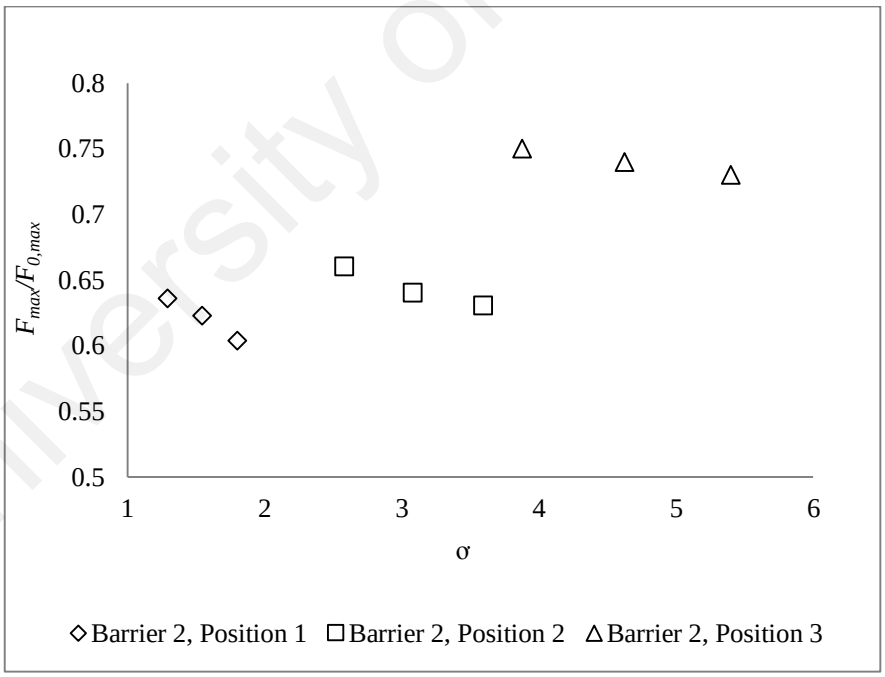

Figure 4.38: Variation of the forces with the changes of the position of the barrier 2

4.3.2.6 Effects of Different Size Upstream Barriers on Building Model With Opening

A similar set of experiments was performed with the building model having 50 % opening. In this case, model was fronted by different upstream barriers located at the three specified positions. The size of the building model was similar to the previous experiments. The only difference was that it contained 50 % opening in its shape. Here, the same barriers were used as those were used with a solid building model test. Previous experiments showed that the presence of opening reduced the forces on the building model. Figure 4.39 depicted the variation of the forces on building model with and without the presence of the barriers. As expected, forces were reduced with the presence of the opening. In this graph, forces were evaluated on the basis of the presence of different barriers at position 1 (d_1). Open building fronted by the barrier 3 provided the best defense against the tsunami forces at lower wave height among all of the cases. As described earlier, longer barrier could deflect the incoming waves that made the flow uneven and affected the exerted forces. This circumstance was more evident with larger reservoir depth compared to smaller one. As like solid building, open building with the barrier 3 located at position 1 (d_1) could reduce the forces more efficiently than the other two types of barrier placed at the same location. Similar to the solid building tests, the effectiveness of placing barrier gradually reduced as the barriers were placed far away from the building model with opening (Figure 4.40).

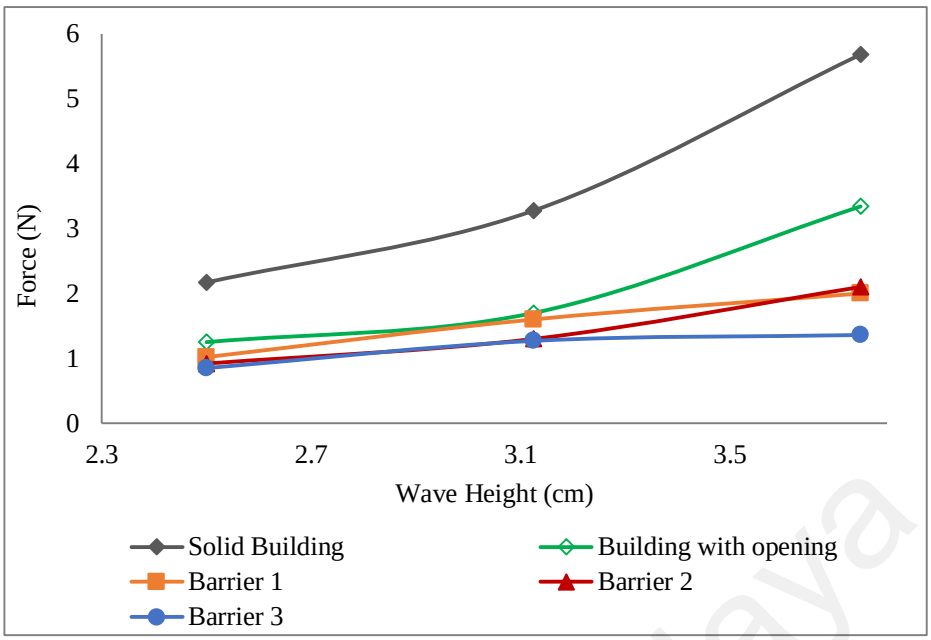

Figure 4.39: Variation of forces on the building having opening as a function of wave height

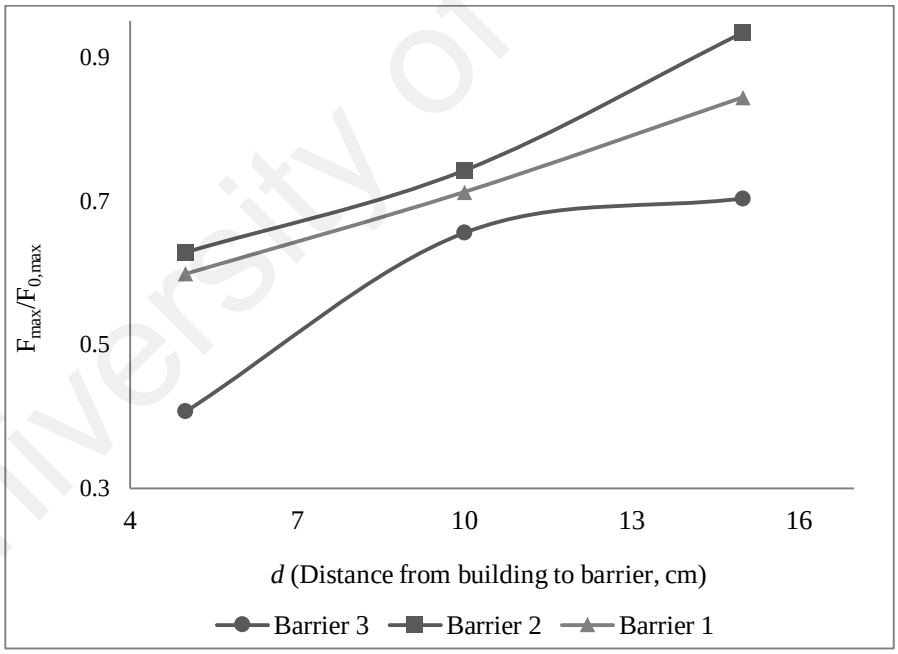

Figure 4.40: Force reductions on building model with opening by the barriers

4.4 Scaling of the Model Structures

The scaling of the experimental data obtained by the model structures to prototype conditions is always a challenging. It is difficult to scale up the obtained results in order to measure the forces in a real tsunami incident. Froude scaling is one of the widely used scaling methods for the free surface gravity flow. The Froude number is given by

$$\text{Froude Number} = \frac{u}{\sqrt{ga}} \tag{4.11}$$

Where, u is the velocity of the flow, a is the wave height, g is the gravitational acceleration. The present experiments were closely associated with the quasi-steady forces which are related to inertia. Therefore, Froude scaling is perfect to achieve the dynamic similitude. Hence, present experiments were designed to follow Froude scaling model = prototype/√[scale factor]) to maintain dynamic similarity.

As different types of model structures with different sizes were used in this present research, different geometric scaling was chosen based on the model and flume size. For example, with the building model (8cm x 8 cm x 8cm), the model scale length ratio was defined by

$$L_r = L_p/L_m = 35 \tag{4.12}$$

Where L_p is the length of the prototype and L_m is the length of the model

The velocity ratio u_r was calculated using Froude scaling

$$\left(\frac{u}{\sqrt{ga}}\right)_m = \left(\frac{u}{\sqrt{ga}}\right)_p \tag{4.13}$$

$$u_r = \frac{u_p}{u_m} = \sqrt{\frac{L_p}{L_m}} = \sqrt{L_r} \tag{4.14}$$

Substituting L_p and L_m to a_p and a_m, respectively, the above equation stands for

$$u_r = \sqrt{a_r} = \sqrt{35} \quad (4.15)$$

Applying Froude scaling to the wave characteristics presented in Table 4.1, the features of the prototype were shown in Table 4.7. As expected, Froude number remained constant.

Table 4.7: Prototype wave properties for various reservoir depths

Reservoir depth (h_0, cm)	Avg. Wave height (cm)	Avg. Wave velocities (m/s)	Average F_r
30	2.58	11.36	2.259
25	2.24	10.53	2.244
20	1.82	9.23	2.182
15	1.35	7.75	2.126

4.5 Conclusion

The impacts of the tsunami forces generally vary with the location of the structures from the coast to the further inland. When coastal infrastructures situated far away from the shore, the consequences of the tsunami incidents become different and several factors play in determining the exerted forces on the structures. In the present experiment, flat bed was used with no bed friction. However in the real tsunami, structures located at the further inland could be affected by the friction coefficient. The present experimental results were valid for the structures located near the shoreline and further researches are required to analyze the tsunami impacts on the coastal structures far away from the coast.

CHAPTER 5

CONCLUSIONS AND RECOMMENDATIONS

5.1 Introduction

In this chapter, the overall results of the experimental research were summarized. A comprehensive study was performed to examine the impact of tsunami-induced forces on different coastal structures. A quick release dam-break mechanism was introduced to simulate tsunami waves under different wave conditions. Measured forces and wave heights obtained during the experiments were extensively discussed and analyzed in chapter 4. This chapter summarizes the research findings and recommends for further research directions.

5.2 Summary of the Research Findings

Based on the analysis of the measured results, the following conclusions can be achieved.

1. Physical experiments were simulated successfully with the fast opening of the dam-break gate. These experiments investigated the impact mechanisms of rapidly advancing tsunami-like waves with structures, Wave characteristics were described extensively with wave velocity and wave height. Wave velocity was estimated based on the water depth time history. It was observed that the changes in the velocity with distance along the flume were more apparent with larger wave height in comparison with smaller wave height. However, wave properties (include wave velocity and wave height) agreed well enough with Chanson analytical solution (Chanson, 2005).

2. Quantitative analyses of the exerted forces on different coastal structures were performed. In the present study bridge structures as well as building structures were considered for the evaluation of the measured forces.
3. In the case with bridge structures, broken as well as unbroken waves were simulated adjusting the reservoir depths and the static water depths. Measured horizontal forces were larger for the broken waves than those of the unbroken waves. For larger reservoir depths, the initial impact forces were higher than the hydrodynamic forces. As the wave propagated, the front edge of the wave hit the model with high velocity at the base of the bridge pier and attained the peak value of forces instantaneously with relatively smaller water surface elevation. The wave height became high when the velocity, as well as the forces started declining. The similar trends were observed for all of the cases regardless of the reservoir depths. When the girder was located in higher position forces were larger than that of the girder placed at lower position. This circumstance indicated that the bridges with higher girder height are more vulnerable to the tsunami attack. As the tsunami wave height increased, the forces on the girder were also increased which was much apparent in the case of the broken waves than those of the unbroken waves.
4. Experiments were performed with about 16 % perforations in the bridge girder to study the effects of perforations in the force reduction. Approximately 10 % to 18 % force reductions were achieved. Results revealed that perforations in girder are effective in reducing tsunami forces as perforations in girder let water be passed through them. Consequently, less bridge damages are expected with the presence of perforations in the girder during tsunami period. Tests were performed with breakwater and results disclosed that the breakwater was

effective in controlling tsunami forces as long as the breakwater height was more than the tsunami wave height.

5. For the case with square building model, the initial impact forces were larger than the hydrodynamic forces with larger reservoir depths. The hydrodynamic force exceeded the impact force with the case of smaller reservoir depth. The average C_D (drag coefficient) value was 1.31 which was very close to FEMA 55 suggested value; however, it was much lower than FEMA 646 value. The main reason for recorded small value of C_D was due to the limited height of the building model which was easily overtopped by the waves. So, it was difficult to idealize the full impacts of the waves during the turbulent flow condition. The overflowing waves did not contribute to the force measurement.
6. The performances of building with sufficient opening during tsunami event were evaluated in chapter 4. Approximately 10 % to 42 % of forces were reduced with 30 % opening, whereas 22 % to 65 % declinations of forces were obtained from 60 % opening with different reservoir depths. Larger openings in the building model in the coastal region provide more safeguard against the tsunami forces. The presence of the opening allows water to pass through the opening, thus creating counteracting forces inside the building and contributes to the force reduction.
7. The experimental results described in chapter 4 has been clearly demonstrated the efficacy of seawall in the force reduction. Seawall with enough height and positioned closer to the building model provided better performance against the tsunami forces. Another research was performed to evaluate the performance of the perforated seawall in lieu of a solid one. As the amount of force reduction attained by the perforated seawall was almost similar to the solid seawall, this study proposed the use of the perforated wall instead of a solid wall. Moreover,

perforated wall allowed easy receding of water to go back to sea, while solid wall trapped the coming water behind and thus, creating additional forces on the building. Additionally, less construction cost of the perforated wall would make it more attractive than the solid wall. Finally, it should be noted that the results of this study were appropriate for this particular type of setup as the distance between the seawalls and the building structures plays a crucial role in the declination of forces.

8. The effects of the upstream barriers on the building model were assessed by placing different size barriers in different locations in front of the model. The benefits of barrier highly depend on their shape, their length along the flow direction and the distance between the barrier and the building. Barrier with adequate size and shape placed closer to the building model was more effective to provide adequate protection against the tsunami forces. At a higher reservoir depth, thinner barrier that was placed close to the building model performed well than other types of barrier and provide more protection against tsunami forces. Similar tests were performed with building model having opening and as expected, thinner barrier performed better than other two types of barrier.

5.3 Recommendations

The survey of the literature demonstrated that limited research had been performed studying the impacts of the tsunami flows on the coastal structures. However, robust experimentation and analysis should have to be made for clear understanding of the relationship among the multiple variables controlling tsunami effects on the coastal structures. The following future works could be made towards improving existing understanding of these phenomena:

1. Vertical distribution of exerted forces and pressures due to dam-break tsunami waves on the coastal structures should be studied.
2. Laboratory experimental data could be validated with the numerical solution. A single-phase three-dimensional weakly compressible Smoothed Particle Hydrodynamics (SPH) numerical model could be used to investigate the real-time analysis of structural response to the tsunami forces.
3. The present study did not consider any types of debris. The impact mechanics of the floating debris should be considered in the future physical as well as numerical experiments.
4. The laboratory results on the effectiveness of mitigation walls as tsunami protective structures could be validated through the use of the numerical solution.
5. This study did not consider the effect of foundation and the effect of structural weight. These are one of the most important aspects of tsunami research. Therefore, impacts of tsunami waves on structural foundation should be incorporated in future research.
6. Further study could focus on measuring scour depth around the coastal structures created by the tsunami waves.
7. Additional experimental work is required to explore further the influence of the foundation and weight of the structure on wave loading. Such experimental results could be validated through numerical simulation in order to correlate model structures with the actual structures.
8. New guidelines should be developed for the estimation of the hydrodynamic and the impact forces on the specific structures.

REFERENCES

Akiyama, M., Frangopol, D. M., Arai, M., & Koshimura, S. (2013). Reliability of bridges under tsunami hazards: Emphasis on the 2011 Tohoku-oki earthquake. *Earthquake Spectra, 29*(s1), S295-S314.

American Society of Civil Engineers (ASCE). (2006). *Minimum design loads for buildings and other structures*. ASCE Publications, 7(5), New York.

Antonios, & Pomonis, E. E. F. I. T. (2006). The Indian Ocean Tsunami of 26 December 2004 : Mission Findings in Sri Lanka and Thailand *Earthquake Engineering Field Investigation Team (EEFIT)*. United Kingdom, Austria.

Araki, S., Ishino, K., & Deguchi, I. (2010). Characteristics of Tsunami Fluid Force Acting on Girder Bridge. Paper presented at *the Proceedings of the Twentieth (2010) International Offshore and Polar Engineering Conference*, June 20-25, Beijing, China.

Araki, S., & Deguchi, I. (2009). Experimental study on tsunami fluid force on bridge across narrow river. Paper presented at *the Proceedings of the 5th International Conference on Asian and Pacific Coasts*.

Araki, S., Itoh, S., & Deguchi, I. (2008). Experimental study on fluid force on bridge beam due to tsunami. Paper presented at *the Proceedings of the 18th International Offshore and Polar Engineering Conference*, ISOPE.

Arikawa, T. (2008). Behaviors of concrete walls under impulsive tsunami load. Paper presented at the *AGU Fall Meeting* Abstracts (Vol. 1, p. 1331).

Arnason, H., Petroff, C., & Yeh, H. (2009). Tsunami bore impingement onto a vertical column. *Journal of Disaster Research, 4*(6), 391-403.

Arnason, H. (2005). *Interactions between and incident bore and a free-standing coastal structure.* (Ph.D. Thesis), University of Washington, Seattle, 172 pp.

Asakura, R., Iwase, K., Ikeya, T., Takao, M., Kaneto, T., Fujii, N., & Ohmori, M. (2002, July). The tsunami wave force acting on land structures. In *Coastal Engineering Conference* (Vol. 1, pp. 1191-1202). American Society of Civil Engineers (ASCE).

Bahlburg, H., & Spiske, M. (2012). Sedimentology of tsunami inflow and backflow deposits: key differences revealed in a modern example. *Sedimentology, 59*(3), 1063-1086.

Bahlburg, H., & Weiss, R. (2007). Sedimentology of the December 26, 2004, Sumatra tsunami deposits in eastern India (Tamil Nadu) and Kenya. *International Journal of Earth Sciences, 96*(6), 1195-1209.

Ballantyne, D. (2006). Sri Lanka lifelines after the December 2004 great Sumatra earthquake and tsunami. *Earthquake spectra, 22*(S3), 545-559.

Barr, D. I. H., & Das, M. M. (1980). Numerical simulation of dam-burst and reflections, with verification against laboratory data.". *Proc. Institution Civil Engineers,, 69*(2), 359-373.

Bell, S. W., Elliot, R. C., & Hanif Chaudhry, M. (1992). Experimental results of two-dimensional dam-break flows. *Journal of Hydraulic Research, 30*(2), 225-252.

Briechle, S., & Köngeter, J. (2002). *Experimental data for dike-break waves.* Paper presented at the Proc. Intl. Conf. Fluvial Hydraulics (River Flow), Louvain-la-Neuve, Belgium.

Bryant, E. (2001). *Tsunami: the underrated hazard*: Cambridge University Press, London, UK.

Camfield, F. (1980). Tsunami Engineering *Coastal Engineering Research Center, US Army Corps of Engineers, Special Report (SR-6)* (pp. 222).

Canadian Association of Earthquake Engineering (CAEE). (2005). Reconnaissance report on the December 26, 2004 Sumatra earthquake and tsunami. 21 pp.

Carrier, G. F., & Yeh, H. (2005). Tsunami propagation from a finite source. *Computer Modeling In Engineering And Sciences, 10*(2), 113.

Chakraborty, D., & Choudhury, D. (2014). Stability of non-vertical waterfront retaining wall supporting inclined backfill under earthquake and tsunami. *Ocean Engineering, 78*, 1-10.

Chanson, H. (2005). Applications of the Saint-Venant equations and method of characteristics to the dam-break wave problem. *Hydraulic Model Reports Ch55/05*, University of Queensland.

Chanson, H. (2006). Tsunami surges on dry coastal plains: Application of dam-break wave equations. *Coastal Engineering Journal, 48*(04), 355-370.

Chock, G., Robertson, I., Carden, L., & Yu, G. (2011). *Tohoku tsunami-induced building damage analysis including the contribution of earthquake resistant design to tsunami resilience of multi-story buildings.* Paper presented at the Proceedings of the international symposium on Engineering Lessons Learned from the.

City and County of Honolulu Building Code (CCH). (2000). Chapter 16. Article 11. Department of Planning and Permitting of Honolulu Hawaii, Honolulu, HI.

City of Honolulu. (2003). "Revised ordinances of Honolulu." Chapter 16, Article 11, Dept. of Planning and Permitting, Honolulu, HI. ⟨http:// www1.honolulu.gov/council/ocs/roh/⟩ (Retrieved 25, March, 2013).

Cox, D. C., & Mink, J. F. (1963). The tsunami of 23 May 1960 in the Hawaiian Islands. *Bulletin of the Seismological Society of America, 53*(6), 1191-1209.

Cross, R. H. (1967). Tsunami surge forces. *Journal of the Waterways and Harbors Division, Proceedings of the American Society of Civil Engineers, 93*, 201-231.

Cumberbatch, E. (1960). The impact of a water wedge on a wall. *J. Fluid Mech, 7*(3), 353-373.

Dames, & Moore. (1980). Design and construction standards for residential construction in tsunami prone areas in Hawaii *Prepared for the Federal Emergency Management Agency*.

Dias, P., Fernando, L., Wathurapatha, S., & De Silva, Y. (2005). *Structural resistance against sliding, overturning and scouring caused by tsunamis.* Paper presented at the Proceedings of the International Conference of Disaster Reduction on Coasts.

Dressler, R. F. (1954). Comparison of theories and experiments for the hydraulic dam-break wave. *Int. Assoc. Sci. Hydrology, 3*(38), 319-328.

Earthquake Engineering Research Institute (EERI). (2011). *The Tohoku, Japan, tsunami of March 11, 2011: effects on structures*, Special Earthquake Report, Japan, September.

Federal Emergency Management Agency (FEMA). (2005). *Coastal Construction Manual, FEMA 55 Report, Edition 3, Federal Emergency Management Agency,*. Washington, D.C.

Federal Emergency Management Agency (FEMA). (2008). *Guidelines for Design of Structures for Vertical Evacuation from Tsunamis, FEMA P646 Report, prepared by the Applied Technology Council for the Federal Emergency Management Agency*. Redwood City, California.

Franco, A. B. (1996). *Modelacao computacional e experimental de escoamentos provocados pela rotura de barragen.* (PhD Thesis), Instituto Superior Tecnico, Lisbon, Portugal (in Portuguese).

Fritz, H. M., Kalligeris, N., Borrero, J. C., Broncano, P., & Ortega, E. (2008). The 15 August 2007 Peru tsunami runup observations and modeling. *Geophysical Research Letters, 35*(10).

Fujima, K., Achmad, F., Shigihara, Y., & Mizutani, N. (2009). Estimation of tsunami force acting on rectangular structures. *Journal of Disaster Research, 4*(6), 404-409.

Fukui, Y., Nakamura, M., Shiraishi, H., & Sasaki, Y. (1963). Hydraulic study on tsunami. *Coastal Engineering in Japan, 6*, 67-82.

Ghobarah, A., Saatcioglu, M., & Nistor, I. (2006). The impact of the 26 December 2004 earthquake and tsunami on structures and infrastructure. *Engineering structures, 28*(2), 312-326.

Goda, Y. (1974). A new method of wave pressure calculation for the design of composite breakwaters, *Report of the Port and Harbour Research Institute* (Vol. 2(3), pp. 35-68).

Gomez-Gesteira, M., & Dalrymple, R. A. (2004). Using a three-dimensional smoothed particle hydrodynamics method for wave impact on a tall structure. *Journal of Waterway, Port, Coastal, and Ocean Engineering, 130*(2), 63-69.

Goto, K., Sugawara, D., Ikema, S., & Miyagi, T. (2012). Sedimentary processes associated with sand and boulder deposits formed by the 2011 Tohoku-oki tsunami at Sabusawa Island, Japan. *Sedimentary Geology, 282*, 188-198.

Hofland, B., Kaminski, M., & Wolters, G. (2011). Large scale wave impacts on a vertical wall. *Coastal Engineering Proceedings, 1*(32), structures. 15.

Iemura, H., Pradono, M., Yasuda, T., & Tada, T. (2007). Experiments of tsunami force acting on bridge models. *Journal of earthquake engineering, ASCE, 29*, 902-911.

Iemura, H., Pradono, M. H., & Takahashi, Y. (2005). *Report on the Tsunami Damage of Bridges in Banda Aceh and Some Countermeasures.* Paper presented at the Proceedings of the 28th JSCE Earthquake Engineering Symposium, Tokyo, August, 2005.

Iizuka, H., & Matsutomi, H. (2000). Damage due to flood flow of tsunami. *Proceedings of the Coastal Engineering of JSCE, 47*, 381-385 (in Japanese).

International Code Council. (2006). International building code 2006, Country Club Hills, IL.

International Conference of Building Officials (ICBO). (1997). Uniform building code, Whittier, CA.

Jain, S. K. (2011). Quick Report on the Study of the 2004 Sumatra Earthquake and Tsunami Effects *Department of Civil Engineering, Indian Institute of Technology Kanpur*. Kanpur, India. Retrieved 30 th October, 2013. https://www.eeri.org/lfe/clearinghouse/sumatra_tsunami/reports/Quick_Report_Complete_India.pdf

Kasano, H., Oka, J., Sakurai, J., Kodama, N., & Yoda, T. (2012). *Investigative Research on Bridges Subjected to Tsunami Disaster in 2011 off the Pacific Coast of Tohoku Earthquake.* Paper presented at the Australasian Structural Engineering Conference 2012: The past, present and future of Structural Engineering.

Kataoka, S., Kusakabe, T., & Nagaya, K. (2006). *Wave forces acting on bridge girders struck by tsunami.* Paper presented at the Proceedings of the 12th Japan earthquake engineering symposium (pp. 154-157).

Kawashima, K., Kosa, K., Takahashi, Y., Akiyama, M., Nishioka, T., Watanabe, G., . . . Matsuzaki, H. (2011). *Damages of Bridges during 2011 Great East Japan Earthquake.* Paper presented at the Proceedings of 43rd Joint Meeting, US-Japan Panel on Wind and Seismic Effects.

Kirkgoz, M. S. (1983). *Breaking and run-up of long waves, tsunamis: their science and engineering.* Paper presented at the 10th IUGG International Tsunami

Symposium Sendaishi/ Miyagi-ken, Japan, Terra Scientific Publishing, Tokyo, Japan.

Kosa, K. (2012). Damage analysis of bridges affected by tsunami due to Great East Japan Earthquake. *Proc. International Sym. on Engineering Lessons Learned from the 2011 Great East Japan Earthquake*, 1386-1397.

Kusakabe, T., Matsuo, O., & Kataoka, S. (2005). *Introduction of a Methodology to Mitigate Tsunami Disaster by the Pre-Evaluation of Tsunami Damage Considering Damage Investigation of 2004 Tsunami Disaster in the Indian Ocean.* Paper presented at the Proceedings of the 21st US-Japan Bridge Engineering Workshop Tsukuba, Japan, October 3-5.

Lauber, G., & Hager, W. H. (1998). Experiments to dambreak wave: Horizontal channel. *Journal of Hydraulic research, 36*(3), 291-307.

Leal, J. (1999). *Modelação matemática da propagação de ondas de cheia provocadas pela ruptura de barragens em canais de leito móvel.* MS thesis, Instituto Superior Técnico, Lisbon, Portugal (in Portuguese).

Leal, J., Ferreira, R., Cardoso, A., Bousmar, D., & Zech, Y. (2002). *Dam-break waves on movable bed.* Paper presented at the Proc. River Flow 2002, D. Bousmar and Y. Zech, eds., Balkema, Rotterdam, the Netherlands, 2, 981-990.

Leal, J. G., Ferreira, R. M., & Cardoso, A. H. (2006). Dam-break wavefront celerity. *Journal of Hydraulic Engineering, 132*(1), 69-76.

Lekkas, E., Andreadakis, E., Alexoudi, V., Kapourani, E., & Kostaki, I. (2011). *The Mw= 9.0 Tohoku Japan earthquake (March 11, 2011) tsunami impact on structures and infrastructure.* Paper presented at the Environmental Geosciences and Engineering Survey for Territory Protection and Population Safety (EngeoPro) International conference, Moscow.

Liu, P. L.-F., Lynett, P., Fernando, H., Jaffe, B. E., Fritz, H., Higman, B., . . . Synolakis, C. (2005). Observations by the international tsunami survey team in Sri Lanka. *Science, 308*(5728), 1595-1595.

Lukkunaprasit, P., & Ruangrassamee, A. (2008). Building damage in Thailand in the 2004 Indian Ocean tsunami and clues for tsunami-resistant design. *The IES Journal Part A: Civil & Structural Engineering, 1*(1), 17-30.

Lukkunaprasit, P., Ruangrassamee, A., & Thanasisathit, N. (2009). Tsunami loading on buildings with openings. *Science of Tsunami Hazards, 28*(5), 303.

Lukkunaprasit, P., & Lau, T. L. (2011). Influence of bridge deck on tsunami loading on inland bridge piers. *The IES Journal Part A: Civil & Structural Engineering, 4*(2), 115-121.

Maheshwari, B., Sharma, M., & Narayan, J. (2006). Geotechnical and structural damage in Tamil Nadu, India, from the December 2004 Indian Ocean tsunami. *Earthquake Spectra, 22*(S3), 475-493.

Michelin, A., Lauciani, V., Selvaggi, G., & Lomax, A. (2010). The 2010 Chile earthquake: Rapid assessments of tsunami. *Eos, Transactions American Geophysical Union, 91*(35), 305-306.

Mikami, T., Shibayama, T., & Esteban, M. (2012). Field survey of the 2011 Tohoku Earthquake and Tsunami in Miyagi and Fukushima prefectures. *Coastal Engineering Journal, Japanese Society of Civil Engineers (JSCE), 54*(1), 1250011.

Miller, S., & Hanif Chaudhry, M. (1989). Dam-break flows in curved channel. *Journal of Hydraulic Engineering, 115*(11), 1465-1478.

Mori, N., Takahashi, T., Yasuda, T., & Yanagisawa, H. (2011). Survey of 2011 Tohoku earthquake tsunami inundation and run-up. *Geophysical Research Letters, 38*(null), L00G14.

Murty, T. S. (1977). Seismic sea waves: tsunamis *Bulletin of the Fisheries Research Board of Canada- no. 198, Department of Fisheries and the Environment, Fisheries and Marine Service, Scientific Information and Publishing Branch*. Ottawa, Canada.

Nakao, H., Izuno, K., & Kobayashi, H. (2009). Flow and hydrodynamic force characteristics associated with a tsunami acting on a bridge. *Journal of Structure Engineering, Japan Society of Civil Engineers, 55*, 789-798.

Nii, S., Kosa, K., Shoji, G., & Kimura, K. (2009). Experimental examination concerning tidal wave action power to bridge. *Journal of Structural Engineering*, 471-482.

Nistor, I., Saatcioglu, M., & and Ghobarah, A. (2005). *The December 2004 earthquake and tsunami – hydrodynamic forces on physical infrastructure in Thailand and Indonesia,*. Paper presented at the Canadian Coastal Engineering Conference, Halifax, Canada.

Nistor, I., M., S., & Ghobarah, A. (2006). *Tsunami Hydrodynamic Impact Forces on Physical Infrastructures in Thailand and Indonesia.* Paper presented at the Proc. Annual Conf. of the Canadian Society for Civil Eng., CSCE, Calgary, Canada.

Nistor, I., Palermo, D., Cornett, A., & Al-Faesly, T. (2011). Experimental and numerical modeling of tsunami loading on structures. *Coastal Engineering Proceedings, 1*(32), currents. 2.

Nistor, I., Palermo, D., Nouri, Y., Murty, T., & Saatcioglu, M. (2009). *Tsunami forces on structures, in Kim, Y. C., "Handbook of Coastal and Ocean Engineering",* : World Scientific, 261-286.

Nouri,Y., Nistor, I., Palermo, D., & Cornett, A. (2007). Tsunami-induced hydrodynamic and debris flow forces on structural elements. Paper presented at the9th Canadian Conference of Earthquake Engineering, Ottawa, Canada, June.

Nouri, Y., Nistor, I., Palermo, D., & Cornett, A. (2010). Experimental investigation of tsunami impact on free standing structures. *Coastal Engineering Journal, 52*(01), 43-70.

Okal, E. A. (2003). Normal mode energetics for far-field tsunamis generated by dislocations and landslides. *pure and applied geophysics, 160*(10-11), 2189-2221.

Oshnack, M. E., Aguiniga, F., Cox, D., Gupta, R., & van de Lindt, J. (2009). Effectiveness of Small Onshore Seawall in Reducing Forces Induced by Tsunami Bore: Large Scale Experimental Study. *Journal of Disaster Research, 4*(6), 382-390.

Palermo, D., Nistor, I., Nouri, Y., & Cornett, A. (2009). Tsunami loading of near-shoreline structures: a primer. *Canadian Journal of Civil Engineering, 36*(11), 1804-1815.

Pbase. (2007). http://www.pbase.com/issels/phuket_tsunami&page=all. Retrieved 7 th November, 2013

Peregrine, D. (2003). Water-wave impact on walls. *Annual Review of Fluid Mechanics, 35*(1), 23-43.

Pradono, M., Iemura, H., & Yasuda, T. (2008). *TSUNAMI FORCE ON BRIDGE MODELS AND FORCE REDUCTIONS BY MANGROVE MODELS.* Paper presented at the The 14th World Conference on Earthquake Engineering October 12-17, Beijing, China.

Rahman, S., Akib, S., Khan, M. T. R., & Shirazi, S. M. (2014). Experimental Study on Tsunami Risk Reduction on Coastal Building Fronted by Sea Wall. *The Scientific World Journal, 2014*, 7. doi: 10.1155/2014/729357.

Ramsden, J. D., & Raichlen, F. (1990). Forces on vertical wall caused by incident bores. *Journal of Waterway, Port, Coastal, and Ocean Engineering, 116*(5), 592-613.

Ramsden, J. D. (1993). Tsunamis: Forces on a vertical wall caused by long waves, bores, and surges on a dry bed *Report No. KH-R-54, W.M. Keck Laboratory, California Institute of Technology, Pasadena, Calif, 251 pp.*

Ramsden, J. D. (1996). Forces on a vertical wall due to long waves, bores, and dry-bed surges. *Journal of waterway, port, coastal, and ocean engineering, 122*(3), 134-141.

Richmond, B., Szczuciński, W., Chagué-Goff, C., Goto, K., Sugawara, D., Witter, R., Tappin, D.R., Jaffe, B., Fujino, S., Nishimura, Y., Goff, J. (2012). Erosion, deposition and landscape change on the Sendai coastal plain, Japan, resulting from the March 11, 2011 Tōhoku-oki tsunami. *Sedimentary Geology, 282*, 27–39. doi:10.1016/j.sedgeo.2012.08.005

Richmond, B. M., Jaffe, B. E., Gelfenbaum, G., & Morton, R. A. (2006). Geologic impacts of the 2004 Indian Ocean tsunami on Indonesia, Sri Lanka, and the

Maldives. *Tsunamis, hurricanes and neotectonics as driving mechanisms in coastal evolution, Zeitschrift für Geomorphologie NF, Suppl, 146*, 235-251.

Saatcioglu, M., Ghobarah, A., & Nistor, I. (2005). Effects of the december 26, 2004 sumatra earthquake and tsunami on physical infrastructure. *ISET Journal of earthquake technology, 42*(4), 79-94.

Saatcioglu, M., Ghobarah, A., & Nistor, I. (2006a). Performance of structures in Indonesia during the December 2004 great Sumatra earthquake and Indian Ocean tsunami. *Earthquake Spectra, 22*(S3), 295-319.

Saatcioglu, M., Ghobarah, A., & Nistor, I. (2006b). Performance of structures in Thailand during the December 2004 Great Sumatra earthquake and Indian Ocean tsunami. *Earthquake spectra, 22*(S3), 355-375.

Scawthorn, C., Ono, Y., Iemura, H., Ridha, M., & Purwanto, B. (2006). Performance of lifelines in Banda Aceh, Indonesia, during the December 2004 Great Sumatra earthquake and tsunami. *Earthquake spectra, 22*(S3), 511-544.

Sheth, A., Sanyal, S., Jaiswal, A., & Gandhi, P. (2006). Effects of the December 2004 Indian Ocean tsunami on the Indian mainland. *Earthquake spectra, 22*(S3), 435-473.

Shoji, G., Hiraki, Y., Fujima, K., & Shigihara, Y. (2011). Evaluation of tsunami fluid force acting on a bridge deck subjected to breaker bores. *Procedia Engineering, 14*, 1079-1088.

Shoji, G., & Mori, Y. (2006). Hydraulic model experiment to simulate the damage of a bridge deck subjected to tsunamis. *Annual Journal of Coastal Engineering, 53*(2), 801-805.

Shoji, G., Moriyama, T., Hiraki, Y., Fujima, K., Shigihara, Y., & Kasahara, K. (2009). Evaluation of a tsunami wave load acting on a bridge deck subjected to plunging breaker bores and surging breaker bores. *Journal of Japan Society of Civil Engineers, Ser. B 2(Coastal Engineering), 65*(1), 826-830.

Snodgrass, F. E., Rice, E. K., & Hall, M. (1951). Wave forces on piling (Monterey Field Test) *Univ. California, Berkeley, CA, Inst. Of Engineering Research, Tech. Rept. Series 35, Issue 4, June, 9 pp.*

Stansby, P., Chegini, A., & Barnes, T. (1998). The initial stages of dam-break flow. *Journal of Fluid Mechanics, 374*, 407-424.

St-Germain, P., Nistor, I., Townsend, R., & Shibayama, T. (2013). SPH Numerical Modeling of Structures Impacted by Tsunami Bores. *Journal of Waterway, Port, Coastal, and Ocean Engineering, 0*(ja), null. doi: doi:10.1061/(ASCE)WW.1943-5460.0000225.

Streeter, V. L. & Wylie, E. B. (975). *Fluid Measurement*. *Fluids Mechanics.* 6th edition (McGraw-Hill, USA).

Sugimoto, K., & Unjoh, S. (2008). *Experimental study of damage mechanism for bridge structures subjected by tsunami.* Paper presented at the Proceedings of the 11th Symposium on Ductility Design Method for Bridges. Japan Society of Civil Engineers, 11, 97-100., Japan.

Synolakis, C., & Okal, E. (2005). 1992–2002: Perspective on a decade of post-tsunami surveys *Tsunamis* (pp. 1-29): Springer

Takahashi, S., Kuriyama, Y., Tomita, T., Kawai, Y., Arikawa, T., Tatsumi, D., & Negi, T. (2011). Urgent survey for 2011 Great East Japan Earthquake and Tsunami disaster in ports and coasts – part I (tsunami), English abstract of the technical note of the Port and Airport Research Institute (PARI), (1231) 9.

Thomas, S., & Cox, D. (2011). Influence of Finite-Length Seawalls for Tsunami Loading on Coastal Structures. *Journal of Waterway, Port, Coastal, and Ocean Engineering, 138*(3), 203-214.

Tomita, T., Imamura, F., Arikawa, T., Yasuda, T., & Kawata, Y. (2006). Damage caused by the 2004 Indian Ocean Tsunami on the south-western coast of Sri Lanka. *Coastal Engineering Journal, Japanese Society of Civil Engineers (JSCE), 48*(2), 99-116.

Tobita, T., Iai, S., Banta, C., & Wimpie, A. (2006). Reconnaissance report of the 2004 Great Sumatra-Andaman, Indonesia, Earthquake: Damage to geotechnical works in Banda Aceh and Meulaboh. *Journal of Natural Disaster Science, 28*(1), 35-41.

Triatmadja, R., & Nurhasanah, A. (2012). Tsunami force on buildings with openings and protection. *Journal of Earthquake and Tsunami, 6*(04).

Thusyanthan, N. I., & Madabhushi, S. G. (2008). *Tsunami wave loading on coastal houses: a model approach.* Paper presented at the Proceedings of the ICE-Civil Engineering.

Unjoh, S. (2005). Damage to transportation facilities. The damage induced by Sumatra earthquake and associated tsunami of December 26, 2004, A report of the reconnaissance team of Japan Society of Civil Engineers (pp. 66-76).

Unjoh, S. (2007). Bridge Damage Caused by Tsunami,. *Bulletin of Japan Association for Earthquake Engineering, 6*, 26-28 (in Japanese).

U.S. Army Corps of Engineers. (1960). *Floods resulting from suddenly breached dams, Miscellaneous Paper 2(374), Report 1. US Army Engineer Waterways Experiment Station, Corps of Engineers: .* Vicksburg, Mississippi.

U.S. Army Corps of Engineers. (1961). Floods resulting from suddenly breached dams. US Army Engineer Waterways Experiment Station, Corps of Engineers, Report 1 (Vol. 2, pp. 374). Vicksburg, Mississippi.

Wilkinson, F. (2005). Report On Coastal Design And Tsunami Mitigation For Shelter/House Reconstruction Along West Coast Aceh Province pub: UNHCR.

Yamamoto, Y., Takanashi, H., Hettiarachchi, S., & Samarawickrama, S. (2006). Verification of the destruction mechanism of structures in Sri Lanka and Thailand due to the Indian Ocean tsunami. *Coastal Engineering Journal, 48*(02), 117-145.

Yeh, H. H., Ghazali, A., & Marton, I. (1989). Experimental study of bore run-up. *J. Fluid Mech, 206,* 563-578.

Yeh, H. H., & Mok, K. M. (1990). On turbulence in bores. *Physics of Fluids A: Fluid Dynamics, 2*, 821.

Yeh, H. H. (1991). Tsunami bore runup *Tsunami Hazard* (pp. 209-220): Springer.

Yeh, H., Titov, V., Gusiakov, V., Pelinovsky, E., Khramushin, V., & Kaistrenko, V. (1995). The 1994 Shikotan earthquake tsunamis. *pure and applied geophysics, 144*(3-4), 855-874.

Yeh, H. (2006). Maximum fluid forces in the tsunami runup zone. *Journal of waterway, port, coastal, and ocean engineering, 132*(6), 496-500.

Yeh, H. H.-j., Robertson, I., & Preuss, J. (2005). *Development of design guidelines for structures that serve as tsunami vertical evacuation sites* (Vol. 4): Washington State Department of Natural Resources, Division of Geology and Earth Resources.

Yim, S. C. (2005). *Modeling and Simulation of Tsunami and Storm Surge Hydrodynamics Loads on Coastal Bridge Structures*. Paper presented at the Proceedings of the 21st US-Japan Bridge Engineering Workshop, Tsukuba, Japan, October 3-5.

APPENDIX A

LIST OF PUBLICATIONS

Rahman, S., Akib, S., Khan, M. T. R., & Shirazi, S. M. (2014). Experimental Study on Tsunami Risk Reduction on Coastal Building Fronted by Sea Wall. *The Scientific World Journal,* vol. 2014, Article ID 729357, 7 pages, 2014. doi:10.1155/2014/729357

Rahman, S., Khan, M. T. R., Akib, S., Din, N. B. C., Biswas, S. K., & Shirazi, S. M. (2014). Sustainability of Rainwater Harvesting System in terms of Water Quality. *The Scientific World Journal,* vol. 2014, Article ID 721357, 10 pages, 2014. doi:10.1155/2014/721357

Rahman, S., Akib, S. & Shirazi, S. (2014). Experimental Investigation on the Stability of Bride Girder against Tsunami Forces. *Science China Technological Sciences, 57*(10), 2028-2036.

Rahman, S., Akib, S., Khan, M., & Triatmadja, R. (2014). Performance of Bridge Girder with Perforations under Tsunami Wave Loading. World Academy of Science, Engineering and Technology, International Science Index 86, *International Journal of Civil, Architectural Science and Engineering, 8*(2), 17-22.

Akib, S. and Rahman, S. (2013). Time Development of Local Scour around Semi-Integral Bridge Piers and Piles in Malaysia , World Academy of Science, Engineering and Technology, International Science Index 79, *International Journal of Civil, Architectural Science and Engineering, 7*(7), 22-27.

Akib, S. Mashodi, N. and Rahman, S. (2013). Semi-Integral Bridge Scour Countermeasure Using Gabion and Crushed Concrete Mixed with Palm Shell: A Review. *Journal of Science and Technology, 51*(2B) 59-68.

Jahangirzadeh, A., Akib, S. Kamali, B. Rahman, S. (2012). Optimal Water Allocation: Sustainable Management of Dam Reservoir, World Academy of Science, Engineering and Technology, *72*(2012), 444-446

Akib, S., Jahangirzadeh, A., Wei, L. H., Shirazi S. M., Rahman, S. (2012). Experimental study on the skewed integral bridge by using crushed concrete geobags as scour protection, 6th International Conference on Scour and Erosion ICSE 6, Paris, France, Aug 27-31, 2012.